

ANALYSIS AND PROCEDURES OF MULTIBEAM DATA CLEANING FOR BATHYMETRIC CHARTING

F. M. F. ARTILHEIRO

April 1998



**TECHNICAL REPORT
NO. 192**

PREFACE

In order to make our extensive series of technical reports more readily available, we have scanned the old master copies and produced electronic versions in Portable Document Format. The quality of the images varies depending on the quality of the originals. The images have not been converted to searchable text.

ANALYSIS AND PROCEDURES OF MULTIBEAM DATA CLEANING FOR BATHYMETRIC CHARTING

Fernando Manuel Freitas Artilheiro

**Department of Geodesy and Geomatics Engineering
University of New Brunswick
P.O. Box 4400
Fredericton, N.B.
Canada
E3B 5A3**

April 1998

© Fernando Artilheiro, 1996

PREFACE

This technical report is an unedited reproduction of a report submitted in partial fulfillment of the requirements for the degree of Master of Engineering in the Department of Geodesy and Geomatics Engineering, September 1996. The research was supervised by Dr. David Wells, and it was supported by Fisheries and Oceans Canada, by the Hydrographic Office of the Portuguese Navy, and by the Natural Sciences and Engineering Research Council of Canada.

As with any copyrighted material, permission to reprint or quote extensively from this report must be received from the author. The citation to this work should appear as follows:

Artalheiro, F. M. F. (1998). *Analysis and Procedures of Multibeam Data Cleaning for Bathymetric Charting*. M.Eng. report, Department of Geodesy and Geomatics Engineering Technical Report No. 192, University of New Brunswick, Fredericton, New Brunswick, Canada, 186 pp.

ABSTRACT

Multibeam echosounding (MBES) bathymetric surveying is a new hydrographic methodology. Criteria for the most appropriate ways of using MBES systems in hydrography must be established. This report addresses two questions concerning the “cleaning” of MBES bathymetric data:

1. What rules should the hydrographer follow in MBES data cleaning for bathymetric charting, in order to uniformly achieve the most reliable data cleaning results?
2. What features in multibeam acoustic backscatter data can be used to help identify bathymetric anomalies?

MBES bathymetric data contains blunders. These errors need to be identified and the corresponding soundings rejected. This is the goal of data cleaning task. Currently, one of the major obstacles of using MBES in hydrography is the data cleaning. Frequently this is because the sequence of data cleaning steps is not always the most logical and uniform.

This report summarizes the background information required for the analysis and cleaning of MBES data. Several data cleaning methods are reviewed. For two commercial methods, HDCS (a module from the Hydrographic Information Processing System, Universal Systems Ltd.) and BINSTAT (a module from Neptune, Simrad Norge AS), a logical sequence of steps for their use is proposed; as well suggestions for standardization of processing are made.

As there is a correlation between seafloor bathymetric features and side scan targets, this report assesses, for two case studies, how acoustic seabed backscatter information provided by many MBES systems, can be useful as a potential coadjutant of data cleaning.

The results obtained show that bathymetric features such as wrecks are highlighted by a decrease of the backscatter strength, and boulders are highlighted by an increase of the backscatter strength. It is concluded that the bottom detection parameter (amplitude or phase) is an important data cleaning factor for making decisions about blunders and real features, whereas the acoustic imagery provides a mean to define areas where either automatic or interactive data cleaning should be used.

ACKNOWLEDGMENTS

I would like to thank my supervisor Dr. David Wells for his support, orientation, and advice, not only in this report but also, throughout my studies at the University of New Brunswick (UNB).

I appreciate the support and interest of Dr. John Hughes Clarke and Dr. Larry Mayer in my studies at the UNB, as well as for the transmitted knowledge that I profited from during the last two years.

I would also like to acknowledge André Godin for his friendship and deep experience on multibeam surveying.

Multibeam sonar data and hydrographic data processing software are an essential part in this report. I express my gratitude to the Ocean Mapping Group at the UNB and Canadian Hydrographic Service for the multibeam data, Universal Systems Ltd. and Simrad Norge AS for the software licenses.

Finally, I would like to thank my wife Graça for her unconditional support and care, interrupting her professional career to give the highest priority to my studies. Many others played an important part in the emotional support. Here I would like to thank my parents, relatives, and friends.

TABLE OF CONTENTS

	Page
ABSTRACT	ii
ACKNOWLEDGMENTS	iii
TABLE OF CONTENTS	iv
LIST OF FIGURES	viii
LIST OF TABLES	xi
LIST OF SYMBOLS	xii
1. INTRODUCTION	1
1.1. Motivation	2
1.2. Report Outline	4
1.3. Methodology Used in this Report	5
1.4. Contributions	6
2. MULTIBEAM SONAR PRINCIPLES	8
2.1. Transmission and Reception of Acoustic Waves	9
2.2. Sonar Equation	11
2.3. Acoustic Footprint Dimension	13
2.4. Bottom Detection.....	14
2.4.1. Amplitude Detection.....	15
2.4.1.1. Leading Edge of the Reflected Signal.....	16
2.4.1.2. Maximum Amplitude of the Reflected Signal.....	16

2.4.1.3. Center of Mass of the Reflected Signal.....	16
2.4.2. Phase Detection.....	16
2.5. Backscattering.....	19
2.6. Seafloor Properties.....	22
2.7. Interaction of the Acoustic Waves with the Seafloor.....	24
2.7.1. Lambert’s Law	24
2.7.2. Jackson’s Model.....	25
2.7.2.1. Model Implementation	26
2.8. Acoustic Image	28
2.9. Simrad EM 1000 Data.....	31
3. ERRORS IN THE BATHYMETRIC DATA SET	35
3.1. Definitions.....	35
3.2. Uncertainty on Depth Measurement.....	37
3.3. Seafloor Surface Model.....	41
3.4. Causes for the Occurrence of Blunders.....	45
3.5. Effect of Blunders in the Bathymetric Data Set.....	46
3.6. Blunder Handling in the Bathymetric Data Set.....	47
4. DATA CLEANING METHODS AND PROCEDURES	48
4.1. Data Cleaning Requirements.....	50
4.2. Data Cleaning Tools Based on Redundancy.....	51
4.3. Statistical Methods.....	52
4.3.1. Combined Offline Program	53
4.3.2. Hydrographic Data Cleaning System.....	55
4.3.3. Binning Statistics.....	57
4.3.4. Royal Danish Administration of Navigation & Hydrography Algorithm...	60
4.3.5. Automatic Detection Algorithm	62

4.4. Interactive Methods.....	64
4.4.1. Digital Terrain Model	66
4.4.2. Acoustic Image.....	68
4.5. Dimension of Statistical Cells	69
4.6. Procedures for Multibeam Data Cleaning.....	76
5. TEST DATA ASSESSMENT	86
5.1. Test Data	86
5.2. Test Procedures	88
5.2.1. HDCS	88
5.2.1.1. Empress of Ireland	89
5.2.1.2. Halifax Approaches.....	91
5.2.2. BINSTAT	92
5.2.2.1. Empress of Ireland	94
5.2.2.2. Halifax Approaches.....	96
5.2.3. Backscatter Analysis.....	97
5.3. Results	106
5.3.1. Automatic and Interactive Data Cleaning Tests.....	106
5.3.2. Backscatter Tests on Data Cleaning.....	107
5.4. Improvements to Data Cleaning.....	109
6. CONCLUSIONS AND RECOMMENDATIONS	113
6.1. Automatic Data Cleaning Methods	114
6.2. Potential of the Backscatter.....	116
6.3. Future Studies.....	118
REFERENCES	119

APPENDIX A - Cell's Dimension and Classification Parameters	125
APPENDIX B.1 - Results of Interactive and Automatic Data Cleaning with HDCS for the Empress of Ireland	133
APPENDIX B.2 - Results of Interactive and Automatic Data Cleaning with HDCS for the Halifax Approaches	144
APPENDIX C.1 - Results of Interactive and Automatic Data Cleaning with BINSTAT for the Empress of Ireland	154
APPENDIX C.2 - Results of Interactive and Automatic Data Cleaning with BINSTAT for the Halifax Approaches.....	168
VITA	187

LIST OF FIGURES

	Page
Figure 2.1. Beam ensonifying the seabed.....	13
Figure 2.2. Bottom detection methods.	15
Figure 2.3. Phase detection..	17
Figure 2.4. Backscatter samples	20
Figure 2.5. Beam footprint.	21
Figure 2.6. Computation of Jackson’s model for very fine sand (frequency 95 KHz)...	27
Figure 2.7. Generic curves, from Jackson’s model, for different types of seafloor (frequency of 95 KHz).....	28
Figure 2.8. Side scan trace, across- and along-track resolution	29
Figure 2.9. Side scan trace, depth resolution.....	30
Figure 3.1. Right-hand coordinate system.....	37
Figure 3.2. Total depth measurement uncertainty for the Simrad EM 1000 (simplified model) from 5 to 30 metres	39
Figure 3.3. Total depth measurement uncertainty for the Simrad EM 1000 (simplified model) from 30 to 100 metres..	41
Figure 3.4. Two-dimensional profile, the uncertainty of the measurement for the MBES, is used as the region inside which the soundings are accepted.	43
Figure 3.5. Two-dimensional profile, using smaller cells, the uncertainty of the measurement for the MBES is used as the region inside which the soundings are accepted.	43
Figure 4.1. Processing sequence	49
Figure 4.2. BINSTAT window.....	59
Figure 4.3. Clustering by mode seeking.....	63

Figure 4.4. DTM of the Empress of Ireland.	67
Figure 4.5. Acoustic image of the Empress of Ireland.	68
Figure 4.6. HDCS radius of influence.	70
Figure 4.7. Percentage of overlapping among ensonified areas from consecutive pings, water depth from 5 to 20 metres.	71
Figure 4.8. Percentage of overlapping among ensonified areas from consecutive pings, water depth from 20 to 100 metres.	72
Figure 4.9. Coverage of the seafloor.	73
Figure 4.10. Acoustic footprints resulting from the overlapping of two halves swaths ran in direct and reverse sense. Recommended dimension of the radius of influence (HDSCS).	74
Figure 4.11. Acoustic footprints resulting from the overlapping of two halves swaths ran in direct and reverse sense. Recommended dimension of the cells (BINSTAT).	75
Figure 4.12. Example of the acceptance region in BINSTAT.	82
Figure 4.13. Example of the acceptance region in HDSCS.	83
Figure 5.1. Backscatter information from the <i>Empress of Ireland</i> data set. The amplitude samples were corrected by removing the Lambertian correction and filtered by the use of a moving average filter. The theoretic sediment curves are computed by Jackson's model.	100
Figure 5.2. Backscatter information from the <i>Empress of Ireland</i> data set (same as previous figure). The backscatter strength is now presented by a sixth order polynomial which was fitted to the amplitude samples.	101
Figure 5.3. Backscatter information from the <i>Empress of Ireland</i> data set. This figure represents the detection of a wreck. The amplitude samples correspond to the raw data without corrections (filtered out using a moving average filter in order to reduce the noise).	102
Figure 5.4. Backscatter information from the <i>Empress of Ireland</i> data set. Same as previous figure, but detected from a different azimuth.	103

Figure 5.5. Backscatter strength from the *Halifax Approaches* data set from a rocky area. The amplitude samples were corrected by removing the Lambertian correction and filtered by the use of a moving average filter. The theoretic sediment curves are computed by Jackson's model..... 104

Figure 5.6. Backscatter strength from the *Halifax Approaches* data set for a sandy area. The amplitude samples were corrected by removing the Lambertian correction and filtered by the use of a moving average filter. The theoretic sediment curves are computed by Jackson's model..... 105

Figure 5.7. Backscatter strength from the *Halifax Approaches* data set for a sandy area with lower reflectivity. The amplitude samples were corrected by removing the Lambertian correction and filtered by the use of a moving average filter. The theoretic sediment curves are computed by Jackson's model..... 105

LIST OF TABLES

	Page
Table 2.1. Sediment parameters.....	23
Table 4.1. Summary and comparison of methods used for multibeam data cleaning.....	65
Table 5.1. Meaningful correlations used in the BINSTAT interactive data cleaning.....	93
Table 5.2. Simplified summary of characteristics from HDCS and BINSTAT	110

LIST OF SYMBOLS

\bar{r}	position vector
\bar{K}	two-dimensional wave vector
η	transducer efficiency (percentage)
α	absorption coefficient
λ	acoustic wavelength
θ	incident angle
ζ	surface roughness
β	spectral strength at wavenumber $2\pi/\lambda = 1\text{cm}^{-1}$
γ	spectral exponent
ρ	density ratio
ν	sound speed ratio
δ	loss tangent
ψ	scattered angle
l	distance from two elements of the transducer
Φ	angle of received signal referred to the acoustic beam axis
τ	acoustic pulse length
ξ	number of instantaneous backscatter samples
ε	acceptance region
μ	mean depth
σ	standard deviation
Φ	Vandermonde matrix
θ_x	beam pointing angle in the XZ plane

θ_y	beam pointing angle in the YZ plane
$\Delta\phi$	angular coverage between
$\delta\phi_{sys}$	measurement error of the beam angle
$\mu(x, y)$	estimated surface
σ_v	volume parameter
ε_c	relative sound velocity profile measurement error
θ_g	grazing angle
ε_h	heave measurement error
ε_{noise}	stochastic variations modelled as white noise
ρ_o	average water density (1.028 g/cm ³)
ε_p	pitch measurement error
ϕ_r	aperture of the reception beam
ε_r	roll measurement error
$\varepsilon_{roughness}$	roughness of the seafloor surface
Δr_s	range sampling resolution
τ_s	sampling interval
ε_s	surface sound velocity measurement error
ε_{sys}	multibeam system depth measurement error
ϕ_x	transmit beam width
ϕ_y	reception beam width
ε_z	uncertainty of the depth measurement for the MBES
A	area
b_f	dimension of the footprint on the athwartships direction
BS	bottom backscatter strength
b_w	dimension of the footprint on the fore-aft direction
c	sound speed

D	slant range distance
DI	directivity index
\underline{G}	Gram matrix
h	height of the seafloor
I_0	incident intensity
I_i	incident intensity
I_r	intensity related to the <i>rms</i> pressure p_r
I_s	intensity of the scattered sound
L	array's length
N_0	environmental noise level
NL	noise level
\underline{P}	weight matrix
P_i	input power (watts)
p_r	<i>rms</i> pressure
r	distance from the transducer
R	radius of curvature
S_B	backscatter strength per unit area
SL	source level
SNR	signal to noise ratio
S_w	swath width
TL	transmission loss
w	receiver bandwidth
w_i	weight of the i^{th} sounding
x_{res}	resolution on the along-track direction
y_{res}	resolution on the across-track direction
z_i	sounding at i^{th} position

Chapter 1

INTRODUCTION

The goal of this report is to analyze some of the present multibeam echosounding data cleaning methods, developing rules and guidelines to standardize the data cleaning tasks for bathymetric charting. The acoustic backscatter is also considered as an important factor to be taken into account in the trouble areas, for the identification of wrecks and boulders.

Multibeam echosounder (MBES) systems [de Moustier, 1988; de Moustier, 1993; Instituto Hidrográfico, 1994; US/Canada HCMWG, 1995] are receiving wide attention from the international hydrographic community. These systems are designed to acquire hydrographic data, at high density, covering one hundred percent the seafloor. They have, unequivocally, the potential to improve the quality and quantity of bathymetric data, improving also the confidence level of the data presented in nautical charts.

It is a consensus in the hydrographic community that MBES is a hydrographic surveying technology of the future. However, the majority of hydrographers agree that the conventional methods used for survey planning, data acquisition, processing, and cleaning the data (from single beam echosounder surveys), are no longer adequate for multibeam surveys.

MBES data cleaning is the task by which the hydrographer accepts or rejects the

bottom detections generated by the MBES during the operation. The goal of MBES data cleaning is to obtain a high quality data set. Processing and handling the high density of data from MBES has been a concern since the introduction of multibeam echosounders [Burke et al., 1988; Midthassel et al., 1988; Wells et al., 1990; Pøhner, 1990]. Appropriate algorithms and methods [Guenther and Green 1982; Ware et al., 1991b; Simrad Norge AS, 1995; Eeg, 1995; Du, 1995] have been developed, to provide the hydrographer with tools to process and clean the data collected by multibeam echosounders.

To effectively accomplish the task of data cleaning, the hydrographer needs to be fully aware of the algorithms underlying these methods, as well as having a good knowledge of MBES characteristics and potential sources of errors. On the other hand, the decisions involved in data cleaning are often subjective. One example is the sequence of data cleaning procedures to be used. Another is choosing parameters describing the soundings which should be accepted. These decisions depend on the experience and the perceptiveness of the hydrographer. Removing some of this subjectivity is the issue that the author proposes to discuss in this report.

1.1. Motivation

Multibeam echosounding systems are designed for two purposes: bathymetric mapping for bottom topography and thematic imaging of the seafloor for bottom

characterization. Two different types of data, depth soundings and backscatter strength measurements, are used for mapping the seafloor.

The approaches used in commercial MBES soundings data cleaning software [e.g. Universal Systems Ltd., 1994a; Simrad Norge AS, 1995] are based on statistics of subsets of soundings (also called cells or working windows). The reliability of these statistics are sensitive to the dimension of the cells. These meaningful characteristics should be taken into account not only during the data cleaning phase, but also in planning the survey. Confidence in the result of the MBES data cleaning depends on the operator's knowledge of several factors, ranging from MBES principles to the characteristics of the seafloor.

Despite being designed for bathymetric charting, as far as the author is aware there are, so far, very few examples of the use of MBES data for nautical charts. The reluctance of hydrographers to use MBES data for this purpose is due primarily to two factors. The first is the requirement that not only the depth measurements, but many additional measurements (pitch, roll, heave, yaw, and refraction profiles) must also be accurately and reliably observed in order to obtain useful bathymetry. These measurements were, partially or completely, neglected in the surveys performed with single beam echosounders (SBES), since they were not as vital to the survey accuracy.

The second factor limiting MBES acceptance is related to post-processing, cleaning, and validation of MBES data by a hydrographer. Blunders in the data set must be removed, and real features preserved. The reliability of this data cleaning must be maximized by using methods and specifications which lead to uniformity of tasks and

objectivity of the data analysis. Only then, can MBES bathymetry satisfy the primary goal of the nautical chart, safe navigation.

According to the above discussion, the goals of this report are to:

- describe basic MBES principles (depth measurement, bottom detection, sensitivity error analysis, and processing of multibeam data);
- describe the basis of the interaction of the acoustic waves with the seafloor and of acoustic backscatter imaging;
- describe the various methodologies used in MBES data cleaning;
- establish the criteria and rules for the optimal use of MBES data cleaning methods for nautical chart production;
- investigate the feasibility of using acoustic backscatter strength for the identification of bathymetric artifacts.

1.2. Report Outline

This report is organized as follows: Chapter 2 introduces the essential background on MBES principles concerning the depth measurements. Concepts and models that explain the interaction of the acoustic signal with the seafloor are provided.

Chapter 3 describes the uncertainties on the depth measurements, causes and the effects of errors in the bathymetric data set. Different ways of handling these errors are mentioned and a model of the seafloor surface is presented.

Chapter 4 presents and discusses some of the methods which have been developed for MBES data cleaning. Procedures for HDCS (Hydrographic Data Cleaning System) and BINSTAT (Bin Statistics) are described, and suggestions are made to standardize the use of these two software packages.

Chapter 5 describes the purpose of the data cleaning tests, the test data, test procedures, tests on backscatter and summarizes the results achieved on these tests.

Chapter 6 reviews the conclusions and presents recommendations for further studies.

1.3. Methodology Used in this Report

Two test data sets were used for this report, each from surveys carried with CSS Frederick G. Creed by the Canadian Hydrographic Service with a Simrad EM 1000 MBES. The first set was collected on June 28, 1992, in the area of the *Empress of Ireland* in the Gulf of St. Lawrence off of Rimouski, Quebec. The second data set was collected on August 14, 1993, as part of the “*Hydrographic Ground Truthing*”, conducted by the University of New Brunswick (UNB), Chebucto Head area, in the Approaches of the Halifax harbor [Hughes Clarke, 1993].

Two software packages, HIPS (Hydrographic Information Processing System) including the data cleaning module HDCS [Universal Systems Ltd., 1994a] and NEPTUNE including the data cleaning module BINSTAT [Simrad Norge AS, 1995].

were used for cleaning these two test data sets.

The choice of the two software packages (HIPS and NEPTUNE) was motivated by the fact that a license for HIPS was already provided by the Universal Systems Ltd. to the Ocean Mapping Group (OMG) at the UNB, and a NEPTUNE limited license, for academic purposes, was provided by Simrad Norge AS. Additionally, the OMG software *SwathEditor*, developed by Dr. John Hughes Clarke, was used for particular types of visualization, as well as to access the backscatter information from the *Simrad* MBES data, and to convert it from binary format to ASCII format.

1.4. Contributions

The contribution of this report is an overview of the state of the art of multibeam data cleaning tools. MBES data cleaning effectiveness depends upon having overlapping data in along- and across-track directions and upon data redundancy, i.e., having more than one hundred percent of coverage of the seafloor. These coverage parameters are studied as one of the important factors for reliable statistics on the data set. Several examples are presented to illustrate the role of the variation in the percentage of overlap which should be taken into account when planning the survey.

In summary, the contributions from this report are:

- A concise resume of multibeam principles and acoustic waves interaction with the seafloor, as part of the background required for the task of data cleaning:

- The investigation of the algorithms used in the Hydrographic Data Cleaning System (HDCS) [Universal Systems Ltd., 1994a]. Modifications in the radius of the field of influence are proposed;
- Some experiments on using the BINSTAT [Simrad Norge AS, 1995] which resulted in some suggestions to enhance this software, mainly in the visualization in the spatial domain;
- The definition of rules for automatic and interactive data cleaning, as an attempt to achieve uniformity among some of the present data cleaning methods;
- The investigation of using MBES backscatter strength data as complementary information to be used to enhance data cleaning.

Chapter 2

MULTIBEAM SONAR PRINCIPLES

The purpose of this chapter is to introduce the essential background on multibeam echosounder (MBES) principles, including the measurement performed by these systems, concepts and models that explain the interaction of the acoustic signal with the seafloor.

Multibeam echosounders collect high data volumes. The first MBES were designed for deep water use, with a low ping rate and a small number of beams. For example, in the case of the *SeaBeam 16* (operational since 1977), the acquisition rate is approximately 28,800 soundings per hour (one thousand metres water depth, based on General Instrument Corporation [1975]). At the present time, MBES designed for shallow water have a much higher ping rate (the maximum ping rate is controlled by the depth, i.e., to the maximum round time required between the ping transmission and reception by the transducer) and the acquisition rates can reach 11.4 million soundings per hour. This is the case of the *Simrad EM 3000* [Simrad Norge AS [1996], which is an acquisition rate of 400 times higher than that of the earlier *SeaBeam* system. A new generation of shallow water multibeam systems *Fansweep 20* [STN Atlas Elektronik, 1996] is designed to collect up to 1,440 soundings per ping, increasing maximum acquisition rates by a factor of 6 over the EM 3000.

2.1. Transmission and Reception of Acoustic Waves

In general, the MBES transmitted pulse has a narrow width in the fore-aft direction and a wide width in the athwartships direction. In contrast, during reception of the echo, several beams are electronically formed, which are broad in the fore-aft direction and narrow in the athwartships direction [Clay and Medwin, 1977; de Moustier, 1988; de Moustier, 1993]. The beam geometry produces a dense coverage along a swath of the seafloor. The resulting ensonified area is equivalent to the intersection between the transmitted and received beams, which can be reasonably approximated by a set of overlapping ellipses.

After transmission of the acoustic pulse, the system begins to listen for the returned signal. This signal is amplified as a function of the travel time -- Time Varying Gain (TVG). The purpose of TVG is to compensate for the signal transmission loss, which increases with path length or equivalently with propagation time. The TVG corrected echoes from the seafloor are, in theory, amplified back to the same sound level, independent of their distance from the transducer.

For conventional amplitude detected beams, the amplified signal is sampled and converted from analogue to digital format. After that, the signal is rectified and passed through a low-pass-filter. The result of these operations is the low-frequency envelope of the low passed signal. This envelope is the signal that is passed to the bottom detection unit.

For each beam, a time window for acceptable echoes is superimposed, called depth window. The reason for this window is to disregard undesired echoes resulting from mid-water returns (e.g. returns from plankton, fishes, deep scattering layer, etc.). The width and central depth of this window must be well chosen, otherwise real features, such as, peaks of rocks and masts of sunken ships, may be treated as undesired echoes too. Usually, the depth window is centered on the previous depth and its width is based on the roughness and local slope of the seafloor.

The signal level must be higher than the threshold detection level, otherwise the echo will not be detected. It is important to remove undesired echoes. If the threshold level has too a high value (MBES is not sensitive enough), then weak echoes from the seafloor will also be rejected.

After these steps, the next problem is a derivation of the bottom detection (estimation of the slant range). This involves three issues: the footprint size, the measurement of the time of flight, and how to locate the position of the depth data point. For every beam, the received energy returned from the ensonified footprint will be spread out in time and thus will increase for more oblique incident angles and greater range. It is required to determine, as accurately as possible, the total delay between the transmission and reception, corresponding to the energy propagating along the acoustic axis of the beam (this topic is discussed in Section 2.4).

After estimating the time of flight and knowing the beam angle, the coordinates referred to the transducer “vessel coordinates” are computed and stored in the datagrams; this information is referred as raw data.

2.2. Sonar Equation

The sonar equation for echosounding describes the relationship of detectability as the *signal to noise ratio* (SNR).

$$\text{SNR} = \text{SL} - 2 \text{TL} - (\text{NL}-\text{DI}) + \text{BS}, \quad (2.1)$$

where *SNR* is the signal to noise ratio, *SL* the source level, *TL* the transmission loss, *NL* the noise level, *DI* the directivity index, and *BS* the bottom backscatter strength. For the present study, it is important to describe each term in more detail [Urick, 1975; Kinsler et al., 1982; de Moustier, 1993].

Considering a given input power P_I (watts) and a transducer efficiency η (percent), the *source level* (SL) specifies the intensity of the radiated acoustic signal in decibels (dB), relative to the intensity of a plane wave of *root mean square* (rms) pressure 1 μPa , referred to a point 1 metre from the center of the projector in the direction of the target. At a large distance r from the transducer, the intensity I_r is related to the *rms* pressure p_r by the plane wave equation

$$I_r = \frac{p_r^2}{\rho c} \text{ w/m}^2, \quad (2.2)$$

and the radiated power, for a non directional projector and a nominal acoustic impedance $\rho_o c = 1.54 \cdot 10^6 \text{ Pa} \cdot \text{s/m}$ (associated to a sound speed of 1500 m/s and water density of 1028 Kg/m^3), is given by

$$P = \frac{4\pi r^2 p_r^2}{\rho c} = 8.38 \cdot 10^{-6} p_i^2 w. \quad (2.3)$$

Converting Equation 2.3 to decibels and remembering that $10 \log p_i^2$ is the source level (where p_i is $1 \mu Pa$) yields to the expression,

$$SL = 10 \log_{10} (P_i \eta / 100) + 170.8 \text{ dB re } 1 \mu Pa \text{ m}. \quad (2.4)$$

The *transmission loss* (TL) accounts for the loss of the acoustic power due to geometrical considerations, i.e., the spherical spreading (proportional to r^{-2}) and losses due to absorption (proportional to the absorption coefficient, α). The transmission loss is given by.

$$TL = 20 \log_{10} r + \alpha r. \quad (2.5)$$

where r is the range and α is the coefficient of absorption.

The *noise level* (NL) is defined by the environmental noise level (N_0), in the bandwidth (w) of the receiver,

$$NL = N_0 + 10 \log_{10} w. \quad (2.6)$$

For a continuous line array of length, L , and using an acoustic wavelength, λ , the *directivity index* (DI) is given by,

$$DI = 10 \log_{10} (2L/\lambda). \quad (2.7)$$

The last term of the sonar equation, *backscatter strength* (BS), is a substantial topic with wide application in this report. Section 2.5 provides the reader with the background and certain techniques that are relevant to discussions in later chapters.

2.3. Acoustic Footprint Dimension

The ensonified area is the result of the intersection of the transmitted and received beam patterns and is dependent upon beam pointing angle, beam width, depth, and mean slope of the seafloor. The ensonified area for each beam can be approximated by an ellipse (Figure 2.1). Considering a flat and leveled seafloor, the length of this ellipse in the athwartships direction is approximately given by b_r ,

$$b_r = \frac{2d}{\cos^2 \theta} \tan\left(\frac{\phi_y}{2}\right), \quad (2.8)$$

where d is the mean depth, θ the beam pointing angle, and ϕ_y the aperture of the reception beam in the athwartships direction. In the presence of a slope, defined by an angle ζ , the length of the acoustic footprint is approximately,

$$b_r = \frac{2d}{\cos(\theta)\cos(\theta + \zeta)} \tan\left(\frac{\phi_y}{2}\right). \quad (2.9)$$

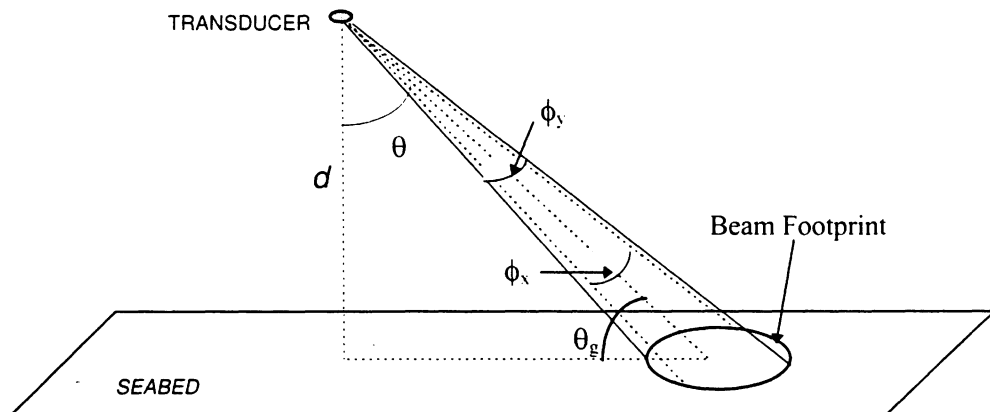


Figure 2.1. Beam ensonifying the seabed.

The width or dimension of the footprint ellipse in the fore-aft direction for a flat seafloor is approximately given by b_w ,

$$b_w = \frac{2d}{\cos(\theta)} \tan\left(\frac{\phi_x}{2}\right), \quad (2.10)$$

where ϕ_x is the aperture of the transmitted beam.

The coverage of the seafloor is a function of the dimension of the ensonified areas, beam spacing across-track, ping rate, ship's speed, yaw, pitch, and roll. In order to achieve one hundred percent coverage of the seafloor, the ensonified areas from consecutive pings must overlap one another, so that every point on the seafloor is ensonified by, at least, one acoustic pulse.

The width of the swath for a flat seafloor is given by.

$$S_w = 2d \cdot \tan\left(\frac{\Delta\phi}{2}\right), \quad (2.11)$$

where $\Delta\phi$ is the angular coverage between the outer beams of the MBES.

2.4. Bottom Detection

Bottom detection is the process used in MBES to determine the time of arrival and the amplitude of the acoustic signal, representing a reflection from the seabed. The reliability of this process affects the quality of the measurements. Blunders can be, among other factors, related to a poor performance of the algorithms used for bottom detection.

Bottom detection algorithms can be categorized into two main divisions: amplitude detection algorithms and phase detection algorithms.

2.4.1. Amplitude Detection

A transducer array emits an acoustic pulse towards the seabed and then starts the listening period. In this phase, the returned signal is sampled in time for each pre-determined beam angle [Simrad Norge AS, 1992]. The travel time of the signal for the correspondent depth point is defined by the detected amplitude of the reflected signal (Figure 2.2).

The most common methods of amplitude detection are as follows:

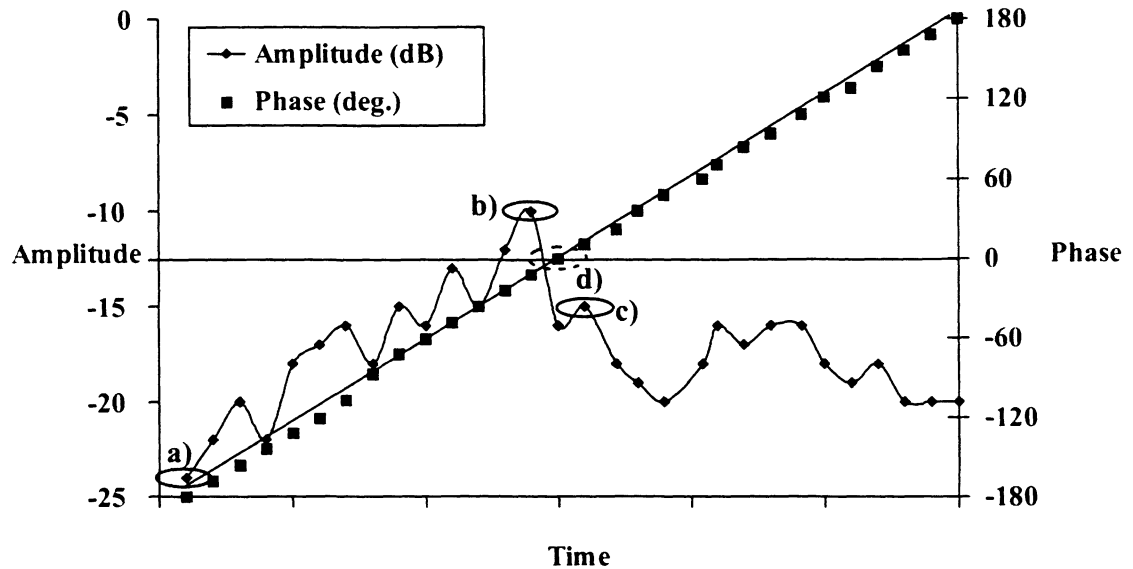


Figure 2.2. Bottom detection methods (signal detection): *a)* leading edge *b)* maximum amplitude *c)* center of mass *d)* zero crossing phase.

2.4.1.1. Leading Edge of the Reflected Signal

This method is commonly used when the angle of incidence of the acoustic signal to the bottom is approximately zero degrees. The bottom detection time is defined for the first arrival inside the beam angle.

With the increasing of the angle of incidence, the returned signal loses its sharp form (short rise time) and the leading edge method no longer performs well. Two other methods can be employed, which take into account the variation of the reflected signal strength samples across the beam footprint;

2.4.1.2. Maximum Amplitude of the Reflected Signal

The bottom detection is defined by the time of maximum backscatter amplitude:

2.4.1.3. Center of Mass of the Reflected Signal

This method is based on the centre of gravity of the signal $s(t)$ inside the depth window $[t_i, t_i + \Delta t]$. This can be obtained by [Instituto Hidrográfico, 1994]

$$\bar{s}(\hat{t}) = \frac{1}{\Delta t} \int_{t_i}^{t_i + \Delta t} s(t) dt, \quad (2.12)$$

where \hat{t} is the time corresponding to the centre of gravity of the signal.

2.4.2. Phase Detection

Amplitude detection is the technique used for the inner beams (close to nadir), where the backscatter amplitude has greater values and a small number of samples. For

the outer beams, the backscatter amplitude decreases and the number of samples becomes very large. Consequently, the echo is so smeared out in time that amplitude detection methods have poor performance. In the presence of a bottom slope in the across-track direction away from the source, the smear of the echo is also enhanced. Hence, the phase detection method is commonly used for large incident angles.

In this technique, the transducer array is divided into two sub-arrays, often overlapping, with the centres of the sub-arrays a number of wavelengths apart. The angular directions are pre-determined and each sub-array forms a beam in that direction, the advantage being that in the presence of simultaneous echoes arrival from different directions, the MBES system

resolves only the echoes in the direction of the formed beam. The sequence of phase difference estimates are then used to estimate the time of arrival of the echo in the pre-determined direction by finding the zero crossing of the phase sequence [de Moustier, 1993]. Figure 2.3 depicts the example of the phase detection method. The

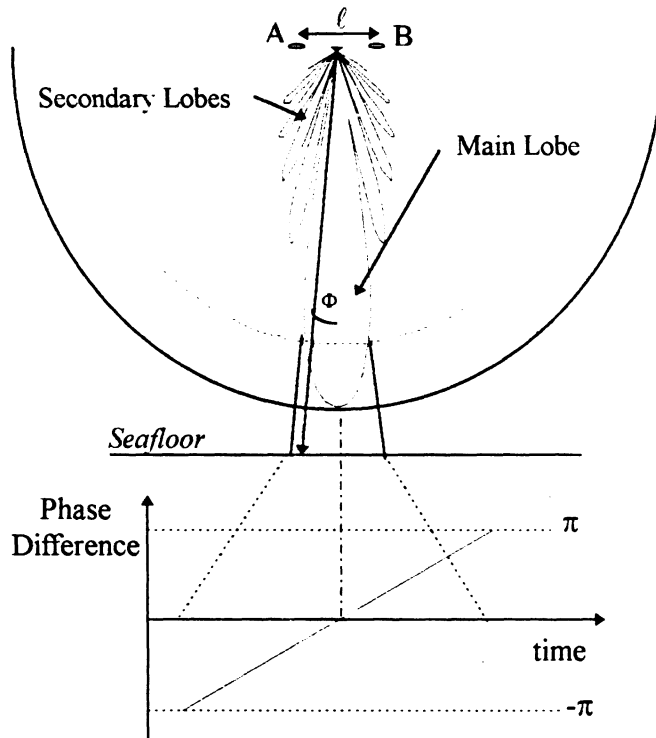


Figure 2.3. Phase detection.

equivalent of the centre of the two sub-arrays are represented by A and B at a distance ℓ from each other, where Φ is the angle of the received signal measured from the acoustical axis. A second order polynomial is fit to a limited sequence of differential phase estimates to refine the detection of the zero crossing phase [Hammerstad et al., 1991]. The phases of the signal received by the two sub-arrays [Du, 1995] will be respectively given by the following equations:

$$P_A(t) = 2\frac{\pi c}{\lambda}t - 2\pi\frac{D}{\lambda\cos(\Phi)} + 2\pi\frac{\ell\sin(\Phi)}{\lambda}, \quad (2.13)$$

$$P_B(t) = 2\frac{\pi c}{\lambda}t - 2\pi\frac{D}{\lambda\cos(\Phi)} - 2\pi\frac{\ell\sin(\Phi)}{\lambda}. \quad (2.14)$$

Thus, the difference of phase is

$$P_A(t) - P_B(t) = 4\pi\frac{\ell\sin(\Phi)}{\lambda}, \quad (2.15)$$

where λ is the acoustic wavelength. When the signal return is from the acoustic axis direction, i.e., $\Phi = 0$, the signal at the two sub-arrays are in phase, and this corresponds to the acoustic travel time.

Across the swath, a combination of amplitude and phase detection is usually required for robust bottom detection. The decision of which method to use depends on the: (1) variance of the curve fit of the phase difference versus time [Hammerstad et al., 1991]; (2) time spread of the echo above a certain threshold [de Moustier, 1993]. Near nadir, the amplitude detection should be used due to the fact that the time series for these beams is too short for a robust phase detection. Amplitude detection is also used in the

case of steep slopes occurring well off-nadir, associated with bathymetric heights, except for the extreme case of a seafloor that is steeply sloping away from the transducer. Phase detection for the nadir beams is more likely to be the result of a gross error (blunder) due to mid-water column returns, or due to higher returns from the sidelobes. Off-nadir detections are mainly by phase, but amplitude detection may be chosen when a higher return is caused by the difference of the reflective properties of the target, by a near specular reflection, or by a large variance of the curve fit. These conditions may occur due to features such as wrecks and boulders.

2.5. Backscattering

Backscattering of sound from the seafloor is of vital importance when using sonar systems, as it can be used as a mean of remotely characterizing some properties of the seafloor, and without which one would not have any return for oblique incidence.

Similar to side scan sonars, multibeam sonars have the capability of collecting backscatter information. The main difference is that MBES measure the angle corresponding to every beam and side scan sonars do not. After correcting each beam backscatter strength for attenuation, spherical spreading, and from the effective ensonified area (dependent on the incidence angle), the result corresponds to the backscatter strength of the seafloor within the instantaneously ensonified area. Because bathymetry is collected simultaneously, multibeam systems provide backscatter strength

that is geometrically corrected (i.e., correct spatial location), and which can be related to the true grazing angle (rather than the assumed flat seafloor and straight ray). This is an advantage over side scan systems.

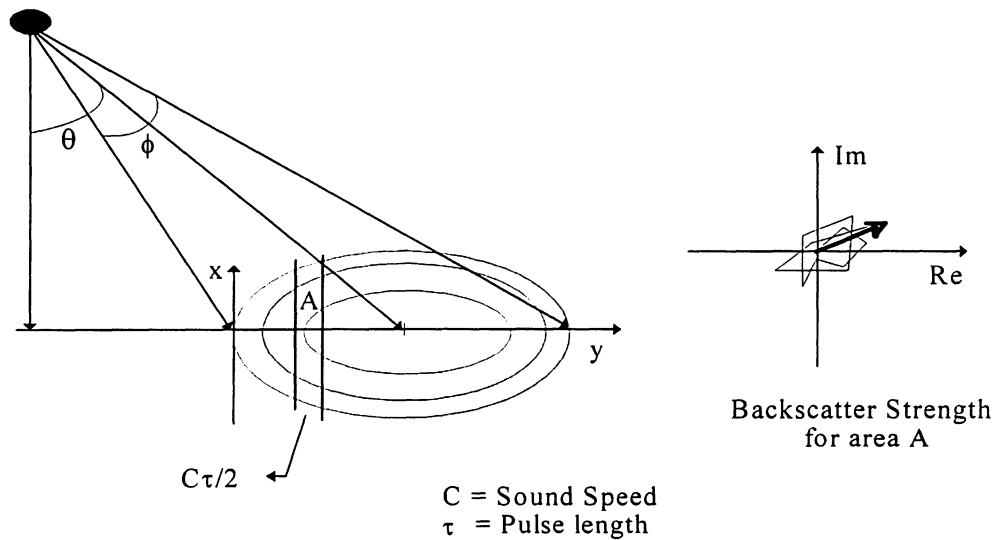


Figure 2.4. Backscatter samples, assuming randomly distributed point scatterers.

The *backscatter strength* (BS), is derived from the sonar equation (Section 2.2) and is usually described as the logarithmic sum of backscatter strength per unit area (S_B , dependent on the reflective properties of the seafloor), and the effective scattering area A (the area of the seafloor that contributes to the backscattered signal) [de Moustier, 1993],

$$BS = S_B + 10 \log_{10} A \text{ dB.} \quad (2.16)$$

The boundaries of the backscattering area are defined by the beam geometry (Figure 2.1), specifically by the beam width (of the transmit beam) in the along-track direction at normal incidence or nadir, ϕ_x , and by the beam width (of the receive beam)

in the across-track direction at nadir, ϕ_y .

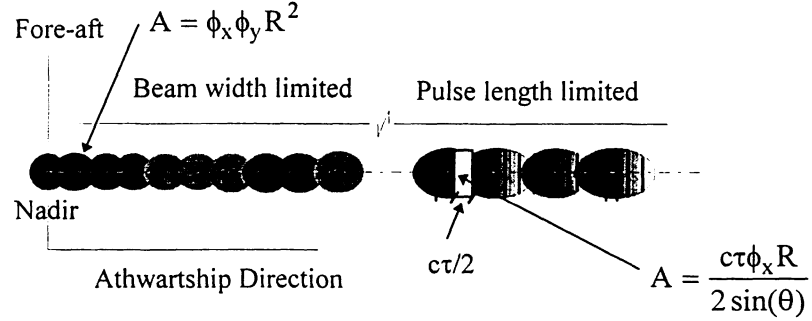


Figure 2.5. Beam footprint and the instantaneous ensonified area A (after Hughes Clarke [1995e]).

For the off-nadir directions, the backscattering area is bounded by the beam width, ϕ_x , and by the transmitted pulse length, τ (Figures 2.4 and 2.5). The backscatter target strength is given by [de Moustier, 1993]:

$$BS = \begin{cases} S_B + 10 \log(\phi_x \phi_y R^2) & \text{for beam width limited case} \\ S_B + 10 \log\left(\frac{c\tau}{2 \sin \theta} \phi_x R\right) & \text{for pulse length limited case} \end{cases} \quad (2.17)$$

where R is the range from the transducer to the point on the seafloor, c the velocity of the sound, and θ the incidence angle. The backscatter coefficient, S_B , is the sum of a term S_0 (related to the roughness and type of the seafloor), and an angular dependence term. For most bottoms S_B is reasonably well matched by Lambert's law for incidence angles between 15 and 65 degrees. Near normal incidence, S_B is a more complicated function of seafloor type and roughness [Jackson et al., 1986a; de Moustier and Alexandrou, 1991] (see Section 2.7).

2.6. Seafloor Properties

The seafloor is characterized by the characteristics of its interface, and by its bulk physical properties. When considering the interaction of the acoustic waves with the seafloor, the fluctuations in the backscatter of the acoustic signal are caused by the nature of incoherent scattering, variations in the interface roughness, and in bulk properties of the bottom substrate.

For reasons of simplicity, seafloor roughness is usually assumed to be isotropic (surface statistics are independent of the direction along the surface [Bendat and Piersol [1986]]) and Gaussian (the distribution of heights $h(\bar{r})$ approximates a normal distribution) [Jackson et al., 1986a; Matsumoto et al., 1993].

Any isotropic and gaussian surface can be represented by a super-position of many harmonic functions, this leading to the concept of a spectrum for the surface. The spectrum of the seabed height variations is, most often, defined by a linear power-law [Jackson et al., 1986a; Matsumoto et al., 1993; Novarini and Caruthers, 1994]. In two dimensions, it is of the form,

$$W(\bar{k}) = \beta \bar{k}^{-\gamma}, \quad (2.18)$$

where \bar{k} is the two-dimensional wave vector, and the magnitude k , is the so called wavenumber. The parameter β is the spectral strength at wavenumber $2\pi/\lambda = 1 \text{ cm}^{-1}$ and γ is the spectral exponent. The parameters β and γ characterize the statistical properties

of the seafloor surface.

In addition to the parameters defined above for the spectral strength and spectral exponent, there are some geoacoustic parameters which are used in seafloor classification models [Mourad and Jackson, 1989; Jackson and Briggs, 1992].

Sediment	ρ	ν	δ	σ_2	γ	β
Rock	2.50	2.50	0.01374	0.002	3.25	0.01862
Gravel	2.50	1.80	0.01374	0.002	3.25	0.01600
Sandy Gravel	2.492	1.3370	0.01705	0.002	3.25	0.012937
Medium Sand	1.845	1.1782	0.01624	0.002	3.25	0.004446
Very Fine Sand	1.268	1.0568	0.01875	0.002	3.25	0.001544
Sandy Mud	1.149	0.9873	0.00386	0.001	3.25	0.000518
Silt	1.147	0.9837	0.00194	0.001	3.25	0.000518

Table 2.1. Sediment parameters [High-Frequency Ocean Environmental Acoustic Models Handbook - APL University of Washington TR 9407 - AEAS 9501, 1994]

The geoacoustic parameters, defined in Table 2.1, are:

Density ratio (ρ) - ratio of sediment mass density to bottom water mass density;

Sound speed ratio (ν) - ratio of sediment acoustic compressional wave speed to bottom water sound speed;

Loss tangent (δ) - ratio of imaginary wavenumber to real wavenumber for the sediment, $\delta = \nu c (\alpha_2 / f) \ln(10) / \pi$, where the ratio (α_2 / f) is a measure of the attenuation in the sediment;

Volume parameter (σ_2) - ratio of sediment volume scattering cross-section to the sediment attenuation coefficient.

Additional geoacoustic properties can be found in Hamilton [1980].

2.7. Interaction of the Acoustic Waves with the Seafloor

This section provides detailed information about Lambert's law and Jackson's model to explain the interaction of the acoustic waves with the seafloor.

Over the last few decades, several researchers have studied and developed theories to explain the high-frequency interaction of the acoustic waves with the seafloor [Urick, 1975; Jackson et al., 1986a; Gensane, 1989; Jackson and Briggs, 1992; Tang et al., 1994].

“Although numerous investigations of high-frequency bottom backscattering have been reported, physical processes responsible for scattering are not well understood.” [Jackson et al., 1986b].

2.7.1. Lambert's Law

Lambert's law assumes the seafloor to be a perfect reflector and is applicable to bottoms with high and random roughness, with no losses at the water/sediment interface, and no transmission to the volume of sediments.

Under these assumptions the acoustic intensity scattered by the seafloor at unit distance from the seabed, can be modelled by Lambert's law [Urick, 1975], which is a

function dependent upon the grazing angle,

$$I_s = \frac{1}{\pi} I_i (\sin \theta_g \cdot \sin \psi) \cdot A, \quad (2.19)$$

where, A is the ensonified area perpendicular to the beam; I_s is the intensity of the sound scattered by the area A ; I_i is the incident intensity; θ_g is the grazing angle; and ψ is the scattered angle.

As far as the multibeam measurements are concerned, they are performed on the backscattered energy (i.e., when $\psi = \theta_g$), thus the previous equation is simplified to,

$$I_b = \frac{1}{\pi} I_i \sin^2 \theta_g \cdot A. \quad (2.20)$$

The *backscattering strength*, BS, is the ratio of the backscattered intensity by the incident intensity, for the case of Lambertian scattering is given by [Urlick, 1975; Gensane, 1989; de Moustier, 1993],

$$BS = 10 \log \frac{I_b}{I_i} = 10 \log \mu + 20 \log (\sin \theta_g) + 10 \log A, \quad (2.21)$$

where $\mu = 1/\pi$.

2.7.2. Jackson's Model

The Jackson's model was developed by Jackson et al. [1986a], and an extension and simplification to their work was performed by Mourad and Jackson [1989]. The main purpose of their work was the development of a model for bottom backscattering,

applicable to frequencies in the band 10 to 100 KHz. The model applies the composite roughness model [Kuo, 1964; McDaniel and Gorman, 1983] for small grazing angles up to 70 degrees, and the Kirchhoff approximation [Clay and Medwin, 1977] for steeper grazing angles.

The frequencies in this band, for which the model was developed, restricts the penetration of the acoustic wave into the sediments. In this case, considering an ideal sediment, the volume parameters of interest are: compressional wave speed and attenuation, sediment density and volume scattering strength. For grazing angles smaller than the critical angle (defined as the angle of incidence after which the refracted ray becomes horizontal), the penetration into a flat bottom can be neglected, as well as the volume scattering.

This model uses the interface roughness and the volume heterogeneity of sediments as the contributors to bottom scattering. The sediment volume scattering strength is treated as a free parameter, which is determined by fits to bottom backscattering data.

2.7.2.1. Model Implementation

The combination of the Kirchhoff approximation and composite roughness is used to compute the scattering at the rough surface; the Kirchhoff approximation is used for steep grazing angles, and the composite roughness is used for moderate grazing angles.

Figure 2.7 is the result of the application of Jackson's model for the characteristic

parameters of a very fine sand. It is important to stress that the application of this model as first stated by Jackson et al. [1986a], is difficult to implement and requires some simplifications (specially in the evaluation of the improper integrals).

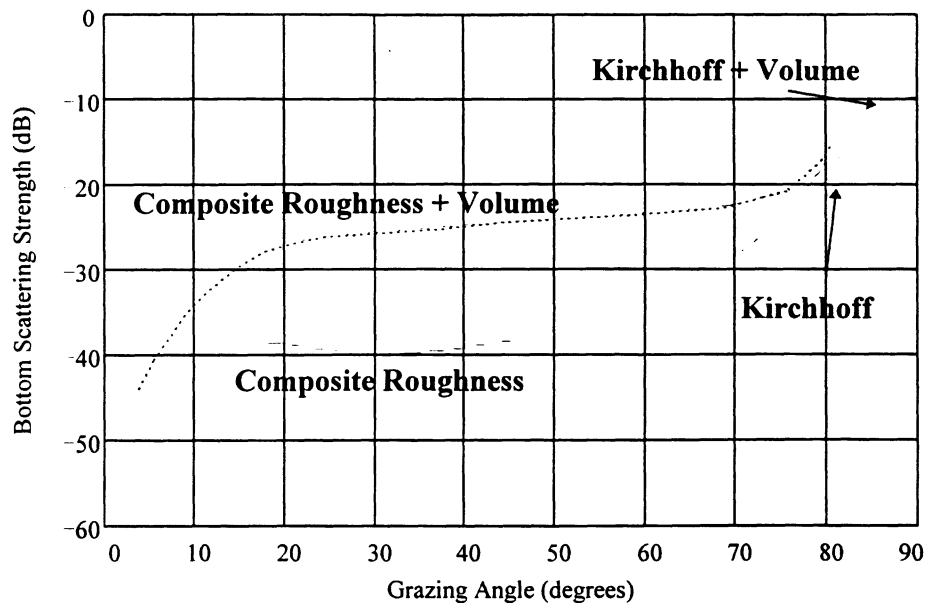


Figure 2.6. Computation of Jackson’s model for very fine sand (and acoustic frequency 95 KHz). Differentiation of composite roughness model and Kirchhoff’s approximation. For both models, the volume scattering was evaluated.

The simplified and extended model [Mourad and Jackson, 1989] took into account those difficulties and came up with a reasonable way to numerically evaluate the integrals of Kirchhoff’s approximation and of the composite roughness model.

Finally, Figure 2.7 presents the calculation of the backscatter for different types of sediments, whose parameters are defined in Table 2.1. This figure is useful to visualize the separation among sediments, and to conclude that the best separation occurs for incidence angles between 20 and 75 degrees.

To use Jackson's model for sediment classification it is necessary to invert the model and search for the best fit of the parameters to the backscatter sample amplitudes [Gott, 1995].

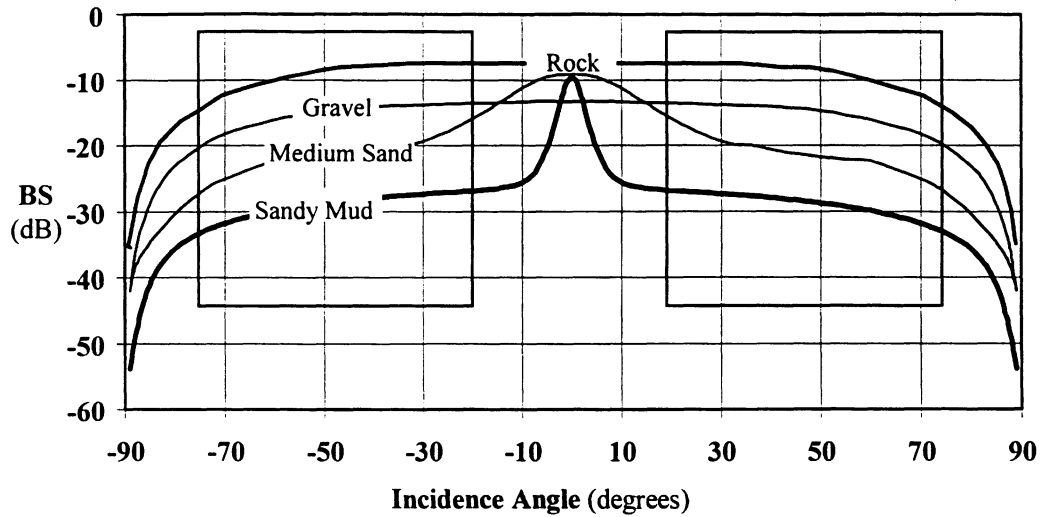


Figure 2.7. Generic curves, from Jackson's model, for different types of seafloor. Calculation performed for a frequency of 95 KHz.

For data cleaning purposes the classification is based on the "graphical comparison" of the observed backscatter amplitudes (after being filtered by the use of a moving average filter and corrected by removing the Lambertian dependence) with the theoretical backscatter response for three types of sediment (mud, sand, and rock).

2.8. Acoustic Image

Each line of the acoustic image corresponds to a slant range corrected backscatter

trace. This trace represents the variation of the backscatter strength along the athwartships profile in the seafloor, defined by the axis of the transmitted beam pattern. Each line is spatially referenced by the projection of the axis of the transmitted beam pattern on the seafloor. However, the coverage of every single ping includes the for-aft width of the beam pattern for each beam footprint. To relate the spatial coverage of one ping to the next, the information of ship's heading, velocity, as well as the attitude of the vessel at each of the transmits, is used [Hughes Clarke, 1995e].

The areas of overlapping are, in the case of multibeam bathymetric surveys, large, and the backscatter strength will have different values, depending on the grazing angle. Therefore, there are some ways to deal with the redundant information in the areas of overlapping, by a definition of priorities according to the beam pointing angle, by overwriting the earlier values, shine through by overwriting the lower backscatter values [Universal Systems Ltd., 1994b].

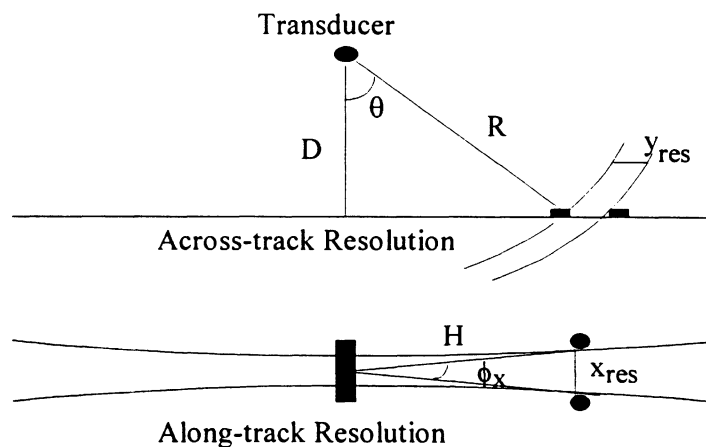


Figure 2.8. Side scan trace, across- and along-track resolution.

The total resolution of the acoustic image is restricted to the resolution of the MBES imagery geometry in the along- and across-track directions. The resolution in the along-track direction depends on the fore-aft beam width, ϕ_x . The resolution in the across-track direction depends on the larger of either time-of-flight sampling resolution Δt (equivalent to the range sampling resolution, Δr), or the pulse length, τ .

The resolution of targets on the backscatter samples, based on Figure 2.8, are equal to x_{res} and y_{res} , respectively for the along- and across-track directions;

$$x_{res} = \frac{d}{\cos\theta} \tan\phi_x \quad (2.22)$$

and

$$y_{res} = \max\left(\frac{\Delta r}{2 \cdot \sin\theta}, \frac{c\tau}{\sin\theta}\right). \quad (2.23)$$

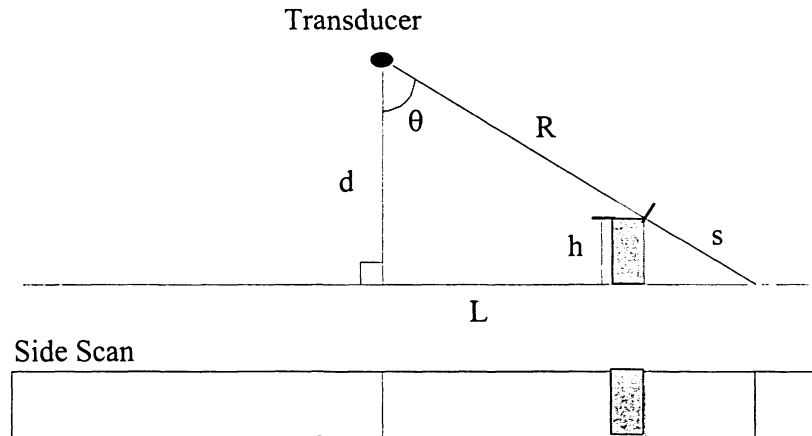


Figure 2.9. Side scan trace, depth resolution.

In addition to the resolution in the horizontal plane, it is possible to define the target resolution or depth anomaly resolution in terms of the obstruction created to the adjacent area of the seafloor. In this case, we are interested in the detection of targets by their shadows, i.e., by the pronounced decrease of the backscatter strength.

Targets are well defined if their dimension is greater than the along-track coverage by the beam width ϕ_r . In the case of a spike laying above a flat seafloor (Figure 2.9), given a particular range sampling resolution, target height, and incidence angle (Δr , h , and θ), the number of instantaneous backscatter samples which do not contain seafloor returns can be obtained by,

$$\xi = \frac{h}{\Delta r \cos \theta}. \quad (2.24)$$

2.9. Simrad EM 1000 Data

The Simrad EM 1000 operates on a frequency of 95 KHz, and has three modes of operation: shallow (water depths from 3 to 200 metres), medium (water depths from 200 to 600 metres) and deep water (water depths from 600 to 1000 metres). The data used for this study was acquired in shallow mode. This mode has the following characteristics:

- 150 degree coverage sector;
- all beams roll stabilized;
- transmission pulse length 0.2 ms;

- 2.5 degree beam spacing;
- every other ping all beams are shifted 1.25 degrees;
- sampling interval, within each beam, is approximately 15 cm range (equivalent to 0.2 ms).

The Simrad EM 1000 raw backscatter intensity are corrected for transmission loss (spherical spreading and attenuation), source power variations, predicted beam patterns, and ensonified areas.

The receivers of the *Simrad* EM 1000 have a limited dynamic range. Therefore, to avoid overload or to have the returned signal masked with noise, a time varying gain (TVG) is applied during the ping reception. As mentioned in Chapter 2 the backscatter strength will drop off with range. Running the TVG provides a flattened or equalized beam sample amplitudes. This is important for the bottom detection and for the display of the acoustical image, where one is principally interested in reflectivity contrasts [Hammerstad, 1994].

From the literature research conducted for one of the earlier Simrad MBES, EM12 [Hammerstad, 1994], it was concluded that for incidence angles larger than approximately 25° degrees, a good approximation was to assume that a uniform flat bottom is characterized by a mean backscatter coefficient S_0 , and that the angular variation follows Lambert's law (see Section 2.7.1),

$$S_B = S_0 + 20 \log(\cos\theta). \quad (2.25)$$

No conclusions were drawn for smaller incidence angles. A reasonably smooth change of

gain is required by the system electronics and the following scheme was implemented in the Simrad MBES from the EM series [Hammerstad, 1994]:

- a) Based on previous pings, the range to normal incidence, R_I , is computed and the mean backscatter coefficients for normal and oblique incidence, S_N and S_θ , estimated;
- b) The gain up to a range of $0.99R_I$ is applied according to the normal incidence assumptions, using the estimated coefficient S_N ;
- c) The gain from a range of $1.02R_I$ is applied according to the oblique incidence assumptions, using the estimated coefficient S_θ with Lambert's law dependence;
- d) The gain in the ranges from $0.99R_I$ to $1.02R_I$ changes linearly with time based on the estimated value S_N and then shifted by $S_N - S_\theta$.

Initially, nominal values for the source level and receiver sensitivity are used. After beamforming, the backscatter sample amplitudes are corrected for both the processing gain and beam pointing angle variations in source level and receiver sensitivity. Then, the estimated backscattering coefficient at oblique incidence, S_θ , is subtracted from the sample amplitudes. Finally, an additional correction is applied to compensate for a presumed Lambertian response (used to modify the backscatter as a function of the incidence angle). This is a valid assumption as long as:

- the incidence angle is greater than 10 degrees,
- the seafloor is flat (leveled or sloped),

- the R_1 value used is correct.

These are corrected sonar image amplitudes and then assumed to be measurements of the seafloor backscatter coefficients S_B [Hammerstad, 1994].

Gensane [1989] concluded that backscattering coefficients near nadir (angles of incidence smaller than 25 degrees) deviate significantly from Lambert's law. Because of that, a revised TVG algorithm has been applied to near normal incidence angles for *Simrad* EM 1000 data acquired later than 1994 [Hammerstad, 1994].

The corrections that are necessary to be applied in the post-processing phase are [Hughes Clarke et al., 1994]:

- local slope (determined from the sounding data);
- local variation in the sea water attenuation coefficient;
- aspherical spreading;
- difference between the apparent grazing angle and the one due to refraction;
- small variations between the estimated and transmit beam pattern;
- removal of the Lambertian correction.

The information from low incidence angles is not useful for seafloor classification. The examples of the backscatter traces used to assess the generic type of sediment are from relatively flat areas. Local slope corrections are assumed to have a negligible effect.

Chapter 3

ERRORS IN THE BATHYMETRIC DATA SET

This chapter describes the uncertainty on depth measurements, causes and effects of errors in the bathymetric data set, and the different ways of handling these errors. A seafloor model is presented as a reference surface for automatic data cleaning.

When using single beam echosounders (SBES), the minimum depth for every measurement is assumed to correspond to the first signal arrival from the seafloor. Mid water returns are, in general, not hard to identify from the continuity of the trace in the echogram. However, digital SBES may have problems with spikes which fall within the depth window.

MBES have a more complex depth measurement process because: the beams are oblique, there are many ancillary sensors (each of which can contribute errors), and the data volume requires efficient automated processing.

3.1. Definitions

The errors in the multibeam bathymetric data set can be divided into three categories: large errors (blunders), systematic errors, and stochastic deviations.

Blunder is the terminology used to define errors made by a machine, caused by defective mechanical or electronic device [NOAA, 1986]. *Outlier* is defined as a value of randomly varying quantity that lies outside certain arbitrary limits. Any value that is larger in absolute value than expected, it is suspected to be a blunder. Hence, the set of outliers is the union of the set of blunders and the set of hazards or minimum depths (e.g. wrecks and boulders).

Systematic errors are mainly the result of the offsets (fixed errors) or biases (errors that vary under different conditions) in sensing movements of the ship, misalignment of the transducer and other sensor mounting angles, and wrong sound speed profile. These errors can be corrected if the shape and size of the systematic error can be determined. Some of the errors in this category are, to some extent, unpredictable. This depends on the data available to check the offsets and biases determined during the calibration [Herlihy et al., 1989; Simrad Norge AS, 1995; Godin, 1996], the redundancy of the data collected in different directions or speeds, as well as check lines.

After removing the blunders and systematic errors from the bathymetric data set, *stochastic deviations* will remain in the data set, usually modeled as “white noise”. White noise has a normal distribution and can be analyzed using statistical techniques.

For hydrographic purposes, the hydrographer is interested in mapping the true seafloor bathymetry and the final product must be as free from blunders as possible. Nevertheless, real features are vital information that need to be preserved for integration in the nautical chart.

3.2. Uncertainty on Depth Measurement

The analysis of depth accuracy used herein is based on the studies conducted by Pøhner [1993]; Hammerstad [1995]; Hare and Godin [1996]. The main objective is to define the effective area in the swath where the measurements meet the accuracy standards of the International Hydrographic Organization. The current “*IHO Standards for Hydrographic Surveys*” (publication S-44, third edition) does not specifically address multibeam uncertainty issues [IHO, 1987], and is currently being revised (draft publication S-44, fourth edition) [IHO, 1996]. For the time being and to author’s knowledge there is no guarantee of the approval of the fourth edition of S-44. In this report the depth measurement accuracy is defined by 1% of the water depth with 95% confidence level.

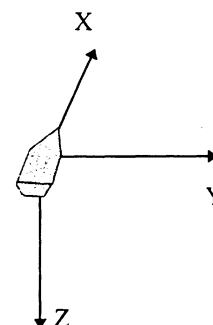


Figure 3.1. Right-hand coordinate system.

The coordinate system is a right-hand system, with the X , Y and Z axes positive respectively in the forward, starboard and downward directions (Figure 3.1). Every sounding can be represented by a vector with coordinates $[x \ y \ z]^T$ relative to the transducer.

The depth measurement error is a function of several factors, such as:

- multibeam measurement error (ϵ_{sys});
- roll measurement error (ϵ_r);
- pitch measurement error (ϵ_p);
- heave measurement error (ϵ_h);
- relative sound velocity profile measurement error (ϵ_c);

The equation of the error of the depth measurement can be presented by,

$$\Delta Z = \epsilon_{\text{sys}} + \epsilon_c Z + \epsilon_p x - \epsilon_r y + \epsilon_h \quad (3.1)$$

considering an incidence angle θ referred to the vertical, one can express x as $z \cdot \tan(\theta_x)$ and y as $z \cdot \tan(\theta_y)$ (the subscript on θ being the plane where the angle is measured, x for the XZ plane and y for the YZ) by substitution of these values in Equation 3.1 and dividing both terms by the mean depth z , we obtain the relative depth measurement error,

$$\epsilon_z = \frac{\epsilon_{\text{sys}}}{z} + \epsilon_c + \epsilon_p \cdot \tan(\theta_x) - \epsilon_r \cdot \tan(\theta_y) + \frac{\epsilon_h}{z} . \quad (3.2)$$

The system errors are dependent on the MBES characteristics and the algorithms used in the bottom detection. The following equations have been developed for the Simrad EM 1000 MBES [Hammerstad, 1995]. The system measurement errors are caused by the uncertainty in the range and angle measurement.

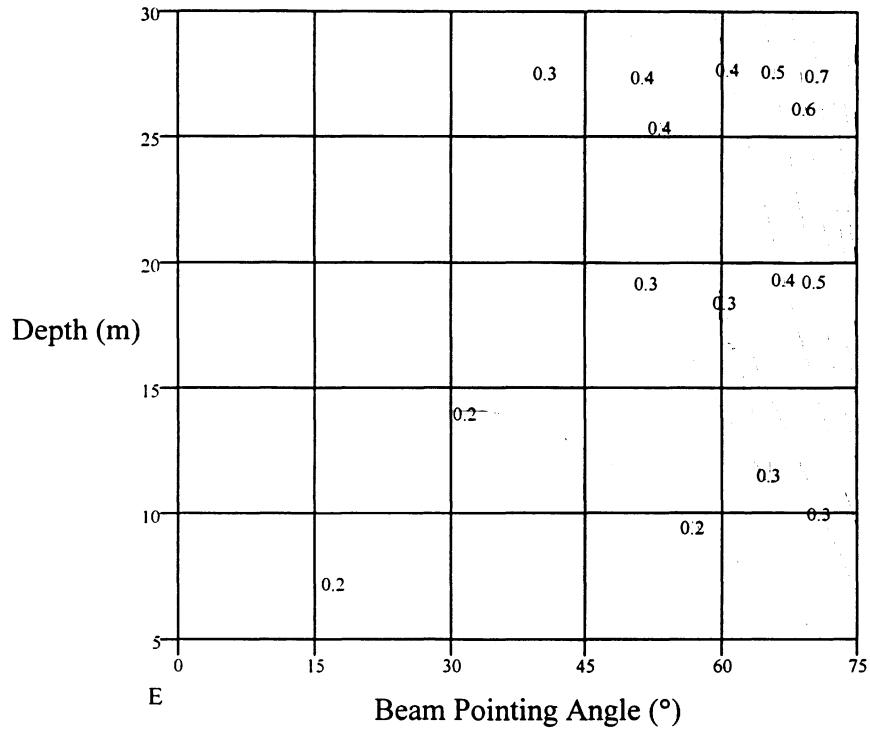


Figure 3.2. Total depth measurement uncertainty, in metres (simplified model [Hammerstad, 1994]), for the Simrad EM 1000 at 95% confidence level. Calculation for roll and pitch error 0.1° and relative sound velocity error 1 m/s.

The range measurement error is dependent on the range sampling resolution Δr_s , pulse length τ , and sound speed c ,

$$\delta R_{\text{sys}} = \sqrt{\left(\frac{\Delta r_s}{2}\right)^2 + \left(\frac{c \cdot \tau}{4}\right)^2} \quad (3.3)$$

The uncertainty in the angle measurement is determined by the method used in the bottom detection. For amplitude detection (in the EM 1000, this is applied when the number of phase samples is less than 12, usual for the inner beams, for shallow waters, and also for sloping surfaces toward the transducer), the error in the measurement of the

beam angle, is given by,

$$\delta\phi_{\text{sys}}(\text{amplitude}) = \frac{\phi_y}{12}, \quad (3.4)$$

where ϕ_y is the athwartships beam width.

For phase detection (applied when the number of phase samples is greater than 12), the uncertainty is given by

$$\delta\phi_{\text{sys}}(\text{phase}) = \frac{0.2 \cdot \phi_y}{\sqrt{n_p}}, \quad (3.5)$$

where the number of phase samples is calculated by,

$$n_p = \frac{\phi_y \cdot d \cdot \tan(\theta)}{\Delta r_p \cdot \cos(\theta)}, \quad (3.6)$$

Δr_p being the range sampling resolution for phase.

Figures 3.1 and 3.2 depict the uncertainty of the total depth measurement.

The *rms* of the absolute system depth measurement error is computed using the equation,

$$\varepsilon_{\text{sys}} = \sqrt{(\delta R_{\text{sys}} \cdot \cos(\theta))^2 + (\delta\phi_{\text{sys}} \cdot d \cdot \tan(\theta))^2}. \quad (3.7)$$

The relative sound velocity profile error is [Pöhner, 1993],

$$\varepsilon_c = \frac{\Delta c}{c_0} (1 - 2 \cdot \tan^2(\theta) + 2 \cdot \tan(\zeta) \cdot \tan(\theta)). \quad (3.8)$$

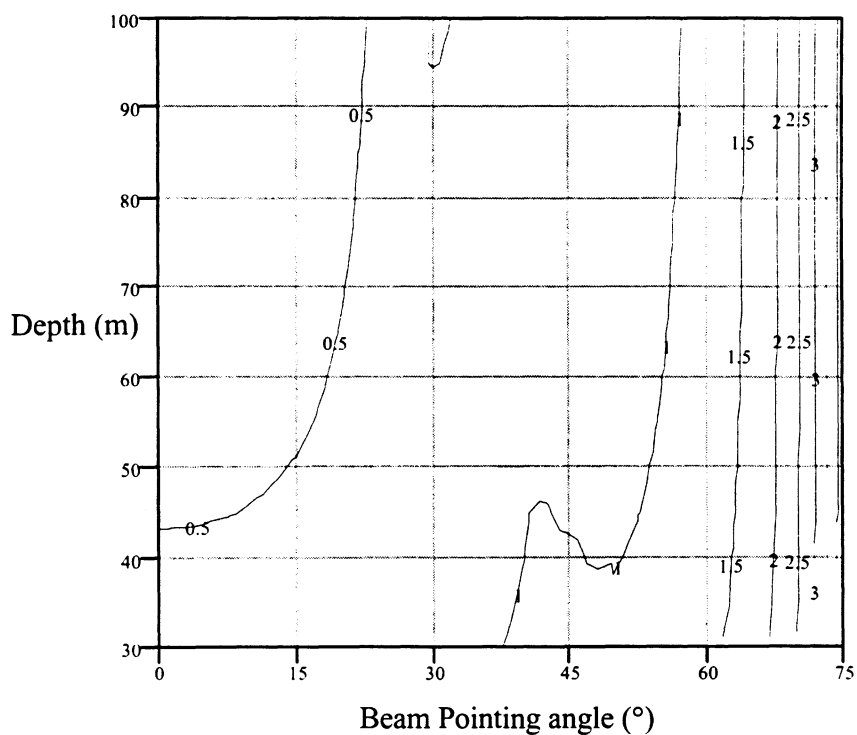


Figure 3.3. Total depth measurement uncertainty, in depth percentage (simplified model [Hammerstad, 1994]), for the Simrad EM 1000 at 95% confidence level. Calculation for roll and pitch error 0.1° and relative sound velocity error 1 m/s.

3.3. Seafloor Surface Model

Multibeam data are three-dimensional spatial points on a surface given by $z(x_i, y_i)$, for $i=1, 2, \dots, n$. This points are irregularly distributed over a two-dimensional region. The multibeam data set can be represented by $\{z(x, y) \text{ with } (x, y) \in \mathbf{R}^2\}$, where \mathbf{R}^2 is the domain of the horizontal positioning (subset of the Euclidean space), usually an irregular

but continuous surface.

An estimated surface $\mu(x, y)$ can be derived in multiple manners. The estimated surface can also be called the topographic trend or mean surface, where each sounding can be represented by,

$$z(x_i, y_i) = \mu(x_i, y_i) + \varepsilon(x_i, y_i), \quad (3.9)$$

where ε is the departure of the sounding under consideration, from the estimated surface.

To clean the blunders and systematic errors automatically, it is necessary to establish an estimated $\mu(x, y)$, which approximates the seafloor, i.e., the seafloor surface model. In this study, the seafloor surface model is defined by a mean surface, given by a weighted moving average surface [Universal Systems Ltd., 1994a] or by patches of least square regression planes [Simrad Norge AS, 1995].

As the local mean surface is only a useful approximation for particular areas, *a priori* data reconnaissance is required, which can be easily done by the use of visualization tools (surface contours or DTMs). Where the seafloor is homogeneous (sinusoidal features, steady slope, or flat), one can assume that the model is a good enough approximation of the seafloor surface. Areas that, by their nature, are not regular surfaces (e.g. wrecks, boulders, and irregular bedrock), should not be approximated by a mean seafloor surface model. The backscatter, the mean surface or the standard deviation surface provide detail about the regularity of the seafloor (high backscatter or variations in the backscatter and high standard deviation are, in general, related to irregular areas). The analysis and cleaning of the data of irregular areas should be performed interactively.

The detail achieved of the seafloor bathymetry in a multibeam survey is a function of several parameters, such as depth, dimension of the ensonified area, beam pointing angle, and beam spacing.

In the same manner as the resolution defined in the previous chapter. Because of the fore-aft beam width and in the matter that the bottom detection is performed to calculate the slant range, it is not possible to resolve topographically a bathymetric feature whose along- and across-track dimensions are smaller than the beam ensonification footprint.

The total depth measurement uncertainty from the MBES, ϵ_z (associated with the confidence level specified for the depth measurement) contributes to a spread of the depth measurements. The example from Figure 3.4 and 3.5 shows that in addition to ϵ_z , it is necessary to add a value related to the roughness of the seafloor surface, $\epsilon_{\text{roughness}}$, for the equivalent of the cell dimension.

Surface roughness can be defined as the root mean square (rms) of the height deviations from the seafloor surface model.

The departure of the sounding in consideration from the seafloor surface model, ϵ , is given by [Ringelberg, 1995],

$$\epsilon = \sqrt{\epsilon_z^2 + \epsilon_{\text{roughness}}^2 + \epsilon_{\text{noise}}^2}, \quad (3.10)$$

where ϵ_{noise} , corresponds to the stochastic variations, resulting from the effect of small-scale features on the seafloor and variation in the properties of the water column.

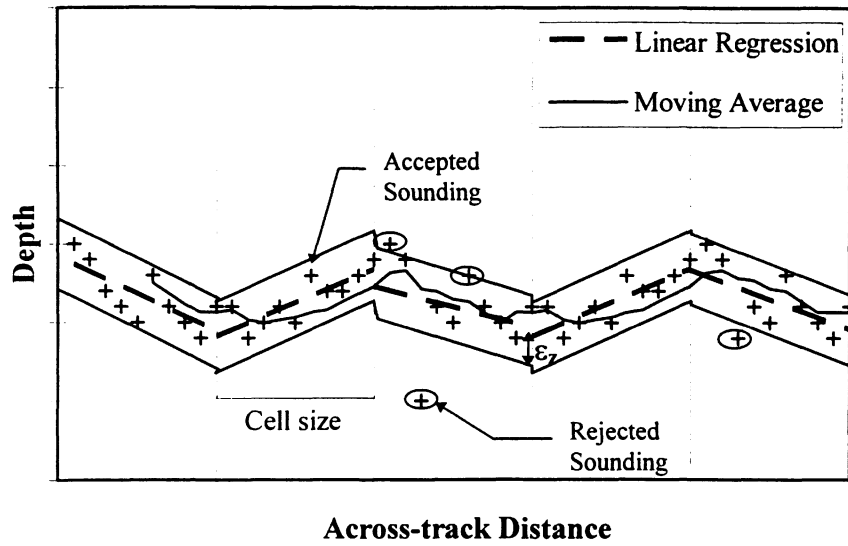


Figure 3.4. Two-dimensional profile, assuming a partitioning into cells, where a regression line is fitted to the data. The ϵ_z represents the uncertainty of the measurement for the MBES, region inside which the soundings are accepted.

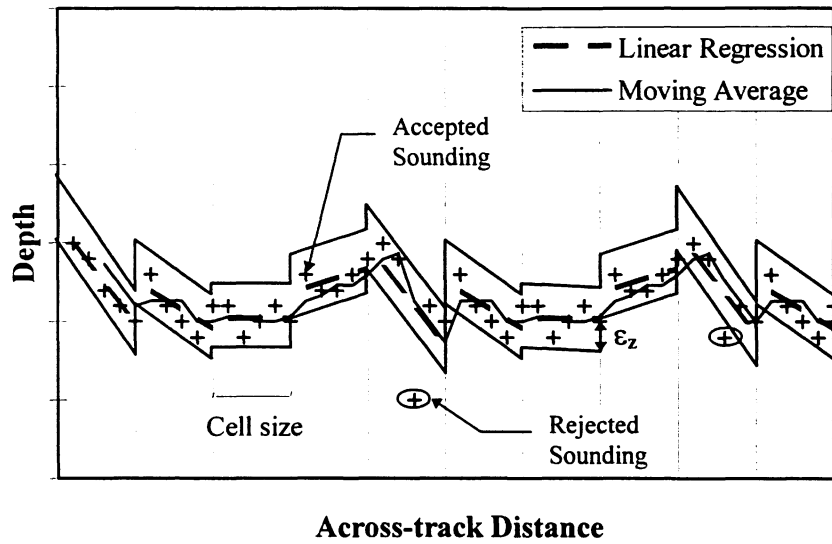


Figure 3.5. Two-dimensional profile, assuming smaller cells, where a regression line is fitted to each cell. The ϵ_z represents the uncertainty of the measurement for the MBES, region inside which the soundings are accepted. These variations are unwanted effects that, in theory, should be removed.

However, because there is no easy way to estimate ϵ_{noise} , its effect must usually be ignored. Accordingly, the region of acceptance for the soundings, should be simplified to,

$$\epsilon = \sqrt{\epsilon_z^2 + \epsilon_{\text{roughness}}^2} . \quad (3.11)$$

The spectrum of seafloor roughness (discussed in Section 2.6) is “filtered” by the stochastic variations ϵ_{noise} , by the footprint size, and by the seafloor surface model cell size.

Considering the relationship between roughness and footprint size: small-scale features act as scatterers (features much smaller than the acoustic footprint size), intermediate features act as local slopes (features of the same order of magnitude as the acoustic footprint size), and topographic features (features greater than the acoustic footprint size) [Berkson and Matthews, 1984]. Local slopes and topographic features may contribute to $\epsilon_{\text{roughness}}$, depending when whether they are smaller or larger than the cell size.

3.4. Causes for the Occurrence of Blunders

Multibeam echosounder measurements are sensitive to several environmental factors, such as, the existence of shoals of fish or kelp in the water column, abnormal sound velocity profiles (e.g. abnormal temperature or salinity), and multiple reflections

or multiple paths, responsible for blunders in the measurements. Another set of factors, responsible for the existence of blunders, are due to internal problems of the system, such as, bottom detection algorithms, outer beam geometry, and equipment malfunction.

The external beams are more sensitive than the inner beams to variations in the sound velocity profile, and systematic errors are more likely to occur on the outer beams. Sometimes, these errors can mask the blunders or the real features on the seafloor, therefore, if one has reciprocal and check lines one would be able to check the calibration values, obtained during the calibration of the MBES for the vessel configuration. Remaining systematic errors, with known causes and known variation rules must be corrected. Systematic errors due to the variation of the sound velocity profile should be identified and the beams which the refraction effect is greater than the accuracy of the measurements, defined for the survey, should be removed before one can look for blunders.

3.5. Effect of Blunders in the Bathymetric Data Set

The bathymetric data set is used for the compilation of nautical charts, which should provide accurate information about bathymetry to the navigator, unrecognized blunders will degrade the accuracy.

Blunders deeper than the neighbors are not a danger to navigation, and they can be removed from the data, even using a subjective criterion. However, shallower

blunders cannot be treated the same way. The methodology used in this case, should guarantee, to the greatest extent possible, that blunders must be removed and real features preserved.

3.6. Blunder Handling in the Bathymetric Data Set

The task of recognizing blunders in the bathymetric data set it is not straightforward. Several approaches have been developed since the early 1980's [Guenther and Green 1982; Ware et al., 1991b; Simrad Norge AS, 1995; Eeg, 1995; Du, 1995]. The MBES systems have also been improving, as well as their bottom detection algorithms. The occurrence of blunders have been decreasing and some error sources have been detected and corrected (e.g. omega artifact, detected on *SeaBeam* caused by the side lobes reported by de Moustier and Kleinrock [1986]).

Almost all the multibeam echosounder systems provide a post-processing package with built in tools for data cleaning. Several techniques are used to deal with blunders, including; statistics over the data set of soundings; comparison of neighborhood profiles or soundings; data visualization of depth contours; color coded bathymetry; and digital terrain models.

The next chapter discusses the data cleaning methods, algorithms, and procedures.

Chapter 4

DATA CLEANING METHODS AND PROCEDURES

This chapter reviews some of the methods developed for multibeam data cleaning. A summary is presented highlighting some of the features for each method. Finally, procedures for two methods, HDCS (Hydrographic Data Cleaning System) and BINSTAT (Bin Statistics), are described in an attempt to standardize the use of these two software packages.

The data acquired by multibeam echosounder systems needs to be processed and validated.

In the post-processing phase, the “vessel coordinates” are converted or transformed into “earth fixed coordinates”. This process requires all ancillary sensors and measurements [Instituto Hidrográfico, 1994; Hughes Clarke, 1995a] be merged with the depths and “vessel coordinates” referenced depths. Finally, for the process to be completed, the huge amount of data must be analyzed to clean out blunders and systematic errors. A major concern is the confidence that the hydrographer is able to put in automatic methods used for this purpose in order to obtain the *basic data product* (Figure 4.1). From this, many different *presentation products* can be derived, such as: bathymetric contours, plots of soundings, acoustical images, Digital Terrain Models (DTMs).

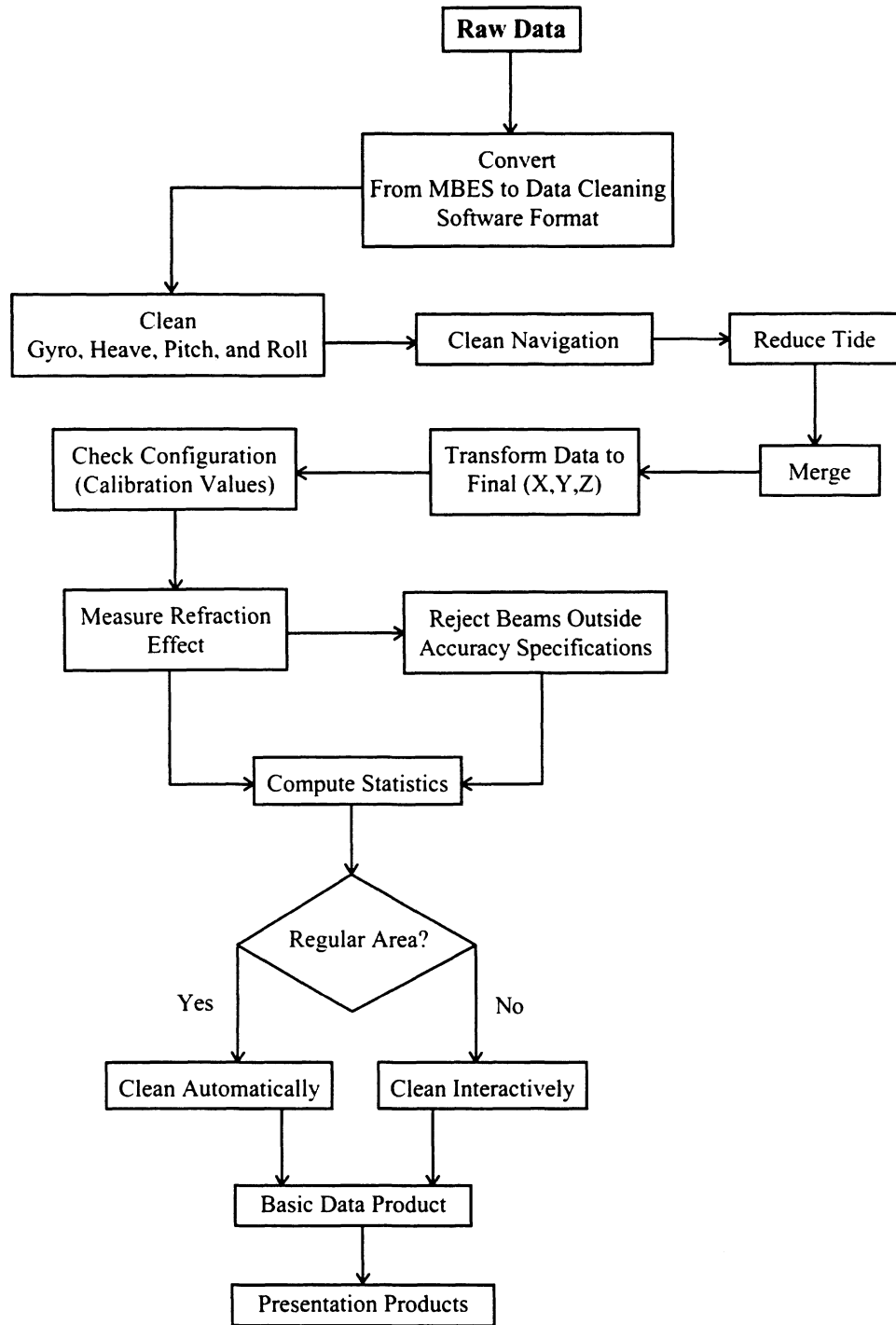


Figure 4.1. Processing sequence.

4.1. Data Cleaning Requirements

The requirements for data cleaning depend on the purpose of the basic data product. In this study, the basic data product is a hydrographic data set. The objective of the hydrographic data set is to have information about the seafloor bathymetry and to preserve information about conspicuous features (wrecks and boulders) which can cause danger to navigation. To achieve this goal, data cleaning must reject the soundings corresponding to:

- gross errors (blunders);
- systematic errors;

and to assess the noise level.

Herein swath mode is used to refer to a single swath and subset mode to refer to an area covered by several lines.

The data cleaning tools need to:

- preserve the complete raw data set (set flags for rejection rather than deleting data);
- be flexible in allowing the overrule of previous rejections;
- be efficient enough to process multibeam data in about as much time as it took to acquire it;
- be of easy implementation and comprehension.

To achieve the design standards, three methods can be followed:

- powerful visualization tools;
- automatic capabilities for cleaning the data;
- interactive capabilities for cleaning the data.

4.2. Data Cleaning Tools Based on Redundancy

All existing data cleaning methods are based on depth data redundancy. Redundancy can be achieved by having plain overlap or overlapping beam footprints within one swath; by running the vessel slowly enough, or the MBES ping rate is fast enough, so that ping-to-ping swaths overlap; and/or by running cross-check survey lines perpendicular to the main survey lines.

Before sounding data points can be analyzed and cleaned, it is necessary to check the ancillary data from each sensor (roll, pitch, heave, and gyro), to detect spikes on these measurements. These erroneous measurements should be rejected and interpolated with the adjacent measurements. Only afterward can the depth data set be clean from gross and systematic errors.

The soundings can be analyzed swath by swath (swath mode) or by areas covered by several swaths (subset mode). The sources of information available to aid the hydrographer in the data cleaning task are:

Soundings in the swath mode

- comparison with soundings corresponding to bottom detection for consecutive pings;

- comparison with soundings corresponding to bottom detection for adjacent beams in the same ping;

Soundings in the subset mode

- comparison with soundings corresponding to the neighboring bottom detections (same or different swaths);

Backscatter associated with the soundings

- assessment of backscatter intensity inside the footprint;
- comparison of mean backscatter strength for the sounding of interest, with respect to that of the neighboring footprints;
- acoustic image of the seabed for the area of interest.

4.3. Statistical Methods

The next sections summarize the following data cleaning methods: Combined Offline Program (COP), Hydrographic Data Cleaning System (HDCS), Binning Statistics (BINSTAT), Royal Danish Administration of Navigation and Hydrography (RDANH) Algorithm, and Automatic Detection Algorithm.

The present tools, used in data cleaning, can be divided into two classes, interactive and automatic tools. The automatic methods are based on statistical tests over the soundings. The interactive tools consist of views along- or across-track profiles,

raster view of soundings using color coding by depths, contour plots, standard deviation surfaces [Universal Systems Ltd., 1994a] and correlation plots [Simrad Norge AS, 1995].

4.3.1. Combined Offline Program

The Combined Offline Program (COP) is a computer program that has been used for processing both Bathymetric Swath Survey System (BSSS) and *SeaBeam* data, by the U.S. National Ocean Service since 1982 [Guenther and Green, 1982; Grim, 1988; Herlihy et al., 1992].

The purpose of this program is to select soundings in the *plottable unit area* (PUA), which corresponds, approximately, to the smallest area on the final chart required to plot one sounding and to verify if the value is reasonable with reference to the neighbors in the PUA. The verification consists of filtering erroneous soundings in the collected data greater than one percent of the water depth.

In the COP algorithm, each sounding, z_i , is compared with the nearest neighbors $\{z_j, j = 1, 2, \dots, n\}$, i.e., with the soundings in the PUA. The PUA is a rectangular area in the swath mode, with n_a soundings along-track and n_c soundings in the across-track direction, the total number of soundings $n_a n_c$, for the same multibeam system depends on the speed of the vessel and on the water depth. If the number of z_j 's within 30 seconds from z_i is less than six, z_i will not be considered as a candidate for the plottable unit area. If the number of z_j 's is greater than six, the mean μ_i and the standard deviation σ_i are estimated from the nearest neighbors $\{z_j, j = 1, 2, \dots, n\}$,

$$\mu_i = \frac{\sum_{j=1}^n w_j z_j}{\sum_{j=1}^n w_j} \quad (4.1)$$

$$w_j = \begin{cases} 2, & \text{if } z_j \text{ and } z_i \text{ belong to the same beam} \\ 1, & \text{otherwise} \end{cases} \quad (4.2)$$

The estimation of σ_i is not given in Herlihy et al. [1992]. The z_j 's that satisfy the condition

$$|z_j - \mu_i| > \alpha \sigma_i, \text{ for } \alpha = 2,$$

are rejected and removed from the PUA, and are called wild points. This procedure is repeated until there are no wild points and the conditions for the nearest neighbors are still satisfied. At this point, z_i is tested against,

$$|z_i - \mu_i| > \beta + \gamma \mu_i, \quad \beta=10.0 \text{ m and } \gamma=1.5\%.$$

If this condition is satisfied, z_i will be flagged and rejected as a candidate.

It is important to stress that this method was developed for deep water MBES, the constant β is equal to 10 metres, however, if one wants to use the system for shallower depths β should be reduced.

4.3.2. Hydrographic Data Cleaning System

The statistical data cleaning module in HIPS (Hydrographic Information Processing System software package from Universal Systems Ltd [1994a]) is called HDCS.

The HDCS uses a *weighted moving average* algorithm. The mean value given by the Equation (4.3) is an estimation of the depth of a particular sample. The value of the mean for a sounding at position p is given by,

$$\mu_p = \frac{\sum_{i=1}^n z_i w_{ip}}{\sum_{i=1}^n w_{ip}}, \quad (4.3)$$

where: μ_p = mean depth at pixel p ;

z_i = depth at i^{th} position;

w_{ip} = weight of the i^{th} sounding (its influence on the mean at pixel p).

For HDCS, the weight value is inversely proportional to the horizontal distance d_{ip} from the depth at position i to pixel p , and is given by the following equation,

$$w_{ip} = \begin{cases} 1 - \frac{d_{ip}}{r} & \text{for } d_{ip} < r \\ 0 & \text{otherwise} \end{cases} \quad (4.4)$$

where r is the radius of the area of influence (see Section 4.5), used to calculate the

mean.

This weight algorithm has the advantage of restricting the area of influence of one sounding to the area defined by the radius, r .

Another parameter calculated in the HDCS is the weighted vertical standard deviation σ_p . For the point p , this is given by,

$$\sigma_p = \sqrt{\frac{\sum_{i=1}^n w_{ip} z_i^2}{\sum_{i=1}^n w_{ip}} - \mu_p^2} \quad (4.5)$$

This equation computes a continuously estimated surface of the standard deviation, derived from the line data points. A point that is anomalous with respect to its neighbors (deeper or shallower), will significantly contribute to the increase of the local variance.

A depth classification algorithm, was developed to restrict and focus the attention of the hydrographer, on the shallow soundings that need to be interactively examined [Wells, 1990; Ware et al., 1991a]. The algorithm classifies depths according to their departure from the mean using Equation 4.6,

$$\text{level}_{ji} = \mu_i + C_3 \sigma_i - j(C_1 \sigma_i + C_2) \quad j = [0,7]. \quad (4.6)$$

The classification of a depth, z_i , is done using the condition,

$$\text{if } (z_i < \text{level}_{ji}) \text{ then flag } z_i \text{ at level } j. \quad (4.7)$$

The constants C_1 , C_2 , and C_3 are used to approximate the seafloor by a base line

given by $\mu_i - C_3\sigma_i$, where C_1 and C_2 define a threshold above the baseline. The first parameter is a constant and the second, is proportional to the standard deviation. These values have to be calculated for each multibeam system based on the uncertainty of the depth measurement, and based on the roughness characteristics of the seafloor. [Ware et al., 1991a].

The roughness of the seafloor is a scale dependent parameter. In this method, increasing the sampling density of soundings and reducing the radius, r , of the weighted area, can be used to separate the roughness signal from the real seafloor from the noise.

After the above considerations, it is possible to state that the algorithm will produce a low standard deviation only in regions where both a smooth seafloor and a low noise exist.

4.3.3. Binning Statistics

The statistical data cleaning module in Neptune (software package for processing MBES multibeam data [Simrad Norge AS, 1995]) is called “BINSTAT”. This module operates on blocks of data, which are assigned to a user defined grid, creating geographical cells.

The depths that fall into the same cell are gathered into a single bin. The statistical treatment is performed for each bin with the calculation of a flat but tiltable plane, using the *least squares method*. The statistic values for each cell are:

- minimum, maximum and mean depth;

- standard deviation for each cell relative to the fitted plane;
- noise (ratio of the standard deviation by the mean depth); and
- residuals (differences between each depth and the fitted plane).

As noted above, the algorithm used in this package is based on fitting a plane to all depths within a given bin cell, using the least squares method [Simrad Norge AS, 1995].

Considering the equation of the plane,

$$z(x,y) = \lambda_1 + \lambda_2 x + \lambda_3 y, \quad (4.8)$$

we can develop the least squares model, using the least squares regression [Vanicek, 1996], to calculate the coefficients λ_1 , λ_2 and λ_3 , that best fit the depths gathered in the same bin,

$$\hat{\underline{\lambda}} = \left(\underline{\Phi} \underline{P} \underline{\Phi}^T \right)^{-1} \cdot \underline{\Phi} \underline{P} \underline{\ell}, \quad (4.9)$$

$$\underline{\Phi}^T = \begin{bmatrix} 1 & x_1 & y_1 \\ 1 & x_2 & y_2 \\ \vdots & \vdots & \vdots \\ 1 & x_n & y_n \end{bmatrix}, \quad (4.10)$$

where $\underline{\Phi}$ is the Vandermonde matrix, $\underline{G} = \left(\underline{\Phi} \underline{P} \underline{\Phi}^T \right)$ is the Gram matrix, \underline{P} is the weight matrix that for this case is set equal to the identity matrix (all data points in each bin are equally weighted) and the observed values are

$$\underline{\ell}^T = [z_1 \quad z_2 \quad \cdots \quad z_n], \quad (4.11)$$

where x_i, y_i are the coordinates for the sounding z_i , for $i = 1, \dots, n$.

For each sounding z_i of one bin, the estimated residual, \hat{r}_i , is the minimum distance that the sounding z_i lies from the fitted plane. The standard deviation for the cell is obtained by,

$$\sigma = \sqrt{\frac{\sum_{i=1}^n (\hat{r}_i)^2}{n-3}}, \quad (4.12)$$

where the value in the denominator, $n-3$, corresponds to the number of degrees of freedom, since it is required three points to define the equation of the plane.

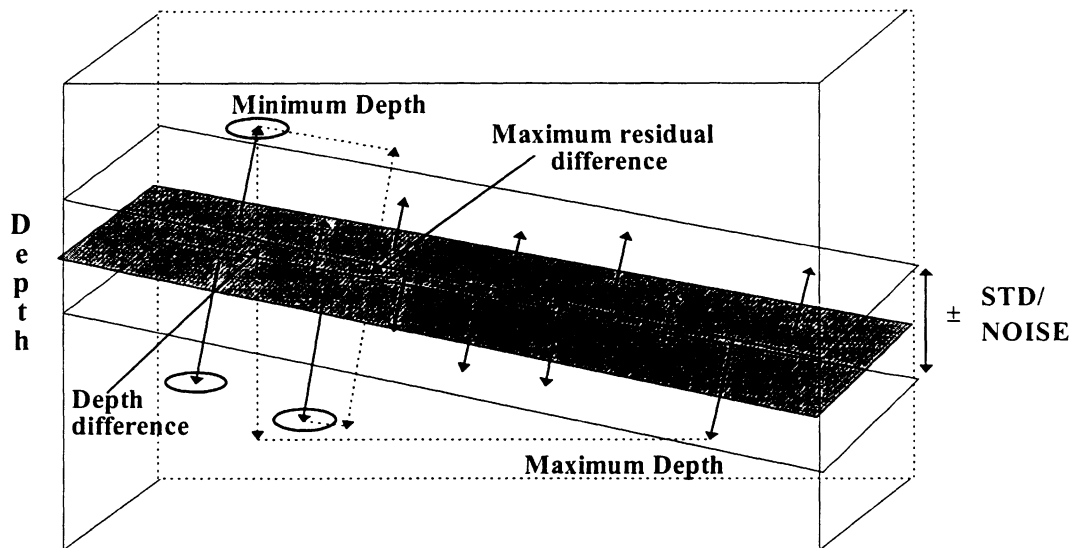


Figure 4.2. BINSTAT window. Example of a set of soundings gathered in the same bin. The arrows represent the difference from the soundings to the fitted plane (after Simrad Norge AS, [1995]).

The method of flagging the data is by the use of rules, which consist on setting some limit parameters [Simrad Norge AS, 1995]. For instance, the limit standard deviation can be set by a value α , and the confidence limits will be defined by,

$$\hat{z}_i - \alpha\sigma < z_i < \hat{z}_i + \alpha\sigma ; \quad (4.13)$$

the soundings z_i that lie outside the confidence region, will be flagged. Among other possibilities, one can define the limits for the residuals and for the noise.

4.3.4. Royal Danish Administration of Navigation and Hydrography Algorithm

This method is described by Eeg [1995], and is based on *least squares adjustments* with equal weights.

Considering a sample of observations, it is possible for each depth to define a set of neighbor depths. For example considering the depth z , the neighbors are z_i for $i = 1, \dots, n$.

The least squares estimate for the depth z , is given by the average depth for the neighborhood of z , including the value of the depth under consideration z (this inclusive mean depth, is given by \bar{z}),

$$\bar{z} = \frac{1}{n+1} \left(z + \sum_{i=1}^n z_i \right), \quad (4.14)$$

and the least squares fit of this model is given by the sum of the squares of the deviations from the mean (*SSD*),

$$SSD = (z - \bar{z})^2 + \sum_{i=1}^n (z_i - \bar{z})^2 . \quad (4.15)$$

Similar equations can be stated for the least squares estimate of z , but now excluding the value of the depth z under consideration [Eeg, 1995]:

$$\hat{z} = \frac{1}{n} \sum_{i=1}^n z_i , \quad (4.16)$$

and

$$ssd = \sum_{i=1}^n (z_i - \hat{z})^2 . \quad (4.17)$$

We represent the values of the new estimate by \hat{z} , the sum of the squares of the deviations from this estimate by ssd , and the sample variance (the average of the squares of the deviations about the sample mean) by s^2 :

$$s^2 = \frac{ssd}{n-1} = \frac{1}{n-1} \sum_{i=1}^n (z_i - \hat{z})^2 . \quad (4.18)$$

The assumption by Eeg [1995], is that “the variance should be of the same order of $|SSD-ssd|$ for the neighborhood of each depth in the swath”. Taking into consideration this assumption, it is possible to define the following quotient,

$$q(z) = \frac{(SSD - ssd)}{s^2} = \frac{(n+1)(z - \bar{z})^2}{\frac{n}{n-1} \sum_{i=1}^n (z_i - \hat{z})^2} \quad (4.19)$$

whose value increases greatly when z is an anomalous depth. The quotient $q(z)$ is used as

the indicator for the inspection of the problematic areas.

The quotient $q(z)$ is very sensitive to the considered neighborhood depths, and this behavior is given by the variance of the neighbor depths. In this sense, the spike detection algorithm requires that z_i 's are, actually, the surrounding depths and this is ensured by the use the Delaunay triangulation [McCullagh and Ross, 1980] to find the set of neighbors.

4.3.5. Automatic Detection Algorithm

One main difference of the method developed by Du [1995] with respect to other methods is its self-calibrating characteristics. Compared to HDCS and BINSTAT, where the user selects the parameters used as the criteria for flagging the blunders and the size of the cells for the statistics (which in the case of the BINSTAT is defined by the user and in the case of HDCS is a fixed cone 10 degree width), Du's method computes this values based on the characteristics of the data set. It uses an algorithm based on clustering by mode seeking technique and the Dixon discordance test [Du, 1995].

The method is developed in two phases:

In the first phase, the data is partitioned into horizontal cells. The cells, also called "working windows", have a fixed size of 10 pings by 10 beams [Du et al., 1995a].

For each working window, a histogram is computed to find gaps between the main mode of soundings and the mode of outliers. Figure 4.2 shows an example of these modes.

The outliers are flagged by the use of the following conditions:

$$L \geq \frac{Lm}{2}, \quad (4.20)$$

and

$$L + \frac{Lm}{2} > C, \quad (4.21)$$

where L is the length of the gap between the main mode of soundings and the mode of outliers, Lm is the span of the main mode, and C is a constant related to the standard deviation of the soundings in the working window.

In the second phase, each sounding under consideration, z_i , is compared with the nearest six soundings z_j (with $j = 1, \dots, 6$) from the same ping.

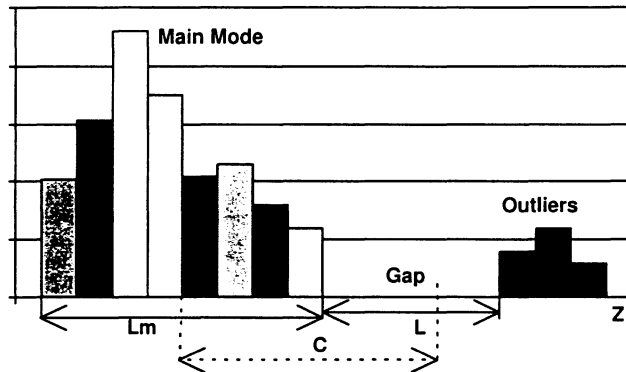


Figure 4.3. Clustering by mode seeking (after Du [1995a]).

In this phase, L is the distance between the soundings under consideration, either the shallowest or deepest of the neighboring soundings and Lm is the distance between the deepest and shallowest neighboring soundings.

The flagging criteria is now defined as $L \geq L_m$.

The idea behind Du's algorithm is to capture the experience of hydrographers skilled in interactive data cleaning. Du et al. [1995b] compared the result of this method and the one obtained by the subjective judgment of a human operator and they concluded that the present method matches the subjective selection 95 percent of the times, and the time required to process the same amount of data was reduced 30 times.

Table 4.1 summarizes the data cleaning methods, discussed in this chapter.

4.4. Interactive Methods

The statistical methods (automatic methods) have objective data cleaning algorithms based on statistical comparisons with neighbor soundings. The interactive methods are visualization tools which make it easy for the operator to detect and flag anomalous soundings; this is, however, a subjective analysis.

Interactive methods are a subset of tools, usually, implemented in every software [Universal Systems Ltd., 1994a; Simrad Norge AS, 1995; Hughes Clarke, 1995b; Sirius Solutions Ltd., 1995]. They use the advantages of the graphical visualization capabilities of the computers.

These tools include line oriented and subset oriented visualization of the data, color-coded contours and three-dimensional views, such as digital terrain model (DTM) and sun illuminated images.

	COP	HDCS	BINSTAT	RDANH	Du's
Window	Nearest neighbors	Field of influence	Rectangular window	Nearest neighbors	Recursive
Window's Dimension	Variable (MBSS dependent)	Variable with depth	User's defined	Voronoi polygon	10 x 10, then 3 x 3 soundings
Weight of Neighbor Soundings	$w = \begin{cases} 2 & \text{same beam} \\ 1 & \text{otherwise} \end{cases}$	$w = \begin{cases} 1 - \frac{r}{d_i}, & d_i < r \\ 0 & \text{otherwise} \end{cases}$	Same weight	Same weight	Same weight
Statistics	Swath mode	<u>Subset mode</u>	<u>Subset mode</u>	Swath mode	Swath mode
Seabed Assumptions	N/A	low frequencies	Approximated by sloping surface at $\lambda < \text{cell size}$	flat	N/A
Test Variable (T)	$z_i - \mu_i$	$z_i - \mu_i$	$z_i - \mu_i$	$\frac{(z_i - \mu_i)^2 \frac{m+1}{m}}{\sigma_i^2}$	$\frac{z_n - z_{n-1}}{z_n - z_1}$
Criteria	$ T > \alpha \sigma_i$ or $ T > \beta + \gamma \mu_i$	$T < C_3 \sigma_i - j(C_1 \sigma_i + C_2)$ with $j = 0, 1, \dots, 7$	$ T < \alpha \sigma_{\text{bin}}$ or $ T < 100 \frac{\sigma_{\text{bin}}}{\mu_{\text{bin}}}$	$\frac{\text{ssd}}{\text{SSD}} > K$	$T > \frac{1}{2}$ or $T > \frac{1}{3}$ large n
Sample Assumptions	1% of depth accuracy	Gaussian PDF	Uniform PDF	Gaussian PDF	Uniform PDF
Detection of Multiple Blunders	Yes	Yes	Yes	By Iterating	Yes
Flagging Procedure	Automatic	Automatic or Interactive	Automatic or Interactive	Automatic or Interactive	Automatic

Table 4.1. Summary and comparison of methods used for multibeam data cleaning.

These tools can depict relevant detail, and can be used to identify features that should be preserved in the data set as well as blunders or spikes that need to be removed.

This section provides some insight to the DTM and acoustical image visualization tools.

4.4.1. Digital Terrain Model

The digital terrain model (DTM) is one of the visualization tools that can be used by the hydrographer to display the seafloor surface. The hydrographer should, however, be familiar with its generation, to use the advantages of this powerful tool [Laurini and Thompson, 1992].

The horizontal positioning for multibeam data has a random distribution. Considering the interpolation of all the accepted positions and depths, a surface can be generated. This surface is built up of triangles, and is considered an irregular DTM. The irregular DTM shows the result of the soundings selected or accepted by the hydrographer during the data cleaning phase, as representing the true seafloor. No average is performed and every sounding in the data set constitutes a point (node) of the DTM.

Another possibility is to superimpose a grid on the survey area and to compute an estimated depth for every point of the grid (regular DTM). In this case, each point is the result of the average performed by a particular method (weighted average for the case of *CARIS Geographic Information System* [Universal Systems Ltd., 1992]). Due to the

average performed in the soundings, the result is a smooth surface, which is not completely useful to detect spikes in the data set.

To check the result of the data cleaning, the hydrographer should, whenever possible, generate an irregular DTM to look for remaining spikes in the data set. If any spike is detected, the hydrographer must re-analyze the data in more detail. Visualization in three dimensions can be employed to highlight different parameters. For example, in the most common case, the depth interval or the slope of the seafloor.



Figure 4.4. DTM of the Empress of Ireland, the DTM is illuminated by a synthetic light source from azimuth 315, 45° declination. The wreck (a) is highlighted by the shadow (image created with HIPS).

Three-dimensional visualization with an artificial sun illumination will highlight faces of the DTM for which the angle formed between the incident ray and the normal to the face nearly coincide (Figure 4.4). In the case of artificial sun illumination, the

hydrographer should display two views, using an azimuth difference of 90 degrees, which allows the detection of all features. If the features have an orientation parallel to the azimuth of the source of illumination in the first view, they are, probably, not detected but they will be, certainly, detected in the second view.

4.4.2. Acoustic Image

The main interest of the use of this image is to provide complementary information about the reflected intensity of the acoustic signal on the seafloor surface. This is dependent upon several factors, such as type of sediment, surface roughness, and grazing angle.

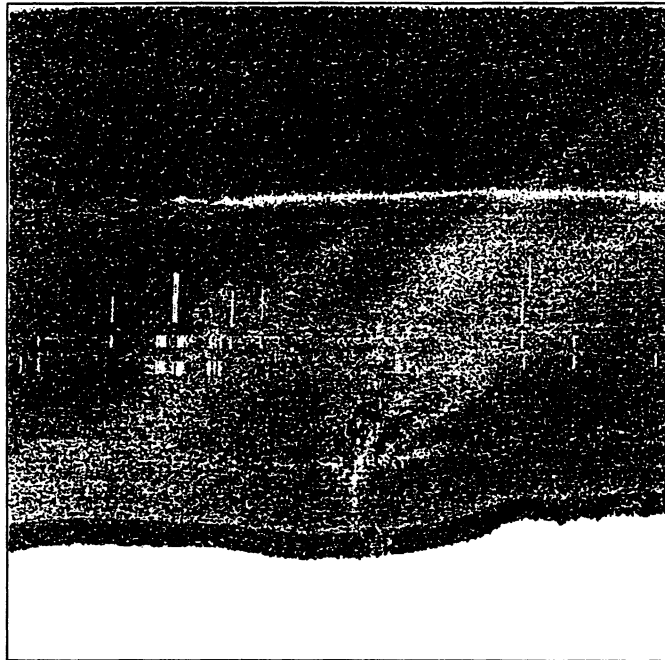


Figure 4.5. Acoustic image of the Empress of Ireland. The wreck (a) is highlighted by the shadow corresponding to low values of backscatter strength (image created with SIPS).

The existence of topographical features on the seafloor can cause changes in the strength of the returned signal, either increasing the signal amplitude (due to the increasing of the grazing angle or to the different properties responsible for the reflectivity) or decreasing of the amplitude (due to the obstruction produced by the feature, causing an area of no return also called a shadow, see Figure 4.5).

Beside the above characteristics, the acoustic image is less sensitive to the problems of errors in the sound velocity profile, and more sensitive to slope or seafloor property variation. Imagery provides complementary information about targets on the seafloor which can be correlated with bathymetric features.

4.5. Dimension of Statistical Cells

It is worthwhile to investigate in more detail two of the commercial MBES data cleaning methods, HDCS and BINSTAT. These methods have the ability to effectively perform automatic data cleaning. Herein, procedures for data cleaning will be discussed and guidelines to standardize the methodology of data cleaning will be suggested.

The pertinent questions are:

- a)* What should the cell dimension be to have meaningful statistics?
- b)* What should the acceptance region be?

The HDCS algorithms use the *weighted moving average surface* and the *weighted standard deviation surface* (Equations. 4.3 and 4.5). These algorithms are sensitive to the

dimension of the radius of influence, for the HDCS the dimension of the cells is a function of the depth. The weighted function used to compute the average and the standard deviation surface has a conical shape, 10 degree width [Wong, 1996], with value one for the center of the cell and zero for the limit of the radius of influence (Figure 4.6).

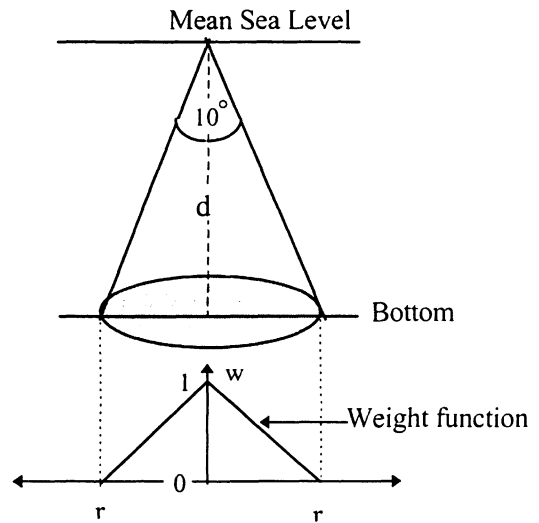


Figure 4.6. HDCS radius of influence.

The HDCS can be used more efficiently if the design of the MBES field survey procedures provides an acceptable overlapping of the swaths. The planning of the survey must take into consideration that, ideally, there should be no gaps among consecutive pings. An average overlapping of 50% means that every point on the seafloor will be sampled twice. An average overlapping of 67% means that every point on the seafloor will be sampled three times.

Figures 4.7 and 4.8 represent the percentage of overlapping for different depths and ship's speeds. From these examples, it is possible to conclude that for the ship speed and multibeam characteristics shown in the Figure 4.8, for depths greater than 70 metres, there are, at least, three footprints that overlap a common point on the seafloor. This number increases for the outer beams. These figures are important for the hydrographer when analyzing the data statistically, and that should be known before handling the data.

For these particular multibeam characteristics and speed of the vessel (5 knots), for depths greater than 70 metres, the overlapping of footprints is more than enough and the survey can be carried out using higher speeds. Nevertheless, the number of soundings for the statistics should be from an area with diameter equal to the average of the acoustic beam footprints for the middle of the overlapping area between two adjacent swaths.

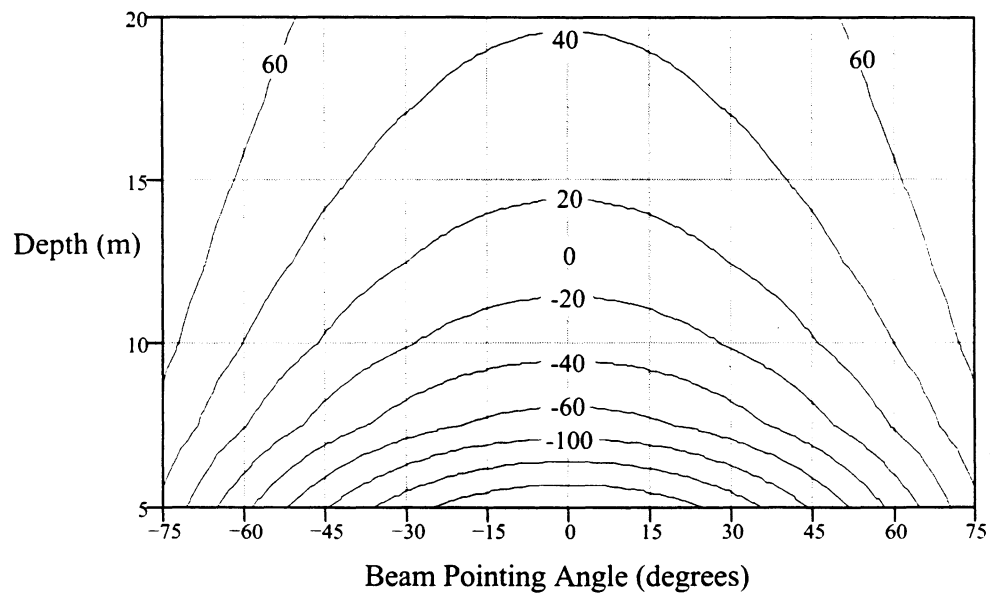


Figure 4.7. Percentage of overlapping among ensonified areas from consecutive pings. Computed for a ship's speed of 5 knots, transmission beam width 3.3° and ping rate 0.25 seconds, assuming no yaw or pitch. The negative overlapping percentages correspond to the percentage of non ensonified area, with respect to the footprint dimension in the along-track direction.

Considering an angle of coverage of 150° and based on some assumptions about system parameters Simrad EM 1000 MBES (see Section 2.8) [Simrad Norge AS, 1992], the area where, the total depth accuracy measurement is better than 1% of the mean

depth (95% confidence level as proposed in the latest draft of S-44, 4th edition [IHO, 1996]), is restricted to 60° for each side of nadir (Figures 2.10 and 2.11). Since the centre of one side of the swath corresponds, roughly, to a beam pointing angle of 60° , then one can use a coverage of two hundred percent, i.e., a line spacing equal to half swath width.

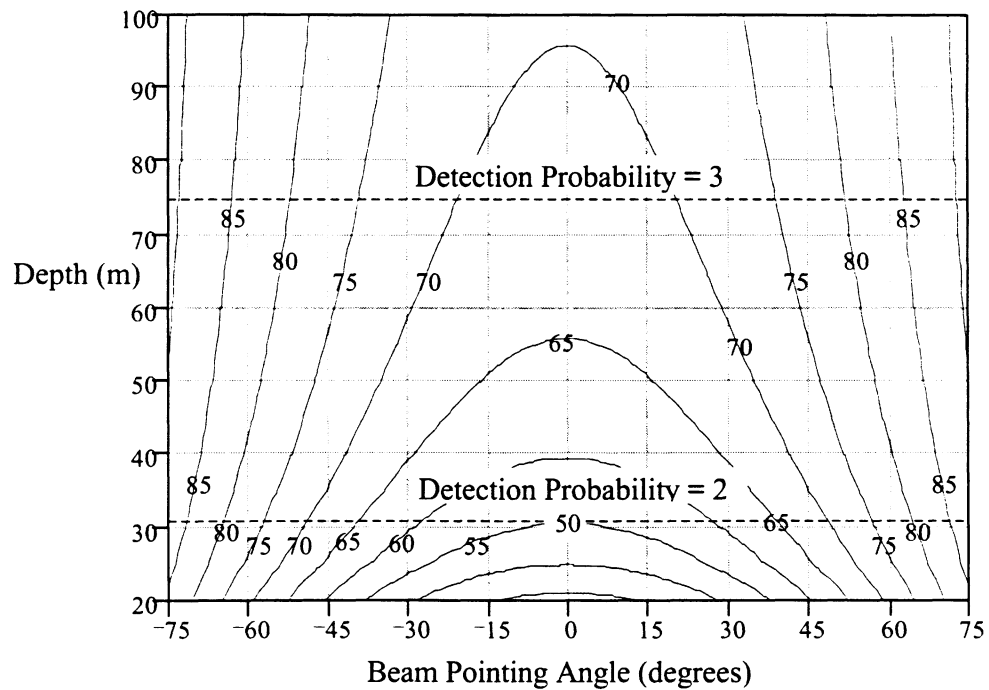


Figure 4.8. Percentage of overlapping among ensonified areas from consecutive pings. Computed for a ship's speed of 5 knots, transmission beam width 3.3° and variable ping rate (function of the depth). The dash horizontal lines represent the minimum detection probability, number of footprints that cover the same point on the seafloor.

The radius of influence should be no smaller than the average of half the footprint dimension, for the intermediate beams (60° beam pointing angle). For a beam width of 3.3° , the radius of influence is approximately 10% of the mean water depth, i.e., the

major semi-axis of the acoustic footprint, which is in accordance with the one used in HDCS $\{ \text{depth} \cdot \tan(5^\circ) \}$.

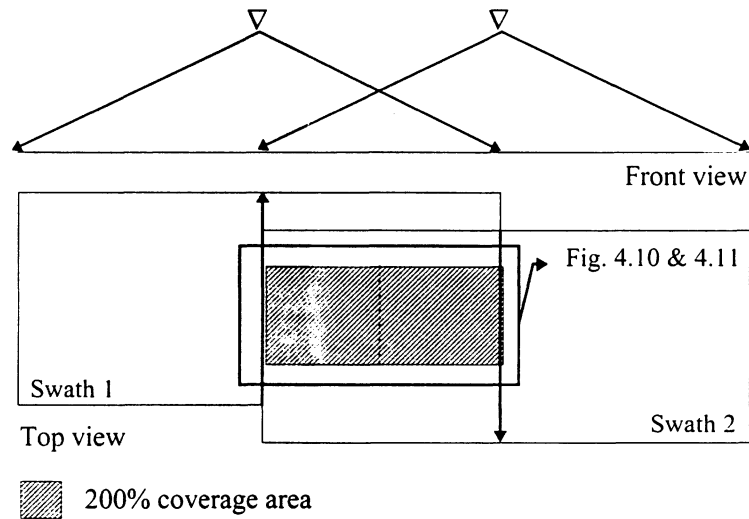


Figure 4.9. Coverage of the seafloor.

Other multibeam systems, with different characteristics (e.g. beam width, beam spacing, and ping repetition rate), will require a different value for the radius of influence. Hence, the cone of aperture should not be a fixed parameter and should be either set by the hydrographer, or calculated by the software based on MBES characteristics and on the overlapping among swaths. The rules to establish the cell dimension should ensure, at least, a number of soundings greater than two degrees of freedom, i.e., three soundings for HDCS and five soundings for BINSTAT.

Figure 4.10 shows one of the possible choices for planning a survey in shallow water and this regards the considerable redundancy required for reliable data cleaning

with the HDCS. In this particular case, one considers no overlapping among the nadir footprints, for consecutive profiles.

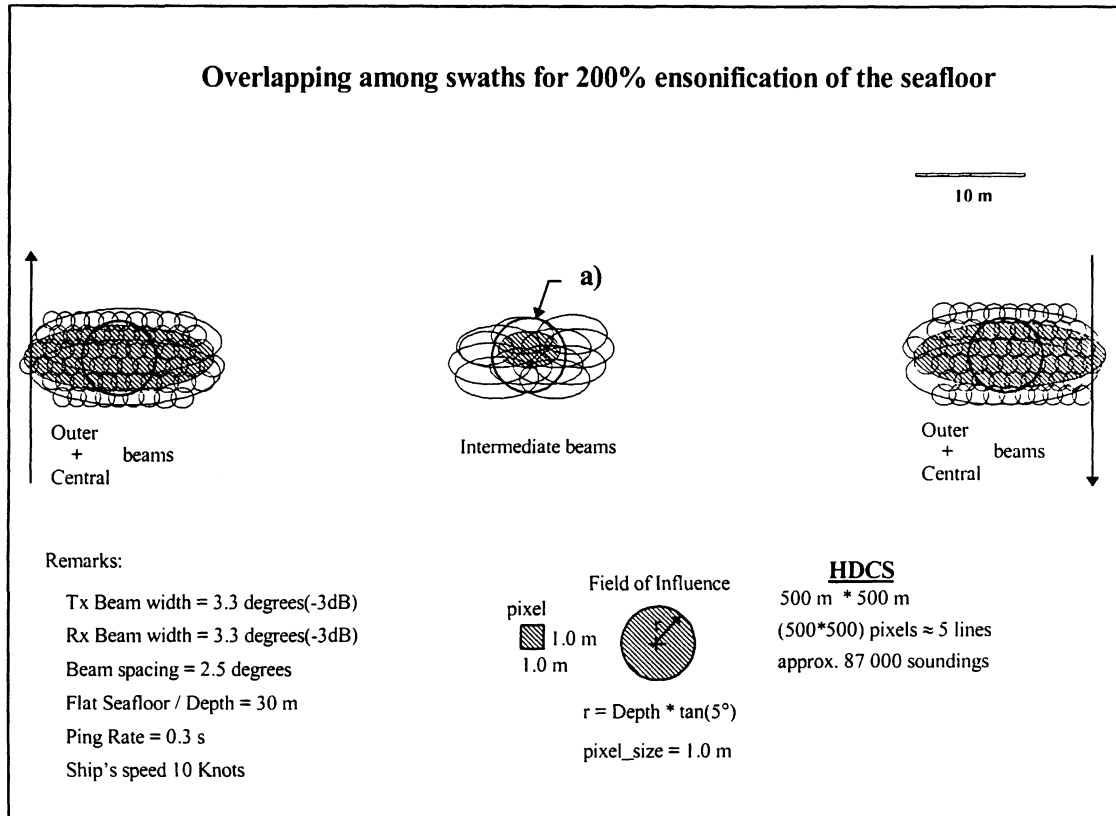


Figure 4.10. Acoustic footprints, resulting from the overlapping of two halves swaths, ran in direct and reverse sense (zoom in from the area defined on Figure 4.9). The circle a) represents the adequate dimension to be used in the HDCS.

As shown in Figure 4.8, for deeper waters, one has a greater overlapping of footprints. Therefore, for statistical data cleaning, the coverage can be reduced to 100 percent, since the present (1987) International Hydrographic Organization depth measurement requirements are met for all the beams. Appendix A presents detailed figures that depict the number of soundings gathered in the same radius of influence for

different MBES characteristics, depths, ship's speed and overlapping.

Similar to the HDCS, for BINSTAT, the data set is partitioned into smaller blocks. The idea is to have a convenient amount of soundings that can be treated without considerable reduction of the processing speed. Each block can be subdivided or their statistics calculated.

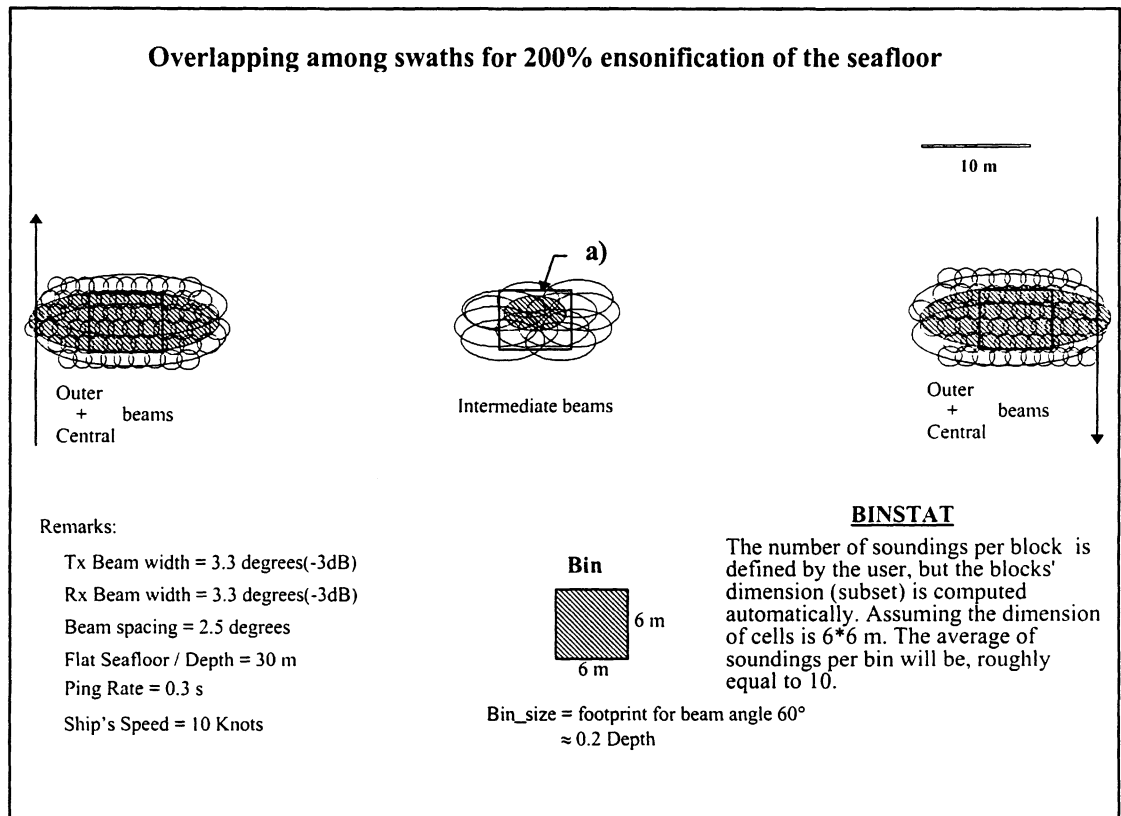


Figure 4.11. Acoustic footprints, resulting from the overlapping of two halves swaths, ran in direct and reverse sense (zoom in from the area defined on Figure 4.9). The square a) represents the adequate dimension to be used in the BINSTAT.

For the statistical computations, the user needs to set the sizes of the rectangular cells in the North and East direction. Considering the same overlapping and MBES

characteristics used in Figure 4.8, the dimensions of the cells should be a square with the sides equal to 20 percent the water depth. Since at least three soundings are required to define a plane, the number of soundings per cell should be greater than this value. BINSTAT provides a display of the number of valid soundings per cell. This is extremely useful to check if the cell dimension is reasonable or not.

Figure 4.9 depicts the recommended dimension of the cells for BINSTAT, as the average of the footprints on the middle of the overlapping, area between two swaths, this assures that the number of soundings will be, in general, greater than two degrees of freedom, i.e., 5 soundings.

4.6. Procedures for Multibeam Data Cleaning

To perform this important task of analyzing and cleaning the multibeam data set, it is important to define procedures. These procedures are important to give the hydrographer the orientation required for comprehensible and uniform methodologies to safely and efficiently accomplish the task of cleaning the data set for hydrographic charts. The result will be a cleaned data set available to be integrated in the nautical chart.

The approaches below are defined for the commercial methods, HDCS and BINSTAT, nevertheless, they can be extended to other methods. The main interest of the following procedures is blunder detection. However, there are further steps that cannot be forgotten, and are included mainly to put blunder detection into context.

As stated in Chapter 3, there are three sources of errors in the MBES measurements: systematic errors, blunders, and stochastic deviations. Systematic errors should be analyzed before the survey by the calibration test, also named *patch test*. The calculation of the MBES system offsets requires to run several lines according to several procedures [Herlihy et al. 1989; Simrad Norge AS 1995; Godin 1996], and their calculation can be performed by both modules HDCS and BINSTAT, blunders by the following set of procedures, and the noise assessed by the final standard deviation surface of the “cleaned” data set.

1. Navigation, attitude, and sound velocity profile errors

The first step of multibeam data processing is to check the positioning, looking for jumps in the coordinates and sudden variations of heading. Gyro, roll, pitch, heave, and tide values need to be checked and sudden variations should be browsed to check for biases in the depth data set. The hydrographer needs to judge when to interpolate or to reject some of the positions or attitude values. After the navigation, attitude, and tide have been validated, the data need to be reduced for the tide and the lines should be merged.

All the following steps should be performed in the subset mode, i.e., by areas, allowing the analysis of the overlapping data of adjacent lines.

2. Systematic errors

The MBES data has systematic errors, which are, in a general sense, the result of

remaining system offsets mainly roll, and sound velocity profile (SVP) errors and they play the most important role in the depth measurement uncertainty. The determination of these calibration values is done before the survey. However, if one has survey lines run in the direct and reverse senses, measuring the depth difference between the outer beams from the two reciprocal lines one will be able to check the configuration determined during the patch test. SVP errors are measured on the inner beams from one line with the outer beams from a line run perpendicularly to the main survey line [Herlihy et al., 1989; Simrad Norge AS, 1995; Godin, 1996]. To accomplish this task, the surveying planning should ideally provide, lines run in reciprocal senses and check lines, the number of lines depends of the dimensions of the surveying area.

The SVP errors result from the variation of the SVP between samples. These errors can be corrected if there is a monitoring of the SVP or tools that can iteratively correct for refraction based on the comparison referred above [Hughes Clarke, 1996]. Neither HDCS nor BINSTAT have this capability, thus the hydrographer needs to check for the effect of the refraction and to define the angular coverage, where the effect is not higher than the depth measurement accuracy specified by the International Hydrographic Organization standards [IHO, 1987].

The results of any remaining systematic errors are reapplied and the data transformed to generate the corrected final sounding positions and depths.

3. Creation and partition of subsets

After known systematic errors had been corrected, there still remain some

systematic errors (mainly due to sound velocity profile variations), gross errors or blunders and noise. The surveying area needs to be divided into smaller areas (i.e., subsets). For this purpose, one can derive color coded contours or standard deviation surfaces (in this case, we should look for small clouds with high standard deviation), to look for irregularities in the subset. The areas with irregularities need to be identified and kept separately. With this technique, one will end up with a number of subsets where some are relatively regular, without conspicuous features and other subsets which have irregularities (blunders or real features).

In this study high standard deviations are associated with irregular seafloor areas, and low standard deviations are associated with regular seafloor areas. The mean surface also provides information to define the irregular areas, i.e., areas with large variations in the bathymetry, and regular areas (bathymetry featureless areas). The acoustic backscatter image is used to identify these areas, in a general way, irregular areas correspond to high backscatter areas (correlated with rock), and regular areas correspond to low backscatter areas (correlated with mud and sand).

4. Analysis of trouble areas

The subsets with irregularities, defined either as areas with high standard deviation or areas with large variation of backscatter strength or rocky areas, need to be interactively analyzed, using the visualization tools that produce profiles (HDCS), or correlation plots (BINSTAT). In the second case, it is necessary to choose a meaningful correlation. From the several experiments carried out for this report, the most useful

correlations are residuals versus depths and standard deviations versus depths. In the particular case of lines oriented in the North-South or East-West directions, correlations of ping number (or time) versus depths and beam number versus depths are also useful.

This work has determined that low standard deviation areas do not necessarily mean an area free from blunders. This is highly dependent on the number of soundings per cell, i.e., a large number of soundings with a blunder will have a lower standard deviation when compared to the same blunder in an area with few soundings. The interactive analysis of the data with HDCS, should be carefully conducted; the safest procedure is to visualize all the soundings by cross-section.

BINSTAT does not provide for the spatial visualization of profiles (except when the lines are either oriented in the North-South or East-West directions). However, this module provides, in addition to the standard deviation and mean surface, other statistical surfaces, such as, maximum residual difference and depth difference. These surfaces provide further detail to investigate blunders, they are efficient and can be used complementary to the standard deviation and mean surfaces. When cleaning the data interactively the hydrographer must use the surfaces of the standard deviation, maximum residual difference, and depth difference to check the irregular areas and look for blunders in order to identify and flag them.

Large features on the seafloor, i.e., greater than the footprint dimension, will be detected by several beams. These features will be highlighted on the acoustical image due to the contrast of seafloor properties, steep slopes, or shadow.

The acoustic image should be used to correlate the targets with the bathymetric features, which is an efficient method to identify real features (see Chapter 5). If the irregularities in the data set are caused by blunders, they must be rejected from the data set and the remaining subset should be analyzed as a regular area.

5. Analysis of regular areas

Regular areas are defined by their low and uniform standard deviation surface. Mud surfaces can be considered regular surfaces, since they do not present high local variation of the standard deviation or backscatter strength. Sand may also have these properties, in the absence of topographic variations such as sand waves.

In this phase, the data set is only cleaned of the known systematic errors. It was defined before that these subsets do not contain conspicuous features. The errors in these subsets are spurious blunders, remaining systematic errors, and noise. These subsets can be treated automatically and it is important to keep in mind that during the survey, there must be at least one beam meeting the survey accuracy measurement specifications, i.e., one hundred percent coverage within an acceptable angular sector according to the IHO depth measurement accuracy.

The region of soundings against which the soundings should be validated or accepted, is a function of several factors, for example, the uncertainties in the depth measurements and the sinusoidal variations on the seafloor. One is not able to obtain further vertical resolution than the defined by ϵ , herein called the ***acceptance region***

(Figures 4.12 and 4.13),

$$\varepsilon = \sqrt{\varepsilon_{\text{roughness}}^2 + \varepsilon_z^2} \quad (4.22)$$

where ε_z , $\varepsilon_{\text{roughness}}$ are the standard deviations, of the system uncertainty (section 3.2) and from the bottom roughness, for the particular cell size. The first value should be defined for the middle of the overlapping region. If the wavelength of the features are much larger than the cell size, $\varepsilon_{\text{roughness}}$ will be neglected. On the other hand, its value will play an important part in ε , when the size of the cell is comparable to the bottom wavelength.

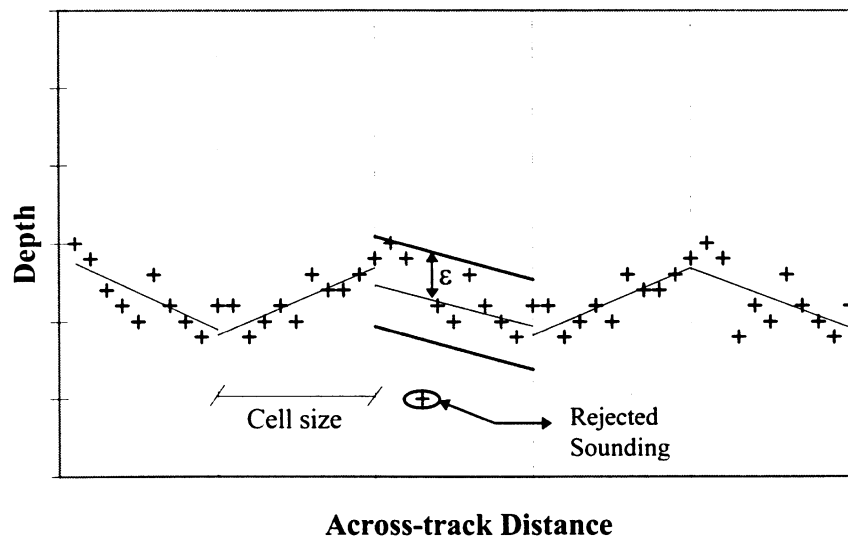


Figure 4.12. Example of the acceptance region in BINSTAT.

The acceptance region, ε , is set in the local rules in the case of BINSTAT by the expression $|z_i - \hat{z}_i|$, representing the distance a sounding z_i lies from the fitted plane, where \hat{z}_i is the estimated depth for the sounding z_i .

In the HDCS method, the acceptance limit can be used by the selection of the

classification levels, using the alternative expression to Equation. 4.6, implemented in HDCS [Universal Systems Ltd., 1994],

$$\text{level}_i = \text{integer}\left(\frac{(z_i - \mu_i) - B \cdot \sigma_i}{L \cdot \sigma_i + O}\right) \quad (4.23)$$

where z_i is the sounding being classified, μ_i and σ_i are the values of the mean and standard deviation for the cell corresponding to the sounding being classified, the values B , L , O are respectively the base scale, the level scale, and level offset. The classification level of z_i corresponds to the integer of the right-hand side of Equation 4.23.

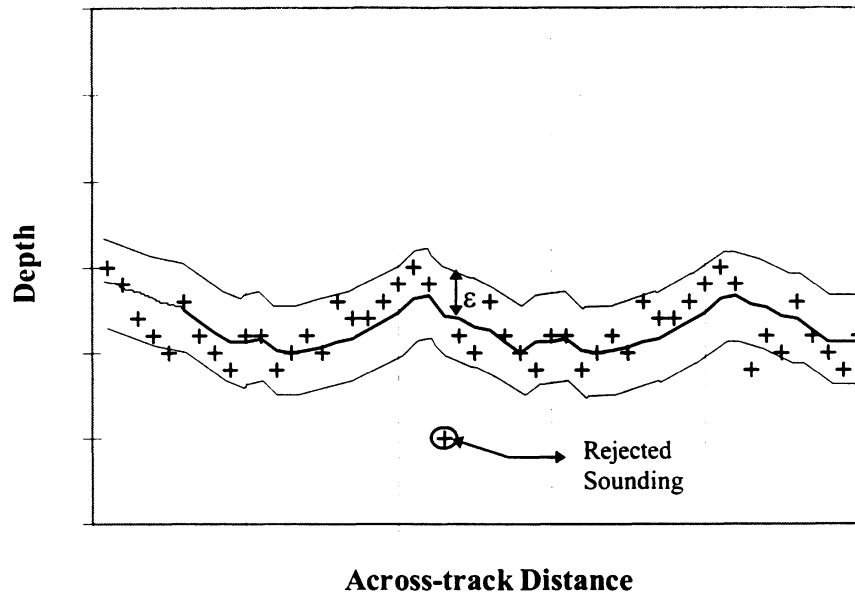


Figure 4.13. Example of the acceptance region in HDCS.

The values for the parameters can be determined experimentally, but their values are somewhat subjective. The base scale, B , allows the hydrographer to shift the classification levels proportionally to the standard deviation (generally speaking, this corresponds to shift the mean surface upward or downward depending whether B is

positive or negative, this should not be used since it produces a biased mean seafloor surface). The level scale, L , scales the classification levels inversely proportional to the standard deviation (soundings which depart the same value from the seafloor but with higher standard deviation for the whole cell will be classified in a lower level). The level offset, O , generates the increase or decrease of the level resolution. Figures a.7, a.8, and a.9 in Appendix A depict the role of each of these parameters.

Parameters B and L , when different from zero, will play an important role in the classification level. These values will induce the classification levels as a function of the standard deviation. On one hand this is useful when the increase of standard deviation results from irregularities in the seafloor. On the other hand blunders or systematic errors (most likely in the outer beams) will increase locally the standard deviation leading to a lower classification level for these soundings.

The use of the standard deviation in the classification criterion in one hand leads to an increase of the acceptance region for areas with bathymetric features, but in the other hand can lead to the acceptance of blunders or of soundings largely affected by the refraction effect. Since this automatic procedure will be applied to regular areas, one should use the simplest form of the classification level, i.e., the one corresponding to the residuals ($B = 0$, $L = 0$, and $O = 1$), reducing Equation 4.23 to $|z_i - \mu_i|$, representing the distance that the sounding z_i lies from the mean seafloor surface, this leads to an objective criterion, without any influence from the standard deviation (and that can be applied in a similar way to BINSTAT rules [Simrad Norge AS, 1995]). One ends up with

eight classes of residuals, from 0 to 7 with one metre intervals, where the highest residual is assigned to level 7, i.e., $\{\text{level}_j, j=0, 1, \dots, 7: [0, 1[, [1, 2[, \dots, [7, \infty[\}$. The hydrographer can reject the classes which residuals are higher than ϵ . If the acceptance region is small, values smaller than 0.70 m, the level offset should be set to $O = 0.1$, with this value the classes, will be of 0.10 m interval, i.e., $\{\text{level}_j, j=0, 1, \dots, 7: [0, 0.1[, [0.1, 0.2[, \dots, [0.7, \infty[\}$, and the hydrographer can easily reject a level and higher levels.

The use of the classification expression with $L \neq 0$, implies that the classification levels will be scaleable by the standard deviation. This can be, for particular cases, a good choice, for example when the seafloor presents high variations but without systematic errors. However, in general, this will lead to a lower classification level for areas that do have systematic errors, mainly due to refraction.

The hydrographer needs to be aware that the presence of a seafloor slope will not affect the residuals in HDCS or in BINSTAT, but will affect the standard deviation. $\epsilon_{\text{roughness}}$ can be calculated from the depth profiles in the HDCS. In BINSTAT it is more difficult to estimate $\epsilon_{\text{roughness}}$, specially if the lines are not oriented in the North-South or East-West directions.

Finally, after all the MBES bathymetric data is cleaned, the values of the standard deviation are a data quality measure combining the effects of data noise level, seabed roughness, cell size, and slope.

Chapter 5

TEST DATA ASSESSMENT

The purpose of the tests with real data can be described as follows:

- Implementation and verification of the procedures for multibeam data cleaning;
- Identification of possible improvements to HDCS and BINSTAT;
- Identification of the potential of some built in functions on HDCS and BINSTAT;
- Definition of relevant features of the backscatter strength for data cleaning.

This chapter describes the test data, test procedures, and tests on backscatter. A summary of the results obtained with the test data is also presented.

5.1. Test Data

In this study, two test data sets were used. The data was collected on surveys carried out with *CSS Frederick G. Creed* by the Canadian Hydrographic Service with a MBES *Simrad EM 1000*. The first set was collected on June 28, 1992, in the area of the wreck of the *Empress of Ireland* in the Gulf of St. Lawrence off of Rimouski, Quebec. The second data set was collected on August 14, 1993, as part of the “*Hydrographic Ground Truthing*”, conducted by the University of New Brunswick (UNB), Chebucto

area, in the Halifax approaches. Hereafter the two data sets will be named “*Empress of Ireland*” and “*Halifax Approaches*”.

Despite the fact that these two surveys were not carried out for MBES data cleaning purposes, they were selected for this study because of their different characteristics. The *Empress of Ireland* data set consists of a total of eleven lines, six in the North-South direction and five perpendicular to these main lines. There is a large overlapping among swaths, seven of which cover the area of the wreck. The adjacent area of the wreck does not present bathymetric irregularities, and the type of sediment is apparently uniform. The area of interest is a subset with dimension of 1000 m x 1000 m, with total of 290 000 soundings, covering a depth range from 20.1 m to 62.2 m. The wreck of the *Empress of Ireland* constitutes an uncommon bathymetric anomaly of about 20 metres of depth, with approximately 180 m length and 30 m width.

The *Halifax Approaches* test data is a subset of the survey data, which consists of 6 lines run in the East-West direction. The overlapping among swaths is restricted to a few of the outer beams. The area has several bathymetric irregularities and there are several types of sediments (rock and sand). The area of interest has a dimension of approximately 1600 m x 3200 m with a total of 410 000 soundings covering a depth range from 24.1 m to 57.6 m.

The tide reduction for both places was based on the predicted tide heights. In the case of the *Empress of Ireland* data set, the prediction was done for Pointe-au-Père; and for the *Halifax Approaches* data set, the prediction was done for Chebucto Head.

Both test data sets have the backscatter strength information which was used to build the acoustical image.

5.2. Test Procedures

This section describes the procedures followed to clean the two data sets and the procedures of the backscatter tests.

Two software packages, HIPS (Hydrographic Information Processing System) — including the data cleaning module HDCS [Universal Systems Ltd., 1994a] — and NEPTUNE — including the data cleaning module BINSTAT [Simrad Norge AS, 1995] — were used for cleaning the two test data sets.

5.2.1. HDCS

Both data sets (Figures b.1 and b.12) were cleaned interactively (Figures b.2 and b.13) and automatically using HDCS (Figures b.3 and b.14), according to the procedures discussed on Section 4.6.

HDCS provides swath and subset tools, which are used respectively to edit single lines and areas covered by several lines. In the subset mode, the user has the capability to visualize soundings by profiles oriented with respect to the orthogonal subset axes.

5.2.1.1. Empress of Ireland

Interactive Data Cleaning

The set of steps used in the HDCS interactive data cleaning for the *Empress of Ireland* are as follows:

1. Each line was examined to check for errors in gyro, heave, pitch, roll, tide, and navigation.
2. The lines were merged to generate final sounding positions and depths.
3. Two reciprocal lines in the North-South direction were used to check for roll offset. First, the offset value was obtained by adjusting two narrow cross-sections of these two lines; then, the data was re-merged to correct the soundings and positioning from the roll offset.
4. The refraction effect was checked using two perpendicular lines. In these procedures the outer beams from one line (much more prone to errors in the sound velocity profile) were compared against the inner beams from the perpendicular line (less affected by errors in the sound velocity profile).
5. The area of interest was divided into four smaller subsets, with some overlapping among them. For each subset, the mean and standard deviation surfaces were computed to highlight trouble areas. The subsets were cleaned by browsing all the soundings, using cross-section profiles.

Automatic Data Cleaning

The first four steps described in the interactive data cleaning for this data set (*Empress of Ireland*) were followed. Subsequently, the following set of procedures was used:

- a) The mean and standard deviation surfaces were computed for the whole data set to classify the areas where interactive or automatic methods should be used. According to those surfaces, the test area was divided into seven subsets, with some overlapping among them. The subsets were chosen to cover the area surrounding the wreck of the *Empress of Ireland* (a regular area with a low standard deviation). Figure b.4 represents an example of one of the subsets, Figures b.5 and b.6 represent the subset cleaned interactively and automatically.
- b) The soundings from the wreck and from its neighborhood (irregular area with high standard deviation) were interactively cleaned.
- c) For each subset, the mean and standard deviations surface were computed to highlight the trouble areas, as in the interactive method (Figures b.7, b.8, and b.9 represent the respective standard deviation surfaces of Figures b.4, b.5, and b.6). Any area with high standard deviation was browsed to look for blunders, and for one of the data sets some soundings had to be cleaned interactively. The remaining areas with higher standard deviation were mainly caused by refraction.
- d) The acceptance region, ϵ , was defined as one percent of the average depth in the subset (assumed value for the system accuracy ϵ_z), ranging from 0.4 to 0.6 metres.

The characteristics of the seafloor did not present roughness features to be taken into account, therefore $\varepsilon_{\text{roughness}} = 0$.

- e) The subsets were cleaned automatically by setting the base scale $B = 0$, level scale $L = 0$, and level offset $O = 0.1$.

Each classification level is obtained from

$$\text{level}_i = \text{Integer}\left(\frac{|z_i - \hat{z}_i|}{0.1}\right), \quad (5.1)$$

where *Integer* represents the lower rounded number of the value inside brackets.

Soundings with depth difference from the mean surface (residuals) greater than ε (that is, $|z_i - \hat{z}_i| > \varepsilon$), were flagged by selecting the subsequent classification level and rejecting that level and upper levels (i.e., for $\varepsilon = 0.4$ m rejecting level 4 and for $\varepsilon = 0.6$ m rejecting level 6).

The results of the interactive and automatic data cleaning of *Empress of Ireland* with HDCS are presented in Figures b.2 and b.3.

Figure b.10 and b.11 show the result of cleaning the wreck and adjacent area interactively and automatically.

5.2.1.2. Halifax Approaches

Interactive Data Cleaning

The same sequence of interactive procedures (Section 5.2.1.1) was used to clean

this data set. The test area was divided into four smaller subsets, with some overlapping among them.

The reduced overlapping among swaths and the nonexistence of reciprocal and perpendicular lines, did not allow the use of calibration tools to check for remaining roll offset, and subsequently to assess the refraction effect.

Automatic Data Cleaning

The procedures used in the *Halifax Approaches* data set were identical to the ones used to clean the *Empress of Ireland* data set, with the following exceptions: (1) the area of interest was divided into six subsets (Figure b.14), with different dimensions, and chosen to cover areas with lower standard deviations; (2) only these areas were cleaned automatically; (3) the areas with irregularities, corresponding to higher standard deviations, were cleaned interactively.

The *Halifax Approaches* data set and the results of the interactive, automatic, and automatic data cleaning applied to the whole data set, using HDCS are presented by Figures b.12 - b.15 and their respective standard deviation surfaces by. Figures b.16 - b.19. Figure b.20 depicts the effect of cleaning a boulder, using the automatic method. This leads to the rejection of the minimum depths of the boulder.

5.2.2. BINSTAT

Both data sets were cleaned interactively and automatically using BINSTAT. The statistical values for each data block can be visualized in a color coded display, which

allows the identification of the areas with problems. The user can select these areas and bring up the correlation plots to examine the soundings and to flag them. There are several correlation plots supported by BINSTAT module. As far as MBES data cleaning is concerned, only some correlations are meaningful; the correlations often used in the interactive data cleaning procedures are shown in Table 5.1.

The rules for automatic data cleaning are defined in detail in Simrad Norge AS [1995]. One peculiarity of this method is the use of some of the information from the bottom detection method.

X Axis	Y Axis
residual standard deviation time ping number beam number	depth
beam number	depth amplitude residual quality factor standard deviation
ping number	depth amplitude residual quality factor standard deviation
time	depth amplitude residual quality factor standard deviation

Table 5.1. Meaningful correlations used in the interactive data cleaning.

The quality factor (number of amplitude samples for amplitude detection, and a value

proportional to the variance of the curve fit to the phase samples for phase detection) and signal strength (amplitude in dB) are values stored in the datagrams of the Simrad MBES from the EM series. The hydrographer has the capability to select values for the acceptance interval of these parameters.

5.2.2.1. Empress of Ireland

Interactive Data Cleaning

In the analysis of this data set the following steps were used:

1. Each line was examined to check for navigation errors and subsequently processed to generate final sounding positions and depths.
2. A small subset with two reciprocal lines in the North-South direction was used to check for roll offset. The offset value was obtained iteratively using the calibration function, to adjust the reciprocal lines. The data was re-processed to correct the soundings and positioning from roll offset.
3. The test area was divided into four smaller subsets, and for each subset a geographical grid was assigned. The dimension of the cells (bins) for statistical calculations were squares with sides equal to 5 to 12 metres. Which allows, in general, to have at least minimum of 5 soundings per bin. From the several possible bin statistics, the standard deviation surface (*i*) was used to highlight the trouble areas.
4. The subsets were cleaned by browsing the areas in a priority order, from higher to lower standard deviation, using the correlation plots (Table 5.2). Afterward the

minimum depth, depth residual (*ii*), and depth difference (*iii*) surfaces were used to check for further bathymetric details in every block. The blocks were considered cleaned when the high values from surfaces *i*, *ii*, and *iii* were either rejected or identified as bathymetric artifacts. Figures c.12 - c17 depict the use of BINSTAT correlation plots in this data set.

Automatic Data Cleaning

The first two procedures described on the BINSTAT interactive data cleaning for the *Empress of Ireland* were followed. Subsequently, the following set of steps was used:

- a) The mean and standard deviation surfaces was computed for the whole data set to define the areas where interactive or automatic methods should be used. Based on those surfaces and on the side scan image, the area of interest was divided into eight blocks.
- b) The blocks were chosen to cover the area surrounding the wreck of the *Empress of Ireland* (regular area with low standard deviation and/or variations of local backscatter strength).
- c) The soundings from the wreck and from its neighborhood (irregular area with high standard deviation and/or variations of local backscatter strength) were interactively cleaned.
- d) For each block, an identical criterion to the one described for the interactive data cleaning with HDCS, for the *Empress of Ireland*, was used. The areas presenting

higher standard deviation, were caused by refraction affecting mainly the outer beams.

- e) The acceptance region, ε , was defined as in BINSTAT for this same test data. The subsets were cleaned automatically by setting the **basic rule**, i.e., set of flagging conditions applied to the entire block. The value used for the residual interval was $[-\varepsilon, \varepsilon]$, where ε is defined as 1% the water depth. Soundings with residual that is greater than $|\varepsilon|$ were automatically flagged.

The *Empress of Ireland* data set and the results of the interactive, and automatic data cleaning, using BINSTAT are presented by Figures c.2 - c.4, and their respective standard deviation surfaces and noise surfaces respectively by Figures c.5 - c.7 and c.8 - c.10.

5.2.2.2. Halifax Approaches

Interactive Data Cleaning

The interactive sequence of procedures is similar to the interactive BINSTAT data cleaning for the *Empress of Ireland*, except that the test area was divided into four blocks. To each subset a geographical grid was assigned, the dimension of the cells (bins) for statistical calculations were squares with sides equal to 12 to 18 metres.

Due to the reduced overlapping, the lack of reciprocal and perpendicular lines, prevented the use of calibration tools to check for remaining roll offset, and to assess the refraction effect.

Automatic Data Cleaning

1. The test area was divided into four blocks. The acoustical image was used to define the areas with different types of sediments. The areas with higher standard deviation (irregular areas) were correlated with bedrock and the areas with lower standard deviation (regular areas) were correlated with sand.
2. Irregular areas were interactively cleaned using the procedures defined in the interactive data cleaning using BINSTAT for the *Halifax Approaches* and using the same cell dimension.
3. Regular areas were automatically cleaned by the use of **local rules**, that is, a set of flagging conditions applied to the selected soundings inside the block. The value used for the residual interval was $[-\epsilon, \epsilon]$, where the acceptance region is the one defined for the interactive data cleaning using HDCS for the *Halifax Approaches*.

The results of the *Halifax Approaches* interactive, automatic, and whole automatic data cleaning, using BINSTAT are presented by Figures c.19 - c.21, and their standard deviation surfaces, residual surfaces, and depth difference surfaces respectively by Figures c.22 - c.24, c.25 - c.27, and c.28 - c.30.

5.2.3. Backscatter Analysis

Three different backscatter analysis were carried out: (1) detection of anomalies on the seafloor; (2) assessment of the generic type of sediment, in order to assist the hydrographer on the first analysis; (3) assessment of the use of bottom detection

characteristics (type of detection and quality factor) for data cleaning.

BINSTAT allows correlations of amplitude versus beam number. However, as the amplitude is the mean of the instantaneous backscatter samples, it may filter possible targets inside the footprint size. Furthermore, BINSTAT does not allow, under general conditions (lines not oriented according to the projection axes), the visualization of a unique ping or a group of pings. This is due to the fact that statistics are always calculated for a block (subset mode), with bins oriented in the North and East direction and is not possible to rotate them. Thereupon, one needs to work with profiles and use the information from instantaneous samples. The backscatter samples reveal detail that the average can cancel out.

From the analysis of the backscatter traces (derived using *SwathEdit* software) used in this study (Simrad EM 1000), the backscatter samples present a noise of the order of ± 10 dB. In order to reduce the effect of the random variations of the backscatter, it is necessary to filter the samples. A moving average filter was used for this purpose.

For the *Empress of Ireland* data set, the detection of the wreck is highlighted by the decreasing of the backscatter strength caused by the existence of a shadow area where there is no signal return. In this shadow zone, the backscatter measurements are due to background noise only. The returned signal from the wreck is no higher than the returns from the neighboring seafloor. This can be related to the acoustic reflective properties of the hull and super-structures, to the biological growth which accumulated over the wreck since it sunk in 1914, and to the variation of the grazing angle from the

adjacent seafloor to the wreck.

A higher backscatter strength from beams that hit the wreck was not seen. Nevertheless, the shadow created by the wreck was easy to identify and should be used as backscatter information for the detection of wrecks. The decreasing of the backscatter within the shadow zone is of the order of 30 dB, to a backscatter level below -50 dB.

The difference of the backscatter strength given by Jackson's model, for the extreme types of sediments (rock and mud) is of about 20 dB, for incidence angles 10 degrees off-nadir. The variation of the backscatter created by the shadow of an obstruction is comparable to the backscatter difference from rock to mud. However, this is a relative strength decrease. For a rocky seafloor, the decrease would be about 40 dB, to the approximately same level of -50 dB. With this information, one has a potential tool to identify where the difference of the backscatter strength is a result of an obstruction (backscatter strength below any type of sediment) or a result of different sediment type (following approximately Jackson's model curves).

Jackson's model was implemented as an indicator of seafloor type based on the comparison of the backscatter traces with the theoretical model curves, using the geo-acoustic parameters defined in APL [1994]. The computation of this model was performed for just three types of sediment. In the case of rock, the results were not identical to the ones interpolated from APL [1994] for the frequency of 95 KHz, therefore the theoretical values computed for rock were replaced by the ones from the reference above. For the case when the parameters are known but different from the sample parameters given by APL [1994], if one wants to implement this model for areas

where the parameters are known, Jackson's model can be used to calculate the corresponding curves of the backscatter strength versus the grazing angle.

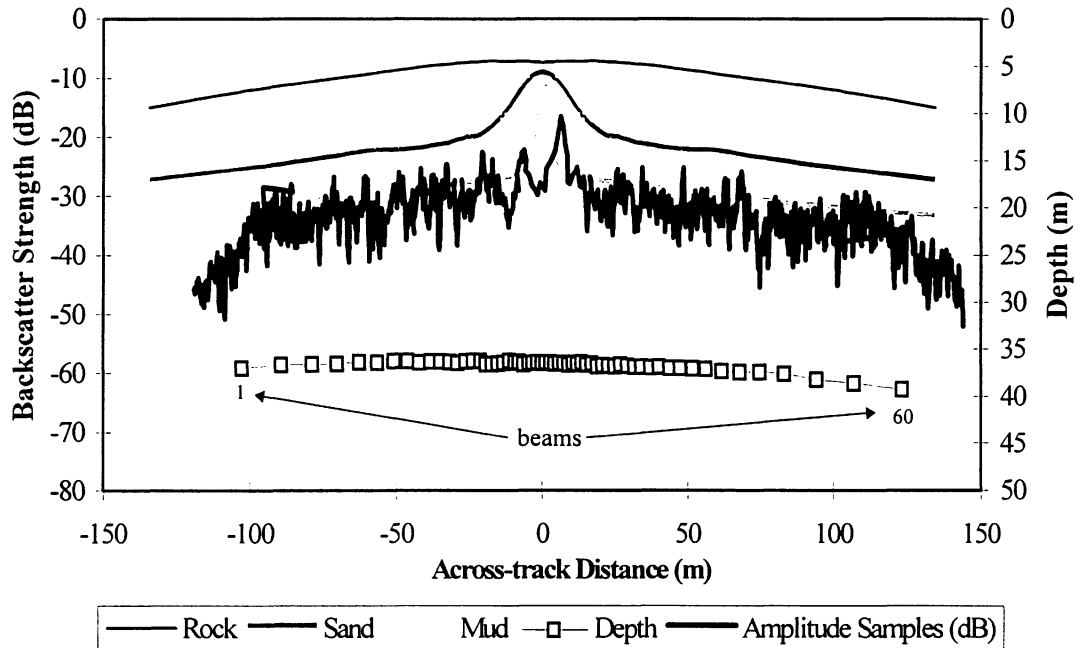


Figure 5.1. Backscatter information from the *Empress of Ireland* data set. The amplitude samples were corrected by removing the Lambertian correction and filtered by the use of a moving average filter. The theoretic sediment curves are computed by Jackson's model.

Figure 5.1 depicts the approach of using the generic sediment curves obtained by Jackson's model (acoustic frequency 95 KHz), for a coarse classification of the seafloor, in the *Empress of Ireland* area. This example indicates that the seafloor is closer to mud than sand or rock.

Figure 5.2 provides basically the same information, but a sixth order polynomial was fitted to the backscatter samples, also corrected by removing the Lambertian effect. If one excludes the most outer beams and the inner beams, it is possible to verify that the differences from the filtered backscatter samples, with respect to the theoretical curve for

mud, are less than about 3 dB, being the trend line parallel to the generic curve.

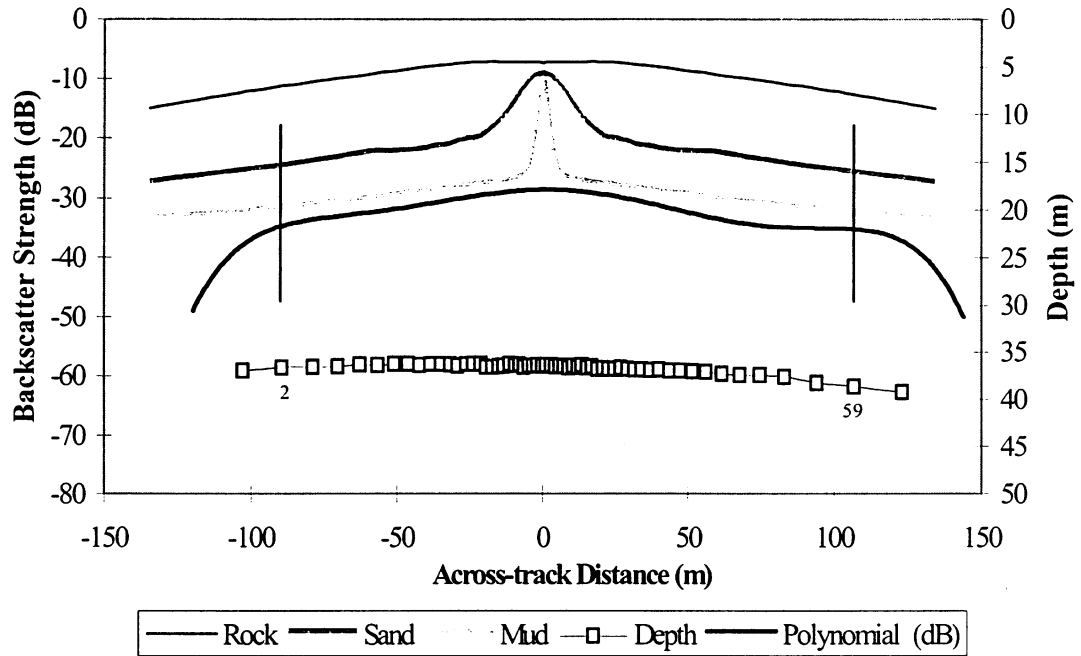


Figure 5.2. Backscatter information from the *Empress of Ireland* data set (same as previous figure). The backscatter strength is now presented by a sixth order polynomial which was fitted to the amplitude samples.

It is important to stress that for the beams near nadir, there are few backscatter samples. When fitting the polynomial to the amplitude samples, the amplitudes of the beams near nadir tend to be more easily filtered out. However, this is the area where the value of S_N is not recorded and it is not possible to correct for the flattening, consequently these values cannot be used in the graphical comparison.

In the presence of profiles from a non-flat bottom, to compare the backscatter strength with the theoretic curves from Jackson's model, further corrections are required (this includes the corrections for slope, i.e., grazing angle, and the corrections for the

enssonified area).

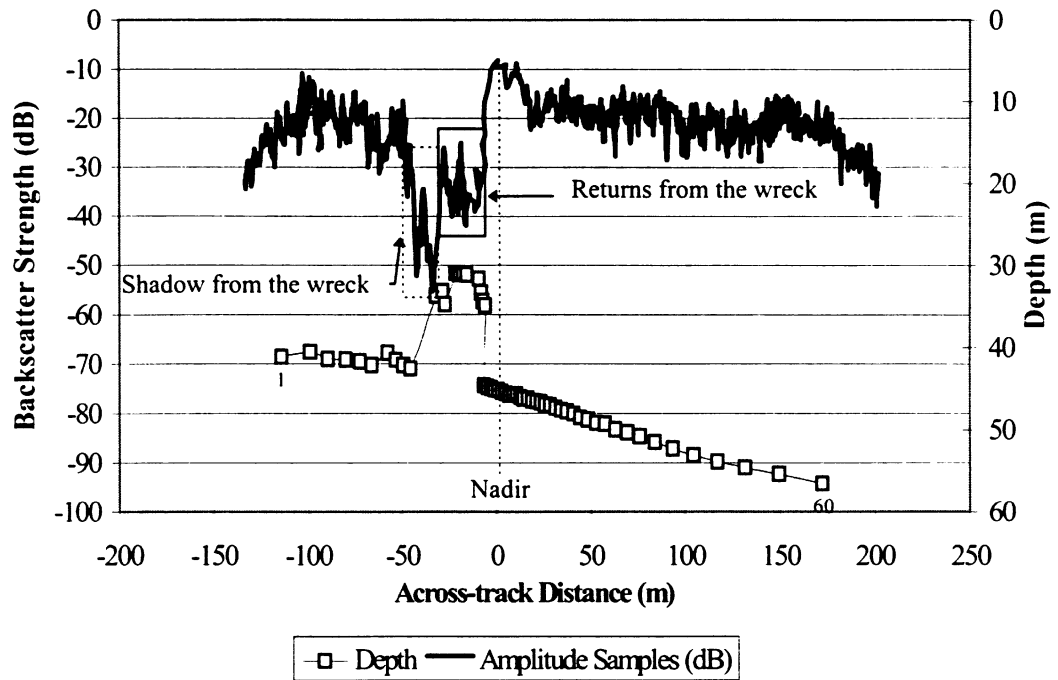


Figure 5.3. Backscatter information from the *Empress of Ireland* data set. This figure represents the detection of a wreck. The amplitude samples correspond to the raw data without corrections (filtered out using a moving average filter in order to reduce the noise).

Figure 5.3 depicts the depth anomaly created by the *Empress of Ireland*; this anomaly is emphasized by the shadow resulting from the obstruction created by the wreck to the propagation of the acoustic wave (approximately athwartships direction). This backscatter strength is given by the strength of the background noise, and it decreases when the returns are from the wreck (to a value of the order of -50 dB). This decrease depends on the reflective properties and on the angle of incidence of the acoustic ray.

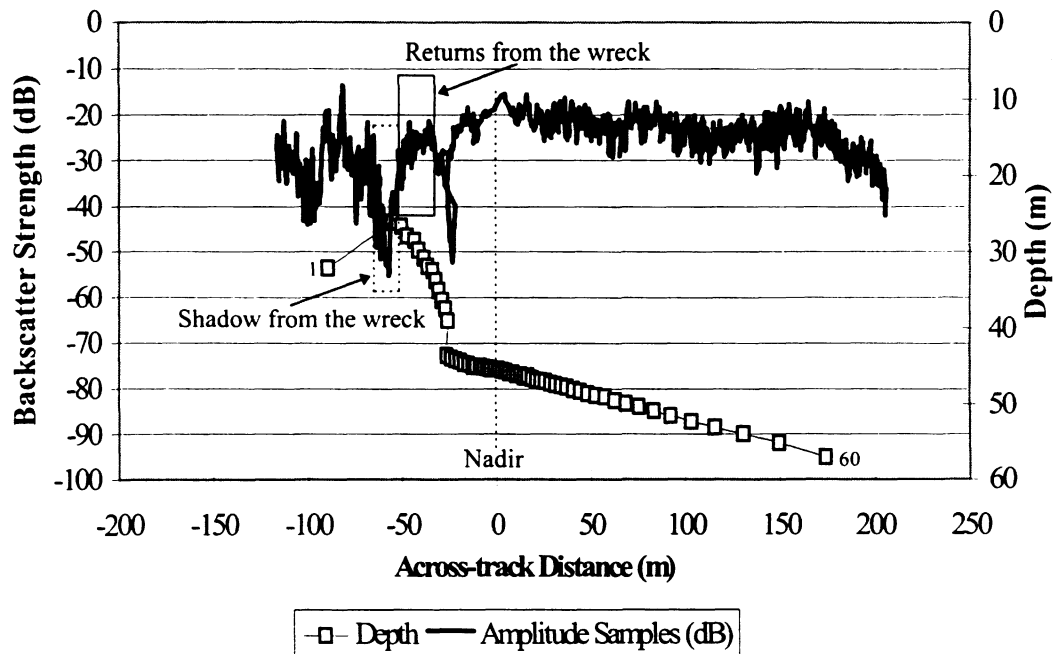


Figure 5.4. Backscatter information from the *Empress of Ireland* data set. Same as previous figure, but detected from a different azimuth.

Figure 5.4 depicts the depth anomaly created by the *Empress of Ireland*, but seen from a different azimuth (approximately fore-aft direction). The anomaly is also emphasized by the shadow resulting from the obstruction, created by the wreck to the propagation of the acoustic wave. The backscatter strength decreases, approximately to the same level (-50 dB). The returns from the wreck are stronger than in Figure. 5.4. From the depth information, one can conceive that this part of the wreck has a more regular surface.

Figures 5.3 and 5.4 exemplify how the backscatter strength can be efficiently used to detect bathymetric anomalies.

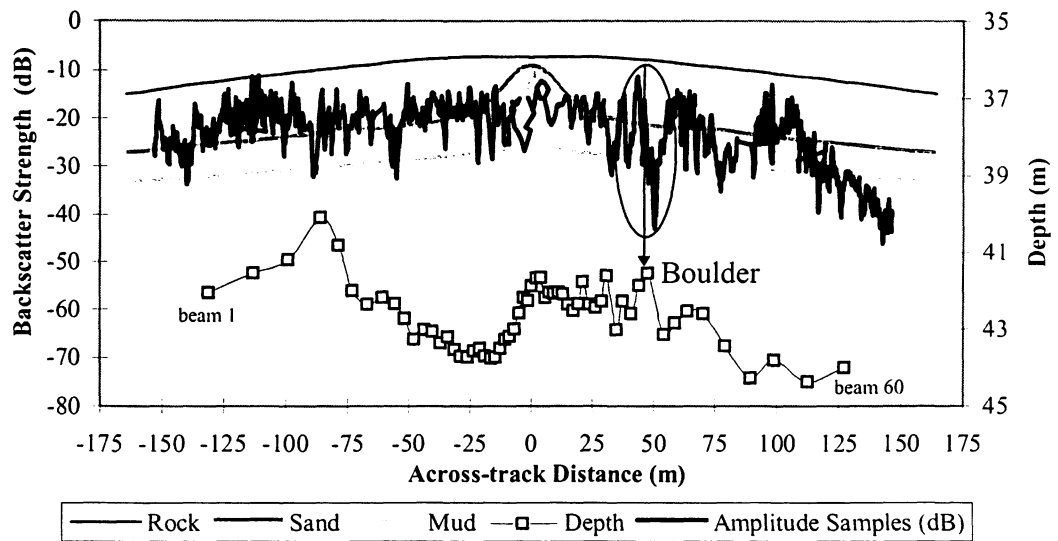


Figure 5.5. Backscatter strength from the *Halifax Approaches* data set from a rocky area. The amplitude samples were corrected by removing the Lambertian correction and filtered by the use of a moving average filter. The theoretic sediment curves are computed by Jackson's model.

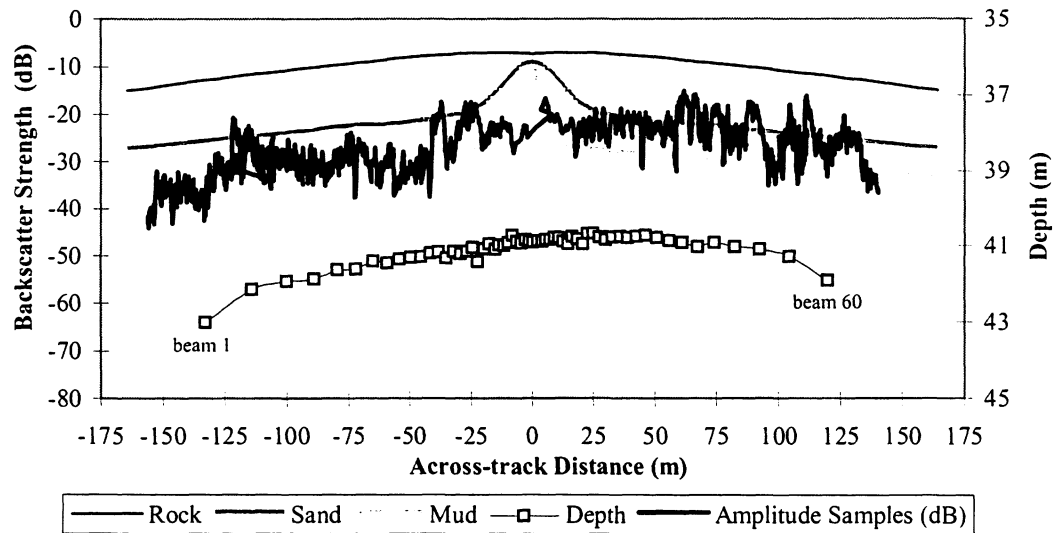


Figure 5.6. Backscatter strength from the *Halifax Approaches* data set for a sandy area. The amplitude samples were corrected by removing the Lambertian correction and filtered by the use of a moving average filter. The theoretic sediment curves are computed by Jackson's model.

Figures 5.5 - 5.7 present plots of the backscatter strength for three sites from the *Halifax Approaches* data set, corresponding to different acoustic sediment types. The location of these samples is approximately the same where sediment samples were collected during the “*Ground Truthing*” project. The graphical comparison of the backscatter traces shows that the backscatter trace from the rocky area, Figure 5.5, is closer from the theoretical curve for sand. The backscatter trace from a sandy area, Figure 5.6, is reasonably close from the theoretical curve for sand, but the backscatter trace from a sandy area with lower reflectivity, Figure 5.7, presents high variation of the backscatter strength and is closer from theoretical curve for mud.

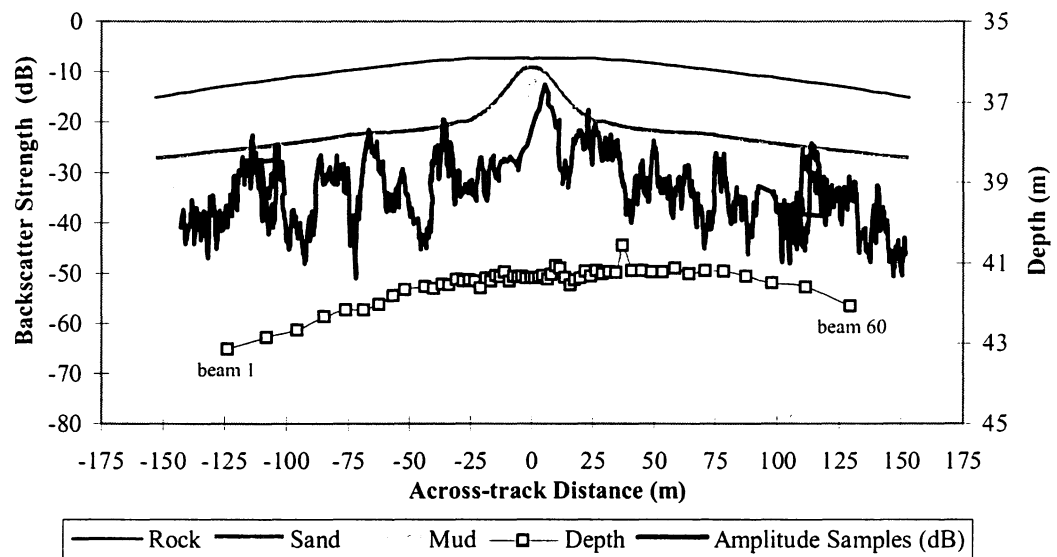


Figure 5.7. Backscatter strength from the Halifax Approaches data set for a sandy area with lower reflectivity. The amplitude samples were corrected by removing the Lambertian correction and filtered by the use of a moving average filter. The theoretic sediment curves are computed by Jackson’s model.

5.3. Results

This section discusses the results from the data cleaning and analysis of the two test data sets. For illustrative purposes, relevant figures concerning this analysis are presented in Appendices B and C.

5.3.1. Automatic and Interactive Data Cleaning Tests

From the comparison of the mean surfaces resulting from the interactive and automatic data cleaning, it is important to stress that the results match quite well. Situations for which differences between the methods occur are identified as follows:

- **regular areas with low redundancy**

The differences are mainly for the outer beams. In hydrographer's interactive analysis, the tendency is to remove soundings inside the measurement uncertainty of the system and to keep the shallower information. The automatic method considers the average of all the soundings, therefore it is a more objective criterion.

- **regular areas with high redundancy**

In the interactive method, when systematic errors exist, the hydrographer tends to be more conservative, keeping the shallowest soundings. In the automatic method, since all soundings are valid information, they are all used to compute the mean surface, which can have a small bias, that is, this method removes objectively the systematic errors without taking into consideration if they are shallower or deeper than the mean

surface.

- **irregular areas (wrecks and boulders)**

The automatic method rejects vital information (minimum depths) when applied to an irregular area. The interactive method tends to preserve, by safety reasons, the minimum depths.

From the two studied cases, there are other interesting results that are important to stress:

- From the *Halifax Approaches*, scattered blunders were detected (Figure c.35). These blunders occurred between beams 24 and 36, with a depth difference of 2 to 3.5 metres (in 30 to 40 metres water depth). These gross errors were better highlighted in the residual and depth difference surfaces than in the standard deviation surface. These blunders were completely flagged out by the automatic methods while the interactive methods had a tendency to leave some of these soundings, when browsing the soundings using the standard deviation surface.
- For the areas with low overlapping among swaths, there were many more soundings flagged out for the outer beams in BINSTAT than in HDCS; this was caused by the larger size of the cell dimension used in BINSTAT.

5.3.2. Backscatter Tests on Data Cleaning

This section presents the results from the backscatter tests for the two studied data sets. For illustrative purposes relevant figures concerning this analysis are also

presented in Appendices B, and C.

- The analysis of the backscatter from the *Empress of Ireland* showed that the target is highlighted by the shadow created on the adjacent area of the seafloor; in the studied cases, the backscatter strength decreased to a level of near -50 dB.
- Backscatter variations on the acoustic image were, in general, correlated with the standard deviation surface. This provides means of clearing up doubts about bathymetric features. (Figures c.18 and c.22).
- The ping analysis, from the *Empress of Ireland* data set, shows that the amplitude samples from beam one and beam sixty, present a considerable decreasing of backscatter strength.
- The data presented a noise of about 10 dB. The raw data needs to be filtered to remove the major part of the noise; in this study, a simple moving average filter was used.
- The comparison of the data with the Jackson's model cannot be used for incidence angles smaller than 10 degrees. The backscatter strength is lower than the estimated with Jackson's model for the theoretic parameters (Figures 5.5 and 5.7).
- The bottom detection revealed that conspicuous features (e.g. wrecks or boulders) were detected by the amplitude method (Figure c.11 and c.44), even for beam angles where the prevailing method is phase detection. This can be explained by the inward face of that object that should produce a higher backscatter return, or due to the high

variation of the line fit to the sequence of the differential phase samples.

- For the *Halifax Approaches*, blunders were detected by phase in areas where the prevailing method is amplitude detection (Figures c.31 and c.35).
- The quality factor (given by the Simrad EM 1000), has different meanings for amplitude and for phase detection. For phase detection, it was seen that the quality factor decreases from the inner to the outer beams approaching zero (Figures c.42 and c.46). However, in the presence of irregularities, the quality factor does not approach zero (Figure c.14). For amplitude detection, the quality factor is low for the inner beams (reduced number of samples, see Figure c.46). For the outer beams, an amplitude detection means the existence of bathymetric features, and usually the quality factor has a higher value. This is due to the increased number of samples used in the algorithm to base the decision on amplitude detection (Figure c.46). The results are not conclusive regarding the use of the quality factor. However, this factor associated with the amplitude detection, can provide additional information.

For the *Halifax Approaches* data set (Figure c.39) a sequence of interactive procedures with BINSTAT is used to analyze an irregular area using the information of the backscatter and of the bottom detection analysis (Figures c.40 - c.46).

5.4. Improvements to Data Cleaning

Table 5.2 is a simplified summary of some of the functions that were used to

investigate the potential of HDCS and BINSTAT.

	HDCS	BINSTAT
Swath Display	phase/amplitude detection side scan side view rear view gyro heave pitch roll profile	N/A
Subset Surfaces	weight mean depth weight standard deviation coverage	mean depth standard deviation minimum depth maximum depth residual difference depth difference valid points beam amplitudes phase/amplitude detection
Swath Flagging Tools	automatic interactive	N/A
Subset Flagging Tools	real-time cross-sections classification level	correlation plots (see Table 5.1)
Systematic Errors	calibration tools	calibration tools
Gyro, Heave, Roll, Pitch and Tide Display	time series editor	N/A
Navigation	positioning editor automatic filter	positioning editor automatic filter
Final Format	Caris format	X, Y, Z format

Table 5.2. Simplified summary of characteristics from HDCS and BINSTAT.

The two software packages have different orientations: HDCS with swath and subset visualization tools by profiles, and BINSTAT with correlation plots of several parameters.

Some suggestions to improve both software packages are:

HDCS

- The radius of the field of influence should be adjusted by the user, as a function of the characteristics of the MBES (beam spacing, ping repetition rate, and ship's speed) and of the overlapping among swaths.
- A residual surface given as a by-product of the mean surface (defined by the difference of every sounding from the mean surface) can be useful to detect blunders in areas with high-density of information.
- Visualization of the side scan image in the subset mode can bring further detail in terms of the spatial distribution of sediment types.
- Visualization of bottom detection method in the subset mode; this feature is relevant for wrecks and boulders identification.

BINSTAT

- Visualization of soundings by profiles, and possibility to rotate the blocks; these features provide an easier way to visualize the data, specially when considering the interactive data cleaning.
- Visualization of the information of gyro, heave, roll, and pitch.
- Store the administrative information (source identification, tide correction, and date) in the final data format.

The following suggestions are proposed for both packages:

- Use the uncertainty of the depth measurement, ϵ_z , as an attribute for every sounding. This attribute can be efficiently used on the calculation of the mean surface, and every sounding could be weighted with this value. This would provide a better comparison of soundings with different accuracies.
- Classification of the soundings using a criterion of residuals proportional to the depth. This is important for areas with large variation in depth.
- The final format of the basic data product should include an attribute assessing the quality of the sounding, which can be set as the standard deviation of the cleaned data set.

Chapter 6

CONCLUSIONS AND RECOMMENDATIONS

For hydrographic paper chart purposes, the main requirement is the detection of all **minimum** depths, rather than the accurate representation of all soundings on the seafloor. With the advent of the electronic chart, both accuracy and high density of information, will be required.

Multibeam systems will contribute, definitively, for the new era of hydrographic surveying by achieving one hundred percent bathymetric coverage of the seafloor and a knowledge of seafloor geology (type of sediment).

Multibeam data cleaning has specific rules that should be quite well understood by the hydrographer, this is due to the beam geometry. Theoretically, there are no restrictions on the distribution of soundings, and it is possible, although not likely, to have structures not connected with the seafloor. In this sense, one can have different depth information of the seafloor, depending on the beam pointing angle, and this can be depicted by a bow of a wreck not laid down on the seafloor. This leads to two different depths depending on when the beams hit the bow of the wreck or when they pass beneath the bow hitting the seafloor (this is an extreme case, however, the hydrographer must be aware of this possibility). In other situations, it is possible to have similar behavior but, in these cases, due to the existence of blunders in the data set. Consequently, it is highly

probable that automatic methods will perform differently from hydrographer's decision in both cases.

In the next sections, conclusions on the data cleaning methods and potential of the backscatter information are summarized.

6.1. Automatic Data Cleaning Methods

Both interactive and automatic tools are required for data cleaning, but the decision on which to use depends on the characteristics of the area. Sandy or muddy seafloor should have relatively smooth bathymetry. Those areas can be analyzed by automatic data cleaning tools. This study concludes that in regions of relatively smooth bathymetry the results for the proposed automatic procedures and for the subjective interactive data cleaning methods are similar. The main differences are for the areas with low density of soundings and affected by systematic errors. This can be solved if every spot on the seafloor has information, at least, from one beam meeting the survey depth measurement accuracy.

For irregular areas or areas with strong bathymetric features (wrecks and boulders), the automatic data cleaning gives different results when compared with the subjective interactive data cleaning. For these areas, one should use the interactive method to preserve all minimum soundings determined to not be blunders.

It is important to stress that, for automatic data cleaning, it is necessary to choose

an appropriate cell dimension and to have available information about the depth measurement uncertainty by beam, assessed by using models, or by the comparison of the depth measurement with a known bathymetric surface.

The sequence of procedures defined in Chapter 4, is an attempt to ensure the objectivity of the data cleaning sequence. By using the same software one ends up with equivalent results. This strategy provides means for filtering almost all the resulting errors from the refraction effect on the outer beams. It is however, concluded that the outer beams, well outside the survey accuracy specifications, need to be rejected before using the use of the automatic procedures.

The residuals in the HDCS are not directly accessible by the users, they need to query several soundings and to calculate the difference of the sounding from the mean surface. A residual surface, as a by-product of the mean surface, can provide useful information about blunders on areas with high-density of soundings.

BINSTAT does not provide visualization of sounding profiles. The implementation of tools to visualize the data by profiles, i.e., in the spatial domain is considered an important possible improvement to this module. An alternative is to provide a means to rotate the blocks. In this way, it would be possible to use the correlation plots to visualize the profiles, by selecting the bins on the athwartships direction.

The value of the acceptance region varies with the depth (percentage of water depth), therefore the acceptance for the residuals should also be set as a percentage of the

water depth. Neither HDCS nor BINSTAT provides the capability of flagging automatically soundings, based on the limit value for the residuals as a function of depth and they should provide this capability.

In general, it is important to stress that the knowledge of the hydrographer about the data cleaning algorithms, multibeam, and seafloor characteristics, will contribute definitely to the improvement of the multibeam data cleaning task.

The survey planning should provide reciprocal and check lines to look respectively for remaining roll offset and sound velocity profile errors.

For deep waters, the risk of hazards to navigation decreases and the footprint coverage for each beam increases. In this sense, one has a greater overlapping in the along-track direction which increases for the outer beams. The achieved redundancy allows a less restrictive use of the automatic procedures.

6.2. Potential of the Backscatter

Backscatter is a source of information for seafloor classification, and for the detection of irregularities on the seafloor. In the case of doubts in the identification of the soundings related to the seafloor, it is strongly recommended to use the backscatter samples, or the acoustic image to look for anomalies. This should be used in extreme situations, or *a priori* to look for areas where troubles exist and in this way, to focus the attention of the hydrographer.

The analysis of the backscatter from the *Empress of Ireland* showed that the target is highlighted by the shadow created on the adjacent area of the seafloor, the backscatter decreases to a level of near -50 dB. The expected increase of the backscatter strength from the wreck returns, was not confirmed. However, for the *Halifax Approaches*, boulders increase locally the backscatter strength, and some of them also presented a decrease of the backscatter (shadow on the adjacent area of the seafloor).

The correlation of the acoustic image with the bathymetry is a useful information, which can provide means of clearing up doubtful features in the bathymetry. The use of the acoustic image in an initial phase of the data cleaning is strongly recommended, not only to detect anomalies in the seafloor, but also for a rough identification of the seafloor type and consequently, to define the regular and irregular areas, where either automatic or interactive methods should be used.

The bottom detection indicators revealed that conspicuous features (e.g. wrecks or boulders), were detected by the amplitude method, even for beam pointing angles where the prevailing method is the phase detection. Blunders were detected by phase in areas where the prevailing method is amplitude detection.

The results are not conclusive for the use of the quality factor. However, this factor associated with the amplitude detection may provide some additional information to decide about the acceptance or rejection of soundings.

6.3. Future Studies

From the present report, further efforts in several directions are recommended.

They are summarized as follows:

- Study of backscatter models for frequencies higher than 100 KHz,
- Study of the reflective properties of materials, used to build hull and super-structures of ships,
- Study the dimension of the features able to be detected by multibeam echosounders,
- Investigation of algorithms used to define regular (sandy and muddy seafloor) and irregular (wreck and bedrock) areas, to define automatically when to apply automatic or interactive methods,
- Study of the surface roughness to be applied in the sounding acceptance region,
- Compare the percentage of outliers from the new generation of shallow water multibeam echosounders, with previous systems.

REFERENCES

- APL (1994). *High-Frequency Ocean Environmental Acoustic Models Handbook*. TR 9407 - AEAS 9501, University of Washington.
- Bendat, J. and A. Piersol (1986). *Random Data*. John Wiley & Sons, Inc.
- Berkson, J. and J. Matthews (1984). "Statistical Characterization of Seafloor Roughness." *IEEE Journal of Oceanic Engineering*, Vol. OE-9, No. 1, pp. 48-51.
- Clay, C. and H. Medwin (1977). *Acoustical Oceanography*. John Wiley & Sons, Inc.
- de Moustier, C. and D. Alexandrou (1991). "Angular Dependence of 12 KHz Seafloor Acoustic Backscatter." *The Journal of the Acoustical Society of America*, Vol. 90, No. 1, pp. 522-531.
- de Moustier, C. and M. Kleinrock (1986). "Bathymetric Artifacts in Sea Beam Data: How to Recognize Them and What Causes Them." *Journal of Geophysical Research*, Vol. 91, No. B3, pp. 3407-3424.
- de Moustier, C. (1988). "State of the Art in Swath Bathymetry Survey Systems." *International Hydrographic Review*, LXV(2), p. 25.
- de Moustier, C. (1993). "Signal Processing for Swath Bathymetry and Concurrent Seafloor Acoustic Imaging." *Acoustic Signal Processing for Ocean Exploration*, J.M.F. Moura and I.M.G. Lourtie Eds., pp. 329-354.
- de Moustier, C. (1995). "Backscatter Theory." *Lecture VII from Coastal Multibeam Hydrographic Surveys*. United States / Canada Hydrographic Commission Multibeam Working Group, St. Andrews, New Brunswick, Canada.
- Du, Z. (1995). *Uncertainty Handling in Multibeam Bathymetric Mapping*, Ph.D. dissertation, Department of Geodesy and Geomatics Engineering, University of New Brunswick, Fredericton, N.B. Canada.
- Du, Z., L. Mayer, and D. Wells (1995a). "An Approach to Automatic Detection of Outliers in Multibeam Echosounding Data." Department of Geodesy and Geomatics Engineering, University of New Brunswick, Fredericton, N.B. Canada.
- Du, Z., L. Mayer, and D. Wells (1995b). "Outliers in Swath Sounding Data and their Automatic Detection." Department of Geodesy and Geomatics Engineering, University of New Brunswick, Fredericton, N.B. Canada.

- Eeg, J. (1995). "On the Identification of Spikes in Soundings." *International Hydrographic Review*, Monaco, LXXII(1), March, pp. 33-41.
- General Instrument Corporation, (1975). *Sea Beam for Precision Bathymetric Survey*. Government Systems Division, United States.
- Gensane, M. (1989). "A Statistical Study of Acoustic Signals Backscattered from the Sea Bottom." *IEEE Journal of Oceanic Engineering*, Vol. 14, No. 1, January, pp. 84-93.
- Godin, A. (1996). "The Calibration of Shallow Water Multibeam Echo-Sounding Systems." *Proceedings of the Canadian Hydrographic Conference '96*, Halifax, NS, Canada, pp. 25-31.
- Gott, R. (1995). *Remote Seafloor Classification Using Multibeam Sonar*. PhD Dissertation, Tulane University.
- Greenburg, A. (1987). "Statistical Filtering of Bathymetric Data". *ASPRS-ACSM*, Fall Convention, Nevada, October.
- Grim, P. (1988). "The COP Algorithm for Selecting Soundings within a PUA". Draft Report, National Oceanic and Atmospheric Administration, Rockville, MD.
- Guenther, G. and J. Green (1982). "Improved Depth Selection in the Bathymetric Swath Survey System (BS3) Combined Offline Processing (COP) Algorithm." National Oceanic and Atmospheric Administration, Technical Report OTES-10, Department of Commerce, Rockville, MD.
- Hammerstad E., F. Pøhner, F. Parthiot, and J. Bennett (1991). "Field Testing of a New Deep water Multibeam Echo-sounder." *Proceedings IEEE Oceans '91*, pp 743-749.
- Hammerstad E. (1994). "Backscattering and Sonar Image Reflectivity." *EM 12/950/1000 Technical Note*, Simrad Subsea AS, Horten, Norway, 6 p.
- Hammerstad E. (1995). "Simrad EM 950/1000 - Error Model for Australian Navy." Extract of Report, Simrad Subsea AS, Horten, Norway, 4 p.
- Hare R. A. Godin (1996). "Estimating Depth and Positioning Errors for the Creed/ EM 1000 Swath Sounding System." *Proceedings of the Canadian Hydrographic Conference '96*. Halifax, NS, Canada, pp. 9-15.
- Herlihy, D., B. Hillard, and T. Rulon (1989). "National Oceanic and Atmospheric Administration Sea Beam System - Patch Test." *International Hydrographic Review*, Monaco, LXVI(2), pp. 119-139.

- Herlihy, D., T. Stepka, and T. Rulon (1992). "Filtering Erroneous Soundings from Multibeam Survey Data." *International Hydrographic Review*, Monaco, LXIX(2), September, pp. 67-76.
- Hughes Clarke, J. (1993a). *Analysis of Residual Roll and Heave Errors Identified During the Matthew Motion Sensor Trials*. DFO Contract FP962-3-4602, Ocean Mapping Group, Department of Geodesy and Geomatics Engineering, University of New Brunswick, Fredericton, Canada.
- Hughes Clarke, J. (1993b). *NSC Frederick G. Creed Cruise Report*. IML 93-042 - 2nd - 21st. August 1993. Ocean Mapping Group, Department of Geodesy and Geomatics Engineering, University of New Brunswick, Fredericton, Canada.
- Hughes Clarke, J. (1995a). "Reference Frame and Integration." *Lecture IV-1 from Coastal Multibeam Hydrographic Surveys*. United States / Canada Hydrographic Commission Multibeam Working Group, St. Andrews, New Brunswick, Canada.
- Hughes Clarke, J. (1995b). "Interactive Bathymetry Data Cleaning." *Lecture X-4 from Coastal Multibeam Hydrographic Surveys*. United States / Canada Hydrographic Commission Multibeam Working Group, St. Andrews, New Brunswick, Canada.
- Hughes Clarke, J. (1995c). "Backscatter Interpretation." *Lecture VII-4 from Coastal Multibeam Hydrographic Surveys*. United States / Canada Hydrographic Commission Multibeam Working Group, St. Andrews, New Brunswick, Canada.
- Hughes Clarke, J. (1995d). "Imaging with Swath Sonars." *Lecture III-4 from Coastal Multibeam Hydrographic Surveys*. United States / Canada Hydrographic Commission Multibeam Working Group, St. Andrews, New Brunswick, Canada.
- Hughes Clarke, J. (1995e). "Sonar Backscatter Mosaicing." *Lecture XI-11 from Coastal Multibeam Hydrographic Surveys*. United States / Canada Hydrographic Commission Multibeam Working Group, St. Andrews, New Brunswick, Canada.
- Hughes Clarke, J. (1996). "Refraction III, Post-Acquisition Corrections", Lecture 39 *Coastal Multibeam Hydrographic Surveys*. United States / Canada Hydrographic Commission Multibeam Working Group, St. Andrews, New Brunswick, Canada.
- Hughes Clarke, J., L. Mayer, and D. Wells (1994), "Shallow-Water Imaging Multibeam Sonars: A New Tool for Investigating Seafloor Processes in the coastal Zone and on the Continental Shelf." *Marine Geophysical Research*, pp. 1-20.
- Huseby, R., O. Milvang, A. Solberg, and K. Weisteen (1993), "Seabed Classification from Backscatter Sonar Data Using Statistical Methods." *Proceedings of the Institute of Acoustics*, Vol. 15 Part 2, pp. 415-420.
- Instituto Hidrográfico (1994). *Curso de Introdução aos Sistemas Sondadores Multifeixe*. Marinha, Ministério da Defesa Nacional, Lisboa.

- IHO (1987). *IHO Standards for Hydrographic Surveys*. Special Publication No 44. 3rd Edition. International Hydrographic Organization, Monaco.
- IHO (1996). *IHO Standards for Hydrographic Surveys*. Special Publication No 44. draft of the 4th Edition. International Hydrographic Organization, Monaco.
- Jackson, D., A. Baird, J. Crisp, and P. Thomson (1986). "High Frequency Bottom Backscatter Measurements in Shallow Water." *The Journal of the Acoustical Society of America*, Vol. 80, No. 4, pp. 1188-1199.
- Jackson, D., D. Winebrenner, and A. Ishimaru (1986a). "Application of the Composite Roughness Model to High-Frequency Bottom Backscattering." *The Journal of the Acoustical Society of America*, Vol. 79, No. 5, pp. 1411-1422.
- Jackson, D., A. Baird, J. Crisp, and P. Thomson (1986b). "High Frequency Bottom Backscatter Measurements in Shallow Water." *The Journal of the Acoustical Society of America*, Vol. 80, No. 4, pp. 1188-1199.
- Jackson, D., and K. Briggs (1992). "High Frequency Bottom Backscattering: Roughness Versus Sediment Volume scattering." *The Journal of the Acoustical Society of America*, Vol. 92, No. 2, pp. 962-977.
- Kuo E. (1964). "Wave Scattering and Transmission at Irregular Surfaces." *The Journal of the Acoustical Society of America*, Vol. 36, No. 11, pp. 2135-2142.
- Laurini, R. and D. Thompson (1992). *Fundamentals of Spatial Information Systems*. Academic Press Ltd., London, United Kingdom.
- Matsumoto, H., R. Dziak, and C. Fox (1993). "Estimation of Seafloor Microtopographic Roughness Through Modeling of Acoustic Backscatter Data Recorded by Multibeam Sonar Systems." *The Journal of the Acoustical Society of America*, Vol. 94, No. 5, pp. 2776-2787.
- McCullagh, M., and Ross, C. (1980). "Delaunay Triangulation of a Random Data Set for Isarithmic Mapping." *The Cartographic Journal*, Vol. 17, N. 2, pp. 93-99.
- McDaniel, T. and A. Gorman (1983). "An Examination of the Composite-Roughness Scattering Model." *The Journal of the Acoustical Society of America*, Vol. 73, No. 5, pp. 1476-1486.
- Midthassel, A., E. Sølvsberg, and F. Pøhner (1988). "Data Management of Swath Sounding Systems." *International Hydrographic Review*, Vol. LXV(2), July, pp. 117-125.
- Milvang, O., R. Huseby, K. Weisteen, and A. Solberg (1993). "Feature Extraction from Backscatter Sonar Data." *Proceedings of the Institute of Acoustics*, Vol. 15 Part 2, pp. 157-164.

- Mourad, P. and D. Jackson (1989). "High Frequency Sonar Equation Models for Bottom Backscatter and Forward Loss." *Oceans '89 Proceedings*, New York.
- NOAA (1986). *The Geodetic Glossary*. National Oceanic and Atmospheric Administration, MA, US.
- Novarini, J. and J. Caruthers (1994). "The Partition Wavenumber in Acoustic Backscattering from a Two-Scale Rough Surface Described by a Power-Law Spectrum." *IEEE Journal of Oceanic Engineering*, Vol. 19, No. 2, pp. 200-206.
- Ogilvy, J. (1992). *Theory of Wave Scattering from Random Rough Surfaces*. IOP Publishing Ltd. London.
- Press, W., S. Teukolsky, W. Vetterling, and B. Flannery (1994). *Numerical Recipes in Fortran -- The Art of Scientific Computing*. Cambridge University Press, New York.
- Pøhner, F. (1990). "Processing of Multibeam Echosounder Data." *The Hydrographic Journal*, No. 56, April, pp. 20-27.
- Pøhner, F. (1993). "Model For Calculation of Uncertainty in Multibeam Depth Soundings." Report from Simrad Subsea AS, Horten, Norway, FEMME 93. 16 p.
- Ringelberg, M. (1995). "Advisory Report: Analysis of Multibeam-Data in Shallow Water." *Proceedings Femme 95*, Biloxi, 19 p.
- Simrad Norge AS (1992). *Simrad EM 1000 - Maintenance Manual*. Horten, Norway.
- Simrad Norge AS (1995). *Neptune Post-Processing System - Operator Manual*. Horten, Norway.
- Simrad Norge AS (1996). *EM 3000 Multibeam Echo Sounder - Product Description*. Horten, Norway, pp. 13.
- Sirius Solutions, (1995). *Seebed - Brochure*. Dartmouth, N.S., Canada.
- STN Atlas Elektronik (1996). *Atlas Fansweep - Shallow Water Multibeam Sweeping Echosounder System*. Preliminary Edition, Germany.
- Tang, D., G. Jin, D. Jackson, and K. Williams (1994). "Analysis of High-Frequency Bottom and Subbottom Backscattering for Two Distinct Shallow Water Environments." *The Journal of the Acoustical Society of America*, Vol. 96, No. 5, pp. 2930-2936.
- Talukdar, K. and R. Tyce (1992). "Relation of Sea Beam Echo Peak Statistics to the Character of Bottom Topography." *Geo-Marine Letters*, New York.

- Universal Systems Ltd. (1992). *CARIS Geographic Information System*. Fredericton, Canada.
- Universal Systems Ltd. (1994a) *CARIS HIPS: Hydrographic Information Processing System*. Document Number HIPS USER-Jan-94-UNIX. Fredericton, Canada.
- Universal Systems Ltd. (1994b) *SIPS: Sidescan Image Processing System User's Guide*. Document Number SIPS USER-Jul-94-UNIX. Fredericton, Canada.
- Urick, R. (1975). *Principles of Underwater Sound*. McGraw-Hill, Inc.
- US/Canada HCMWG (1995). *Coastal Multibeam Hydrographic Surveys*. United States / Canada Hydrographic Commission Multibeam Working Group. St. Andrews, New Brunswick, Canada.
- Ware, C., D. Fellows, and D. Wells (1990). *Feasibility Study on the use of Algorithms for Automatic Error Detection in Data from the FCG Smith*. School of Computer Science, University of New Brunswick.
- Ware, C., L. Slipp, W. Wong, Y. Lee, B. Nickerson, D. Wells, D. Dodd, and G. Costello (1991a). "A System for Cleaning High Volume Bathymetry." *International Hydrographic Review*, Vol. LXIX(2), pp. 77-94.
- Ware, C., W. Knight, and D. Wells (1991b). "Memory Intensive Statistical Algorithms for Multibeam Bathymetric Data." *Computers and Geosciences*, Vol. 17. No. 7. pp. 985-993.
- Vanicek, P. (1996). *Advanced Adjustment Calculus*. Lecture Notes No. 18, Department of Geodesy and Geomatics Engineering, University of New Brunswick, Fredericton, N.B. Canada.
- Wells, D., B. Nickerson, and Y. Lee (1989). "Error Detection and Correction in Processing Large Bathymetric Data Sets." University of New Brunswick, Fredericton, Canada.
- Wells, D., C. Ware, B. Nickerson, Y. Lee, and L. Slipp (1990). "Requirements Analysis and Conceptual Design of Data Cleaning Tools for Large Bathymetric Data Sets." Ocean Mapping Group, University of New Brunswick, Fredericton, Canada.
- Wong, W. (1996). Personal Communication. Universal Systems Ltd., Fredericton, Canada.

Appendix A

CELL'S DIMENSION AND CLASSIFICATION

PARAMETERS

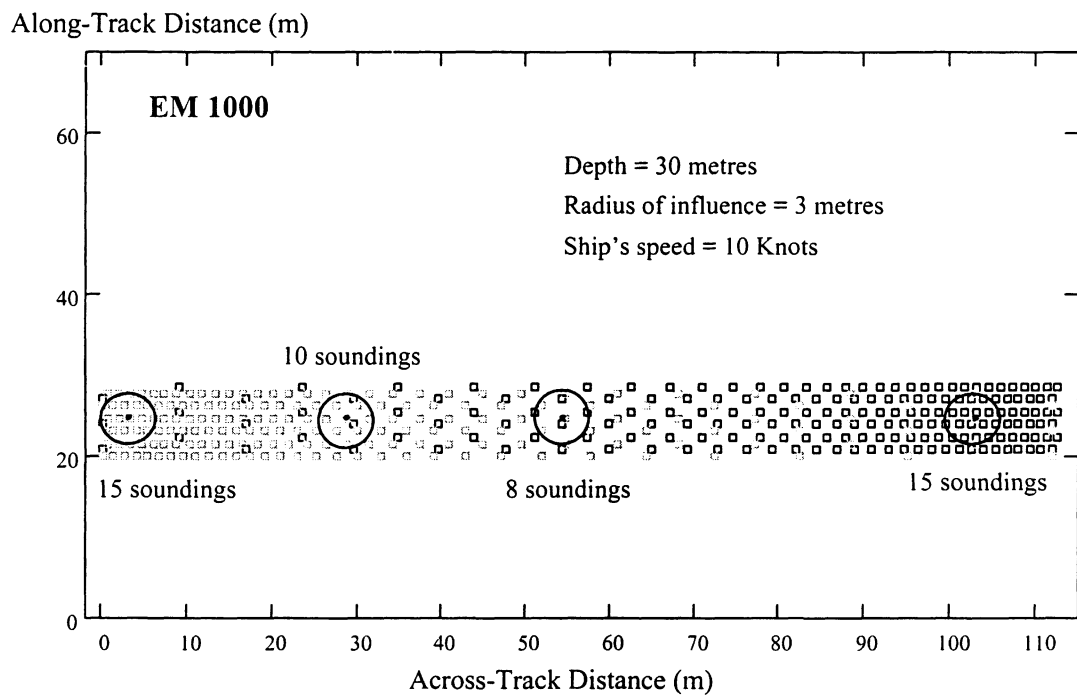


Figure a.1. Number of soundings gathered in the same radius of influence. Multibeam characteristics of the Simrad EM 1000, 200% ensonification of the seafloor, ship's speed 10 Knots, water depth 30 metres, and radius of influence 3 metres.

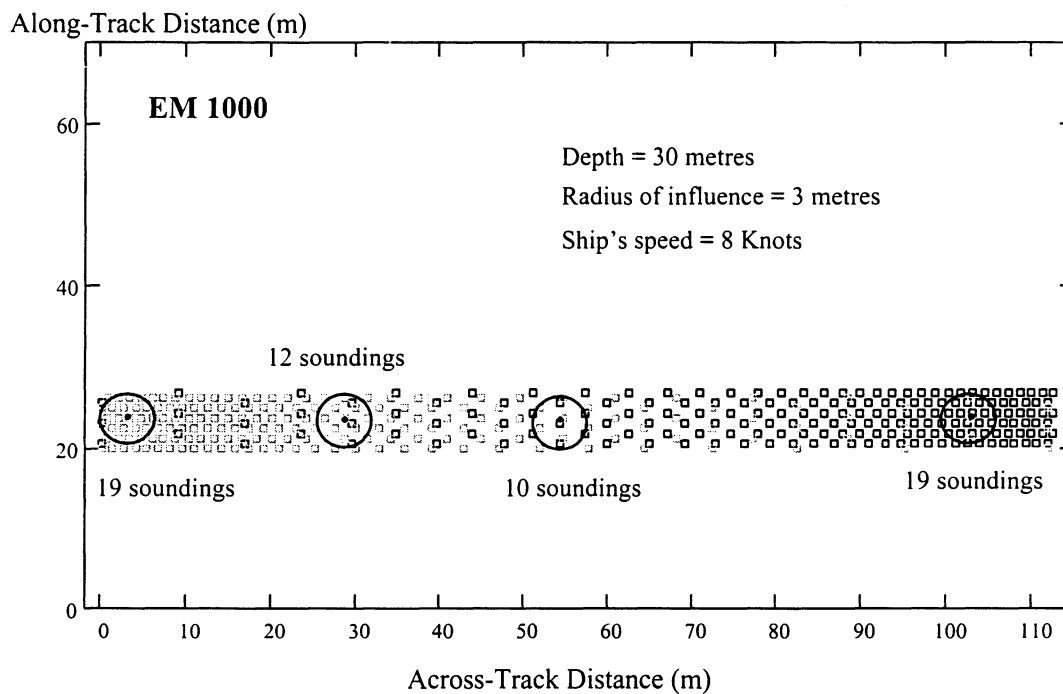


Figure a.2. Number of soundings gathered in the same radius of influence. Multibeam characteristics of the Simrad EM 1000, 200% ensonification of the seafloor, ship's speed 8 Knots, water depth 30 metres, and radius of influence 3 metres.

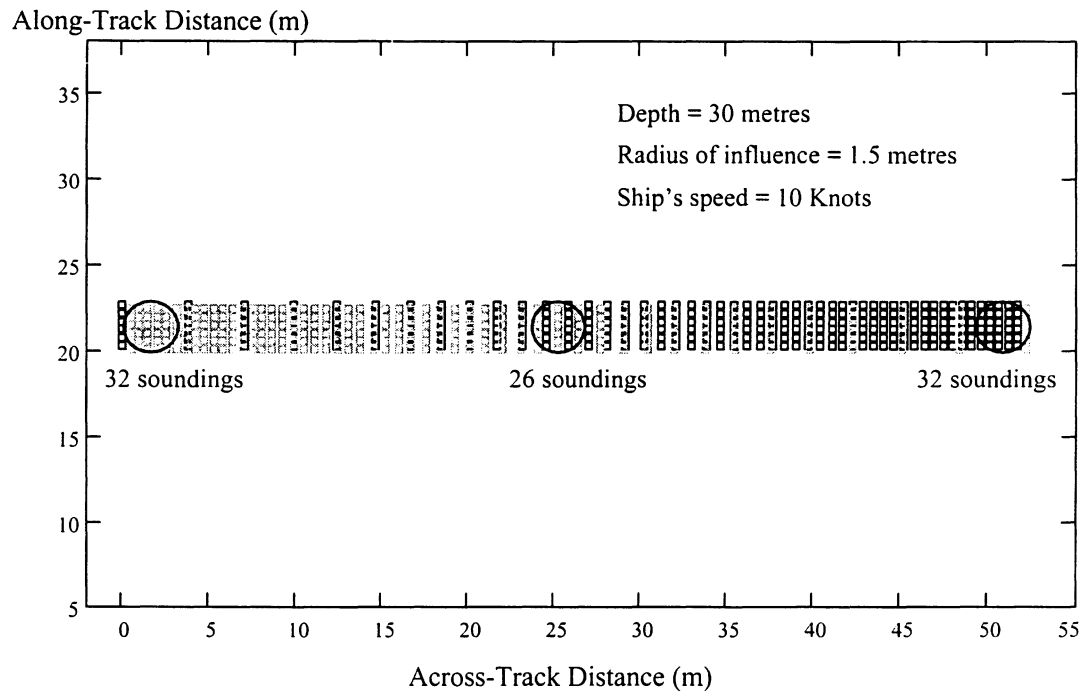


Figure a.3. Number of soundings gathered in the same radius of influence. Multibeam characteristics similar to the Simrad EM 3000, 200% ensonification of the seafloor, ship's speed 10 Knots, water depth 30 metres, and radius of influence 1.5 metres.

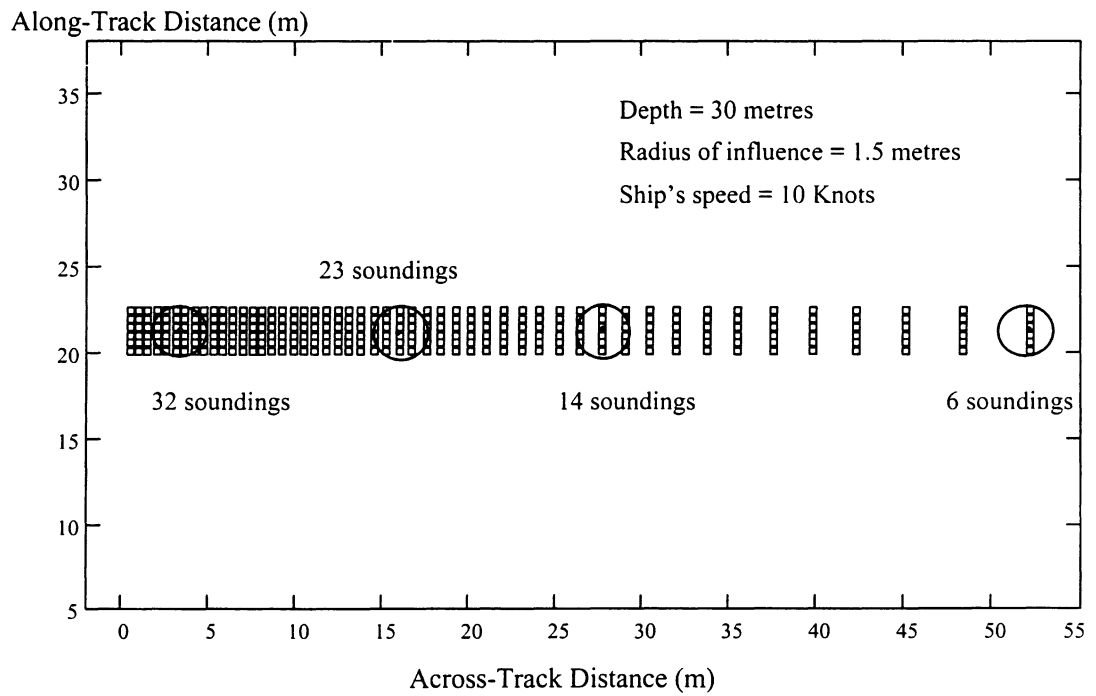


Figure a.4. Number of soundings gathered in the same radius of influence. Multibeam characteristics similar to the Simrad EM 3000, 100% ensonification of the seafloor, ship's speed 10 Knots, water depth 30 metres, and radius of influence 1.5 metres.

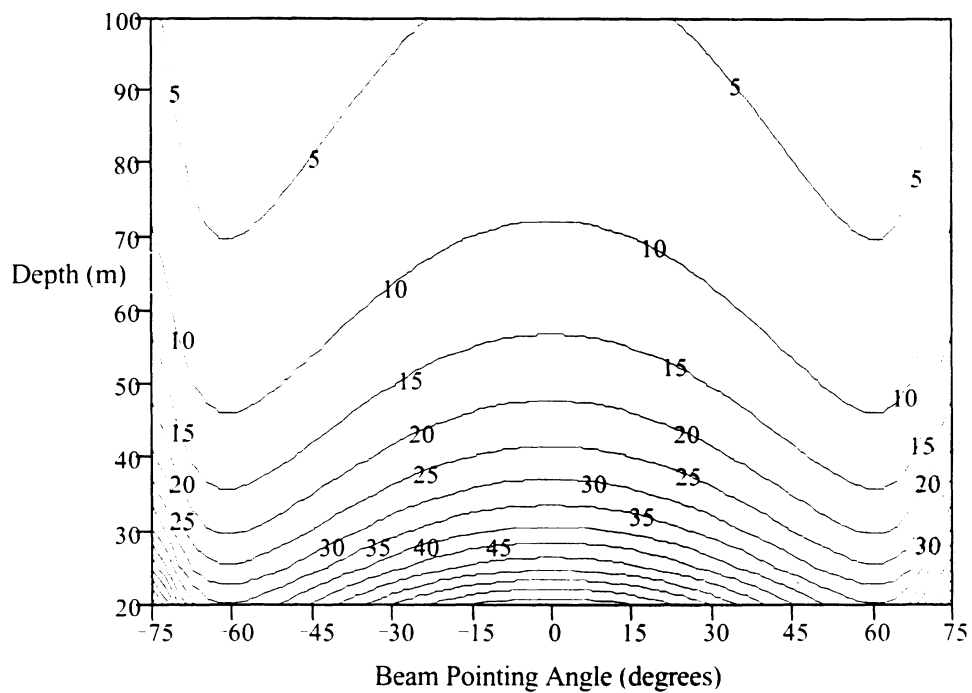


Figure a.5. Number of soundings gathered in the same radius of influence. Multibeam characteristics of the Simrad EM 1000, 200% ensonification of the seafloor, ship's speed 10 Knots, water depth 30 metres, and radius of influence 5 metres.

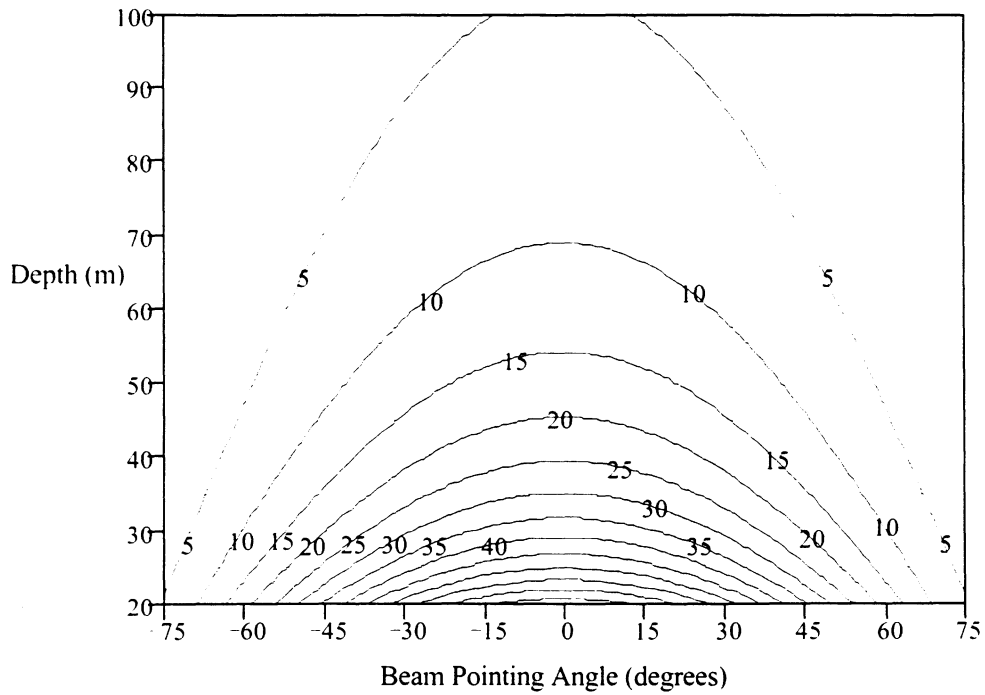


Figure a.6. Number of soundings gathered in the same radius of influence. Multibeam characteristics of the Simrad EM 1000, 100% ensonification of the seafloor, ship's speed 10 Knots, water depth 30 metres, and radius of influence 5 metres.

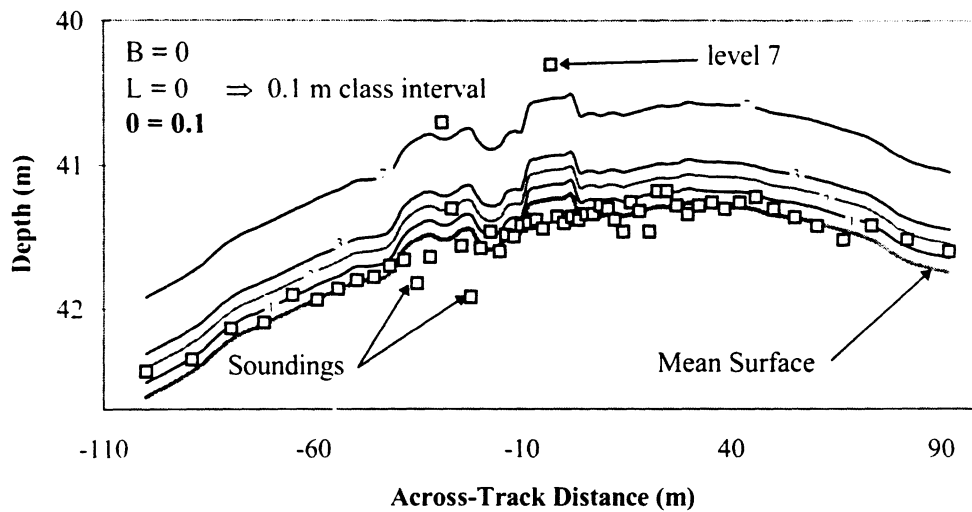


Figure a.7. HDCS classification levels for a profile, using the parameters $B=0$, $L=0$, $O=0.1$. The classification depth intervals are constant each of which with 0.1 metre depth.

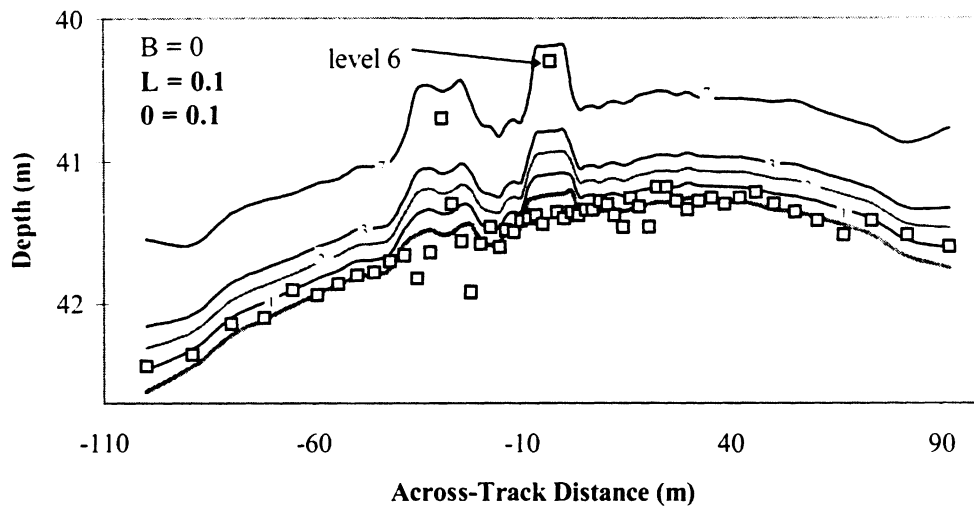


Figure a.8. HDCS classification levels for a profile, using the parameters $B=0$, $L=0.1$, $O=0.1$. The classification depth intervals are constant (i.e., 0.1 metre depth) for standard deviation equal zero. The depth intervals increase proportionally to the standard deviation.

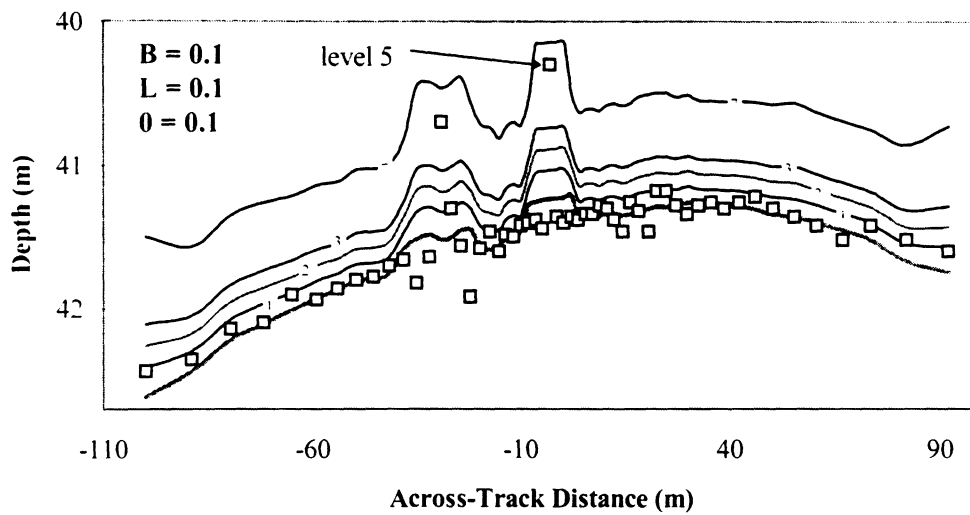


Figure a.9. HDCS classification levels for a profile, using the parameters $B=0.1$, $L=0.1$, $O=0.1$. The classification depth intervals are constant (i.e., 0.1 metre depth) for standard deviation equal zero. The depth intervals increase proportionally to the standard deviation and are shifted with respect to the mean surface due to the effect of the base scale B .

Appendix B.1

RESULTS OF INTERACTIVE AND AUTOMATIC DATA CLEANING WITH *HDCS* FOR THE *EMPRESS OF IRELAND*

The test area has a dimension of 1000 m x 1000 m.

Figures b.1, b.2, and b.3 are color coded contours, from the area used for the experiment, computed with *HDCS* with 1 metre interval.

The area of the experiment was divided into six smaller subsets, with dimension 500 m x 500 m. Figures b.3, b.4, and b.5 represent the mean surfaces generated with *HDCS*, with color coded contours with 1 metre interval.

Figures b.7, b.8, and b.9 represent the standard deviation surfaces, created with *HDCS*, from the subsets presented on Figures b.3, b.4, and b.5. The bright areas correspond to high values of the standard deviation, i.e., higher dispersion of the depths. The darker areas correspond to low values of the standard deviation, i.e., areas with lower dispersion or with few soundings, not enough to calculate the statistics.

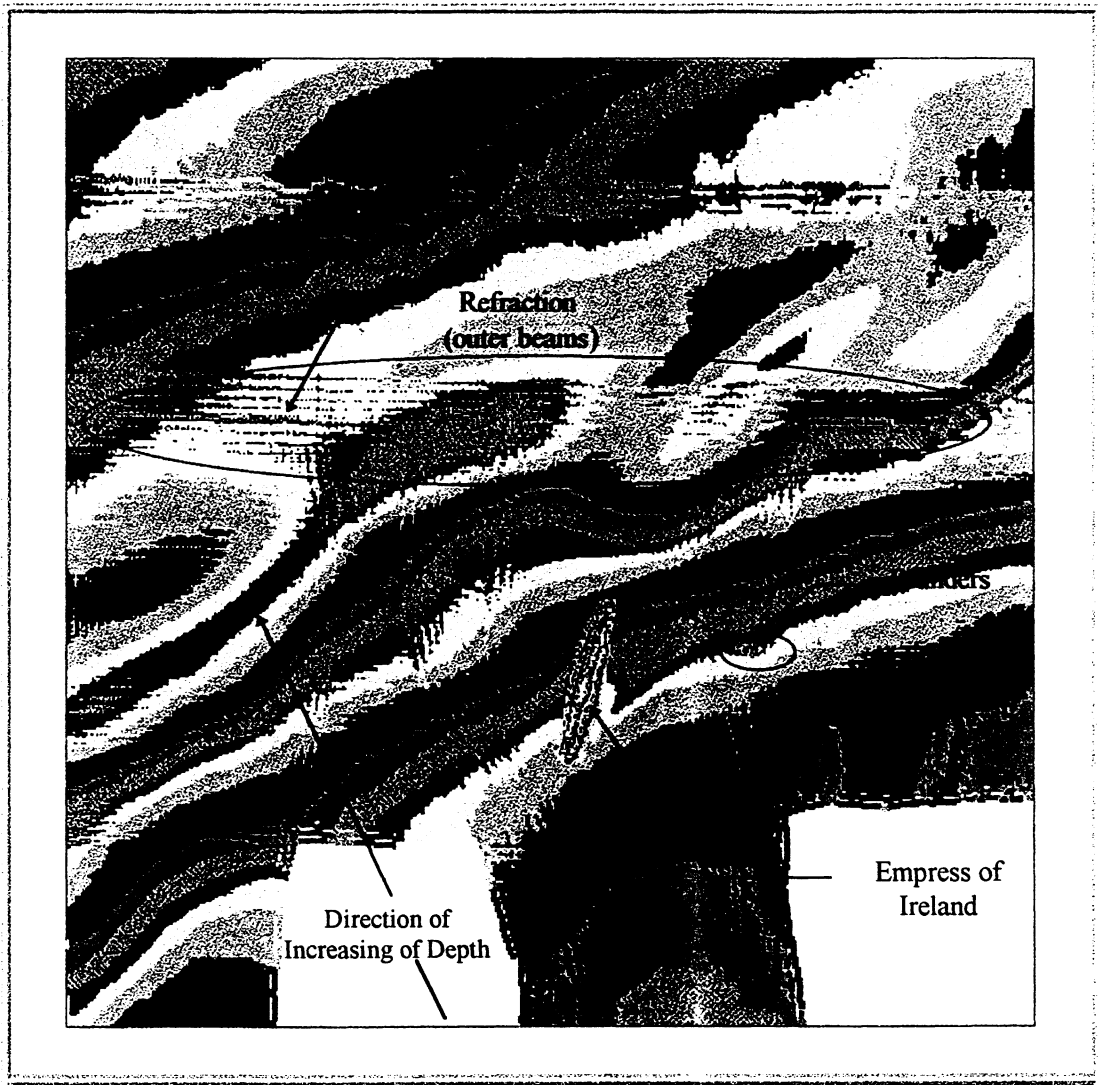


Figure b.1. Mean surface from the depth data after being merged, reduced from tide, and corrected from known systematic errors, using HDCS.



Figure b.2. Mean surface of the area used in the experiment, resulting from the interactive data cleaning, using HDCS.



Figure b.3. Mean surface of the area used in the experiment, resulting from the automatic data cleaning, using HDCS. The subset area is presented in more detail in following figures.

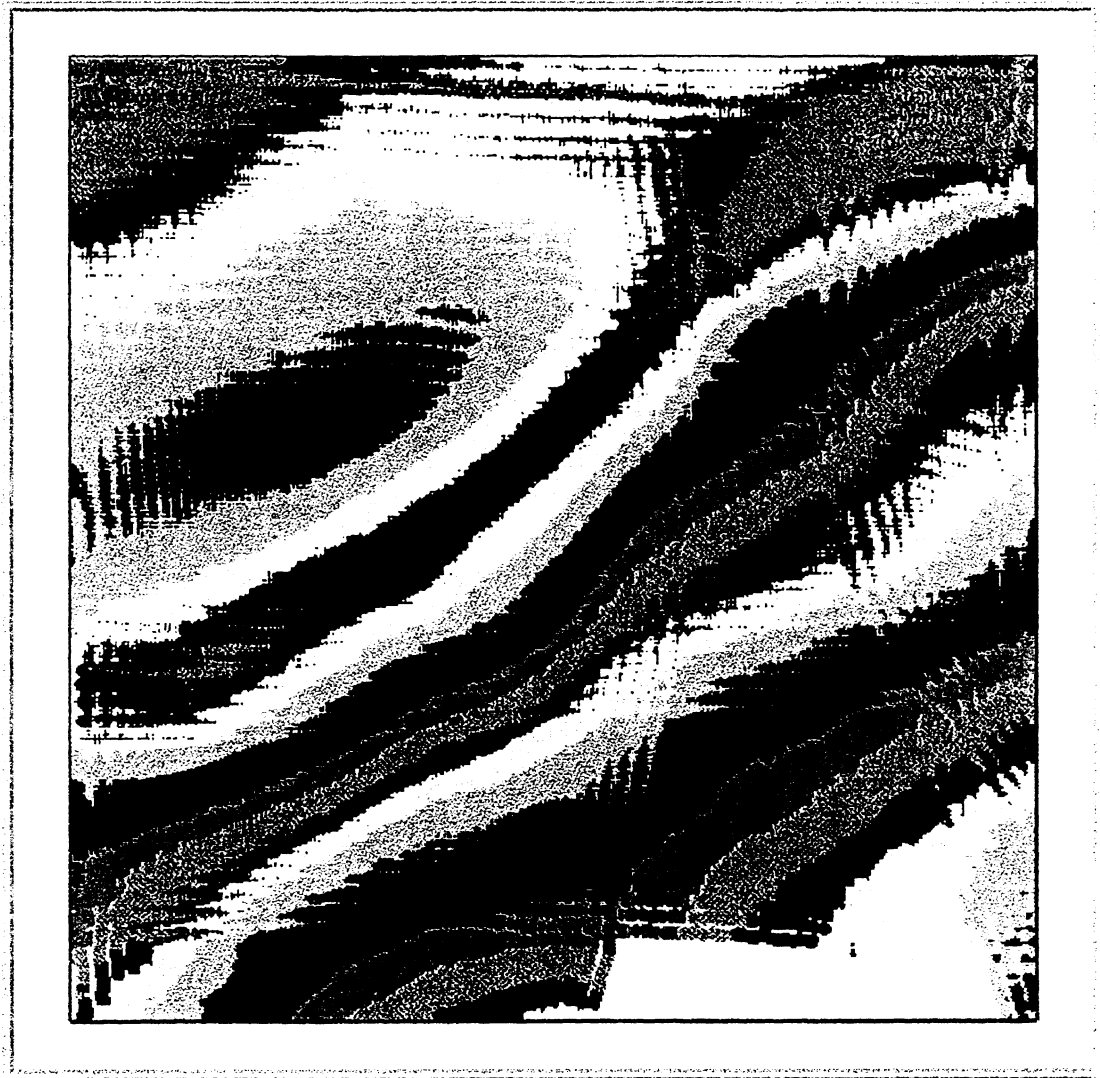


Figure b.4. Mean surface from the subset from Figure b.3 before being cleaned with HDCS. The dimension of the subset is 500 m x 500 m.



Figure b.5. Mean surface from previous subset, resulting from the interactive data cleaning, using HDCS.



Figure b.6. Mean surface from previous subset, resulting from the automatic data cleaning procedures, using HDCS.

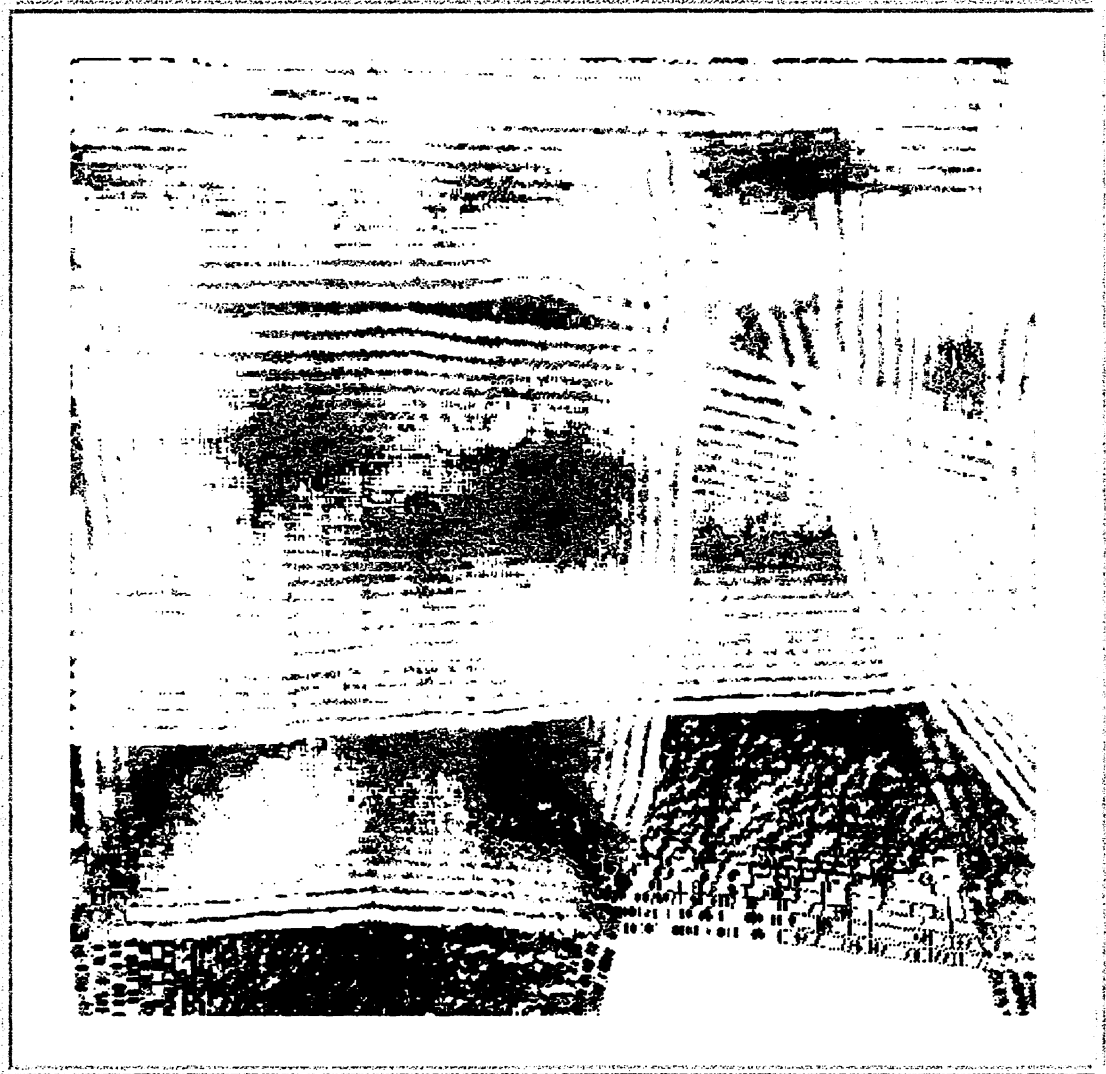


Figure b.7. Standard deviation surface from the subset before being cleaned (Figure b.4) with HDCS.



Figure b.8. Standard deviation surface from the subset after being interactively cleaned (Figure b.5) with HDCS.



Figure b.9. Standard deviation surface from the subset after being automatically cleaned (Figure b.6) with HDCS.

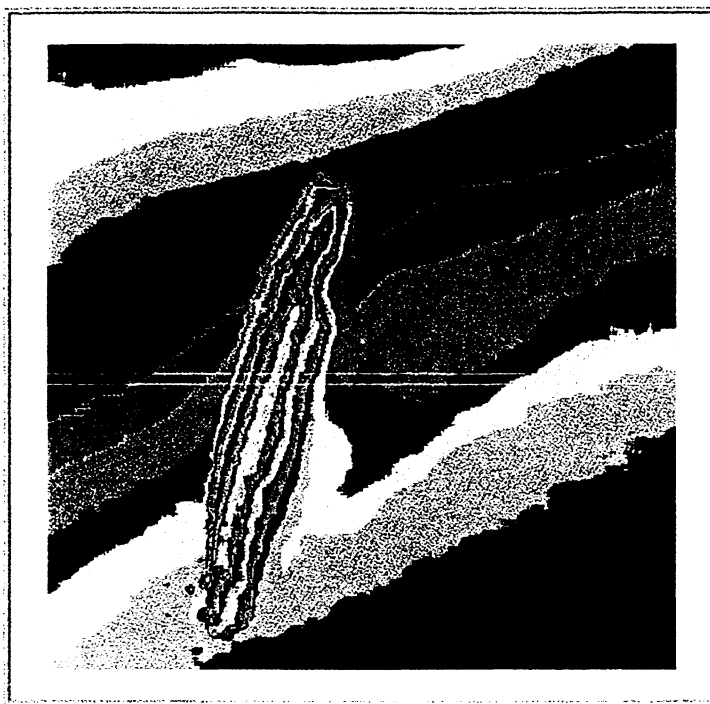


Figure b.10. Subset from the wreck, interactively cleaned with HDCS.

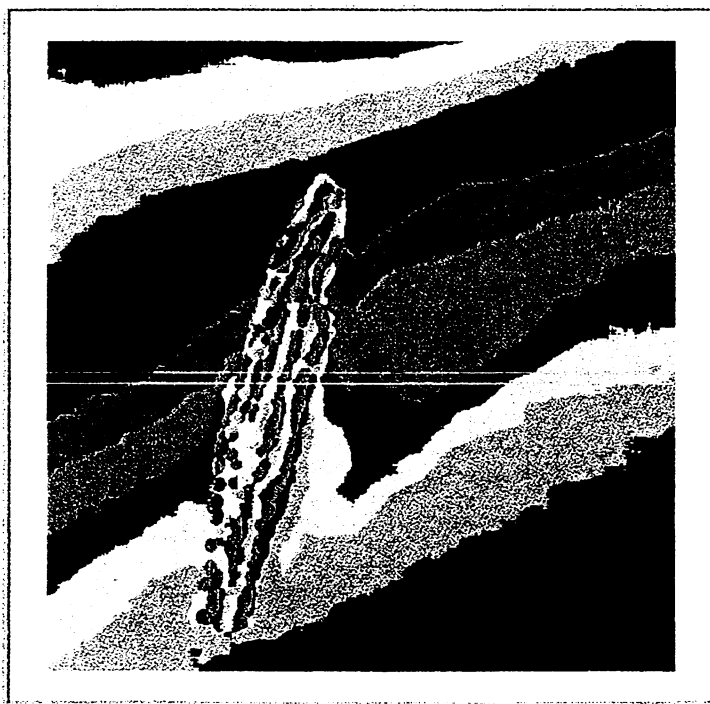


Figure b.11. Subset from the wreck automatically cleaned with HDCS.

Appendix B.2

RESULTS OF INTERACTIVE AND AUTOMATIC DATA CLEANING WITH *HD*CS FOR *HALIFAX APPROACHES*

The test area has an approximate dimension of 1600 m x 3200 m.

Figures b.12 to b.15 are color coded contours, from the area used for the experiment, computed with HD*CS* with 1 metre interval.

Figures b.16 to b.19 represent the standard deviation surfaces, created with HD*CS*, from the subsets presented respectively on Figures b.12 to b.15. The bright areas correspond to high values of the standard deviation, i.e., higher dispersion of the depths. The darker areas correspond to low values of the standard deviation, i.e., areas with lower dispersion or with few soundings, not enough to calculate the statistics.

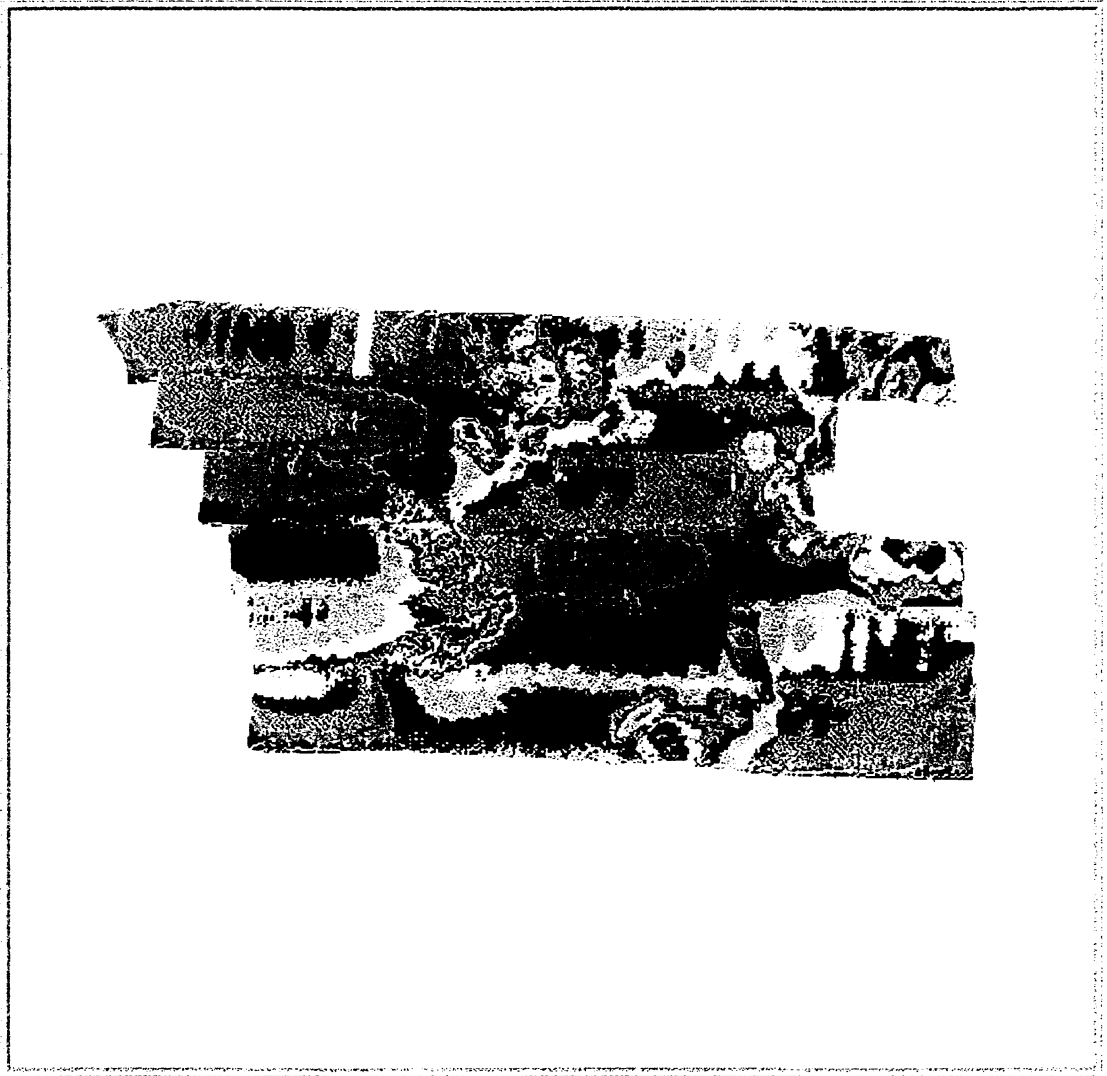


Figure b.12. Mean surface from the depth data after being merged and reduced from tide, using HDCS.

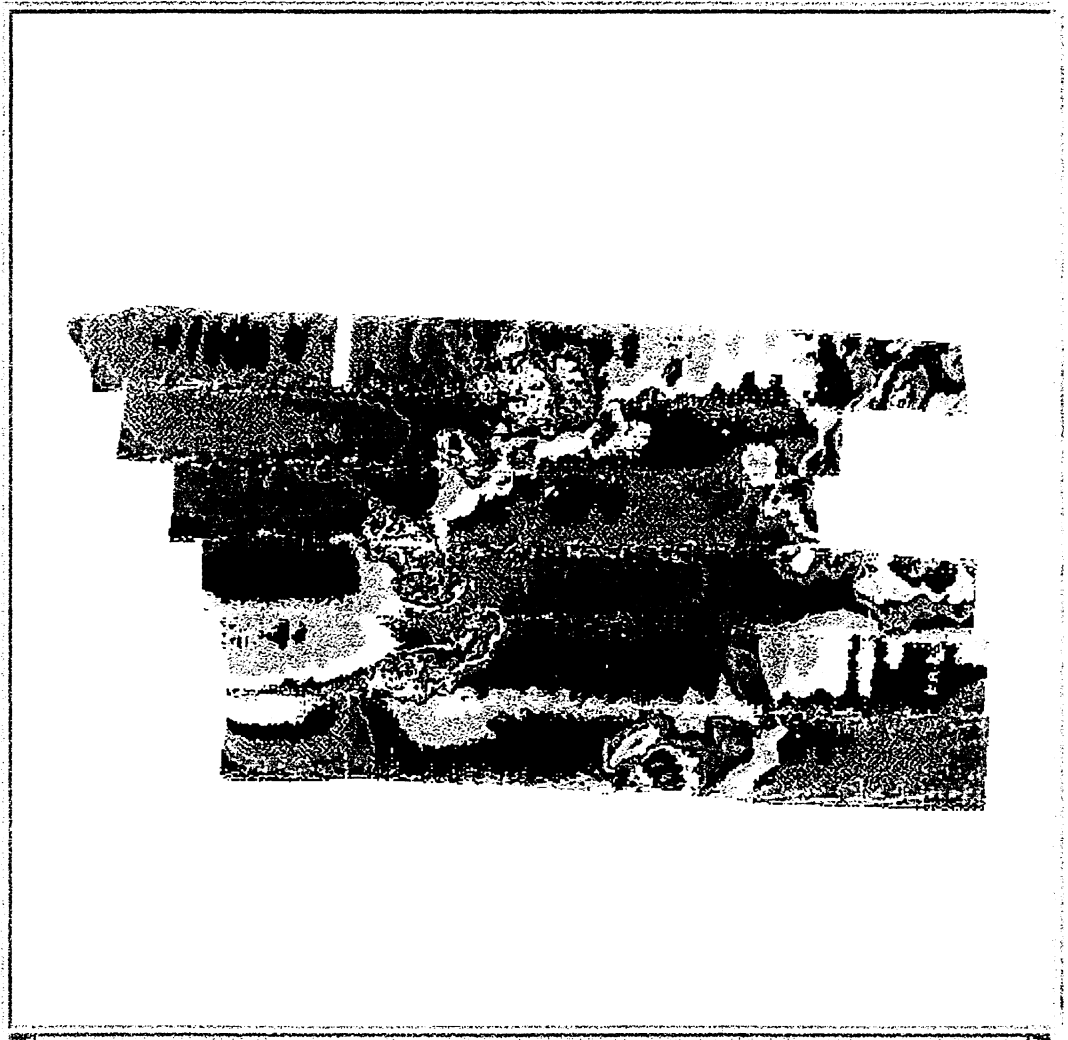


Figure b.13. Mean surface of the area used in the experiment, resulting from the interactive data cleaning, using HDCS.

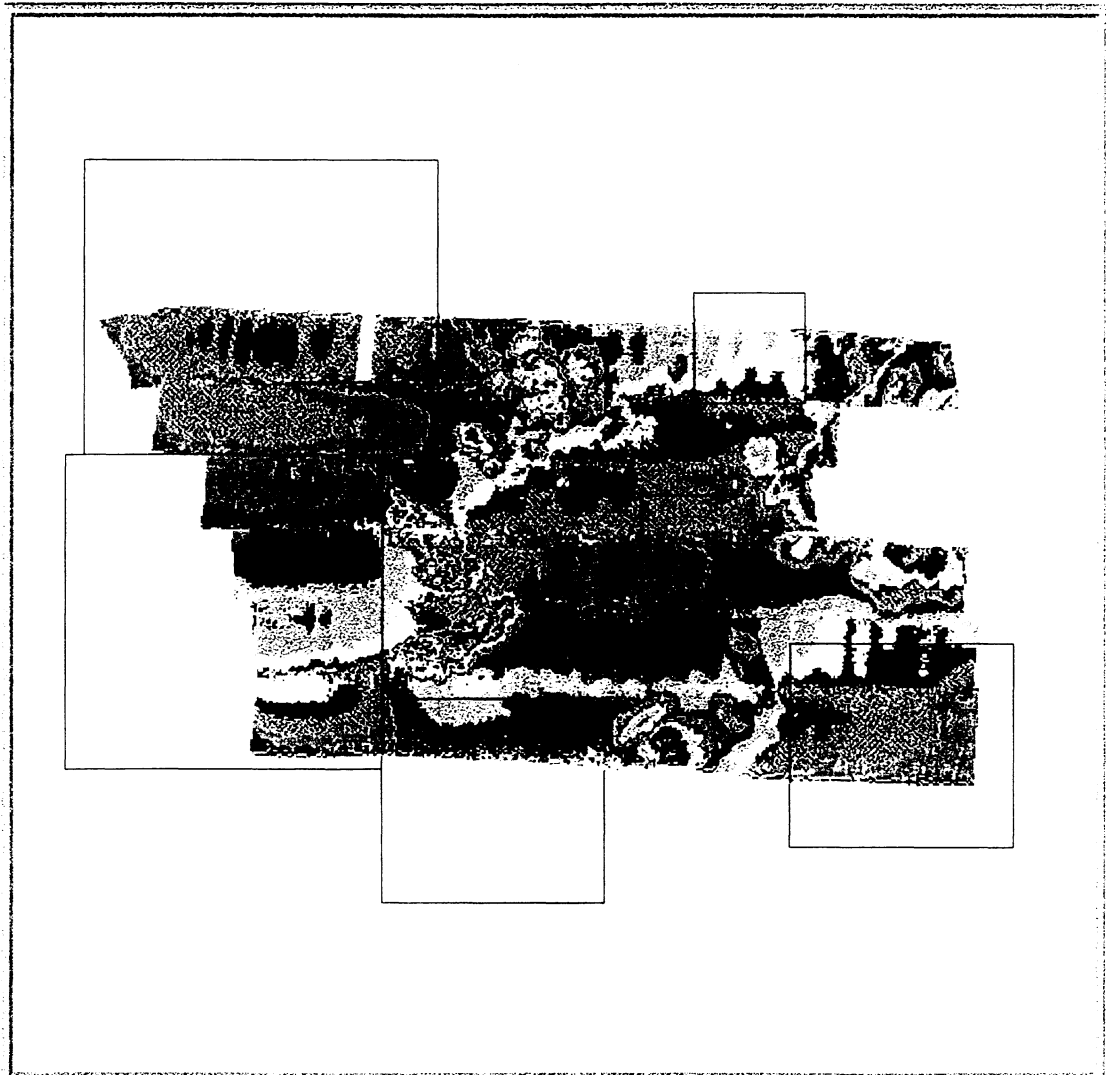


Figure b.14. Mean surface of the area used in the experiment, resulting from the automatic data cleaning using, HDCS. The subsets cleaned automatically are represented by squares.

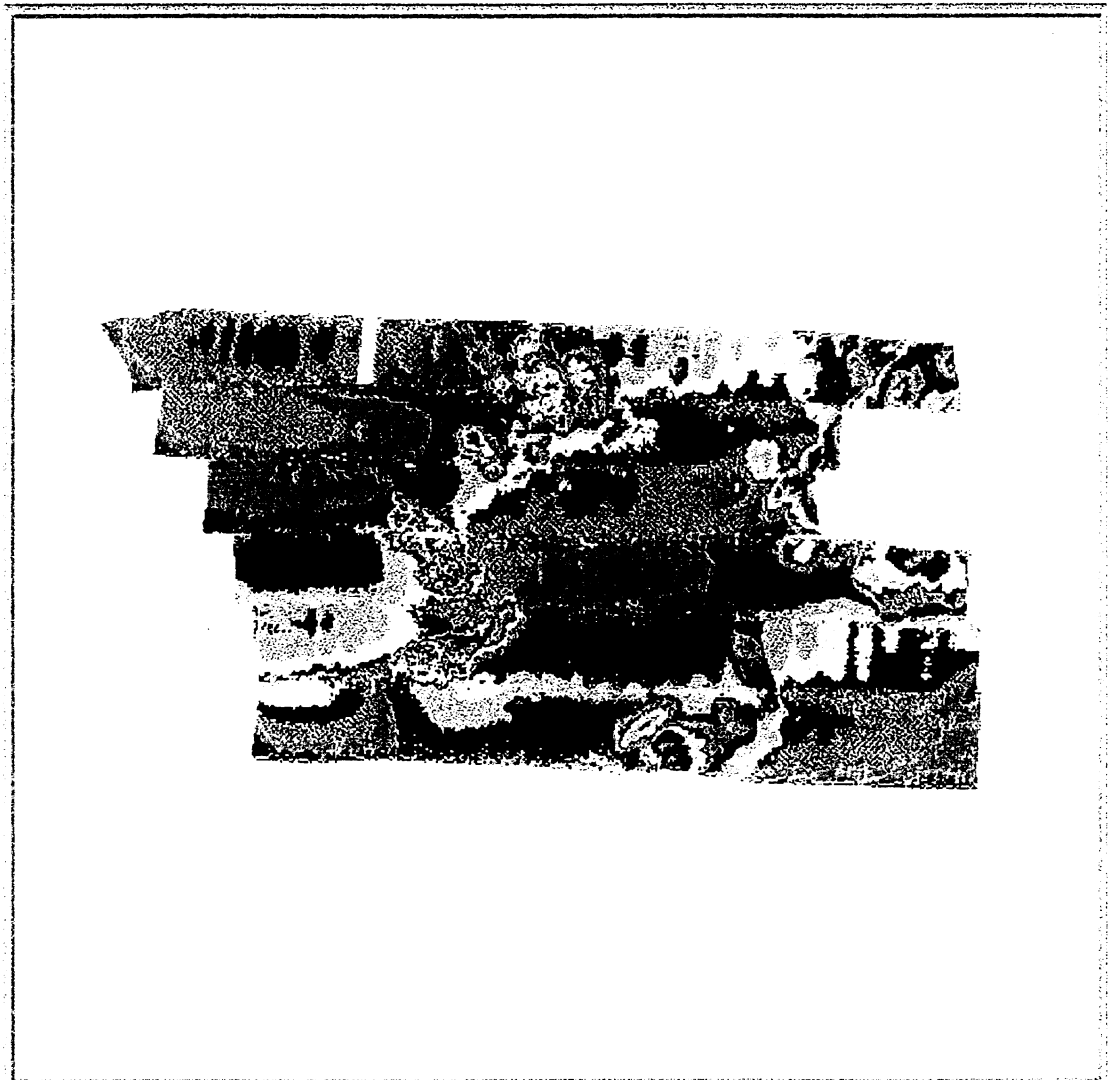


Figure b.15. Mean surface of the area used in the experiment resulting from the automatic data cleaning for the whole area, using HDCS.

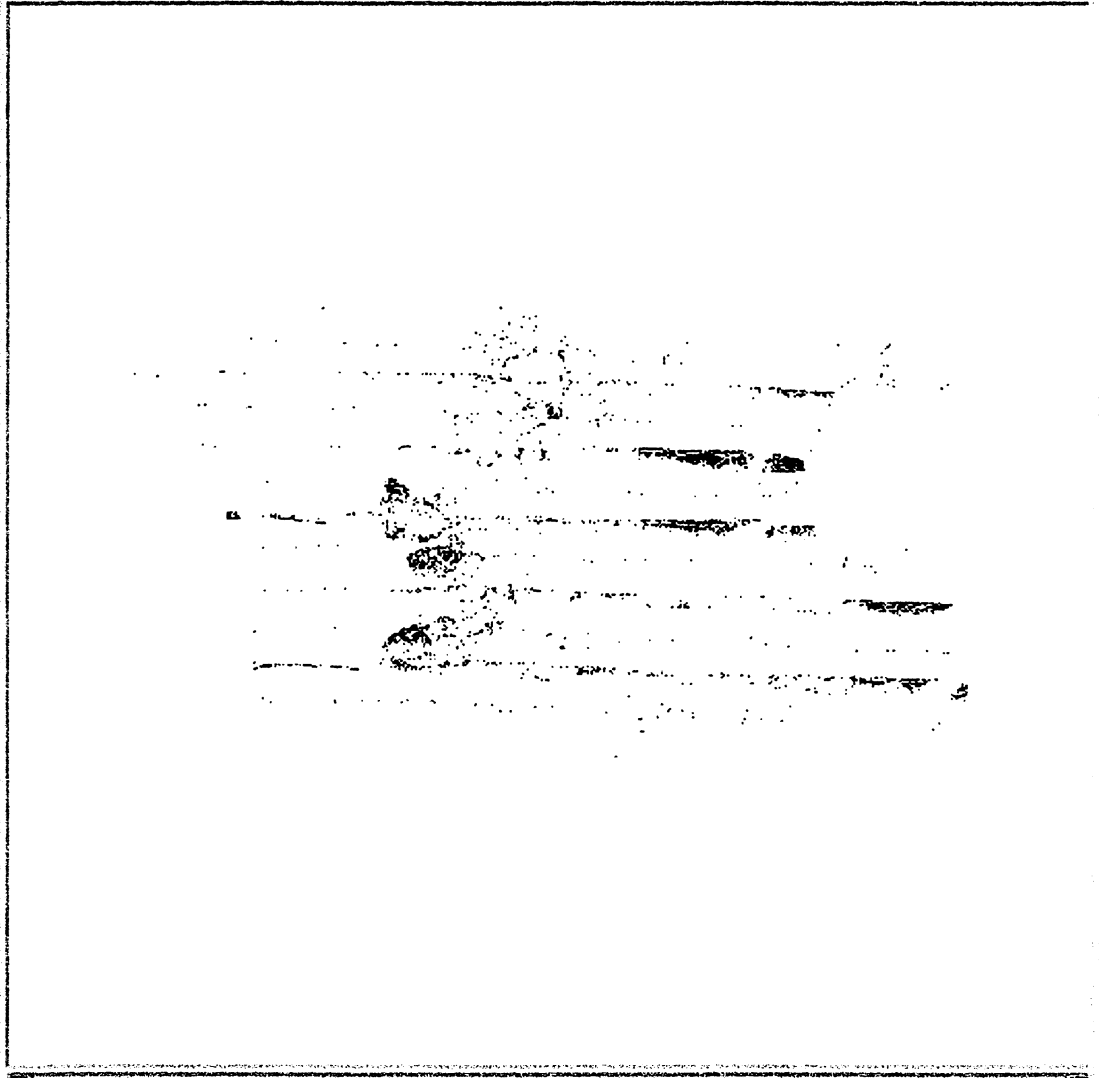


Figure b.16. Standard deviation surface from the depth data after being merged and reduced from tide, using HDCS.

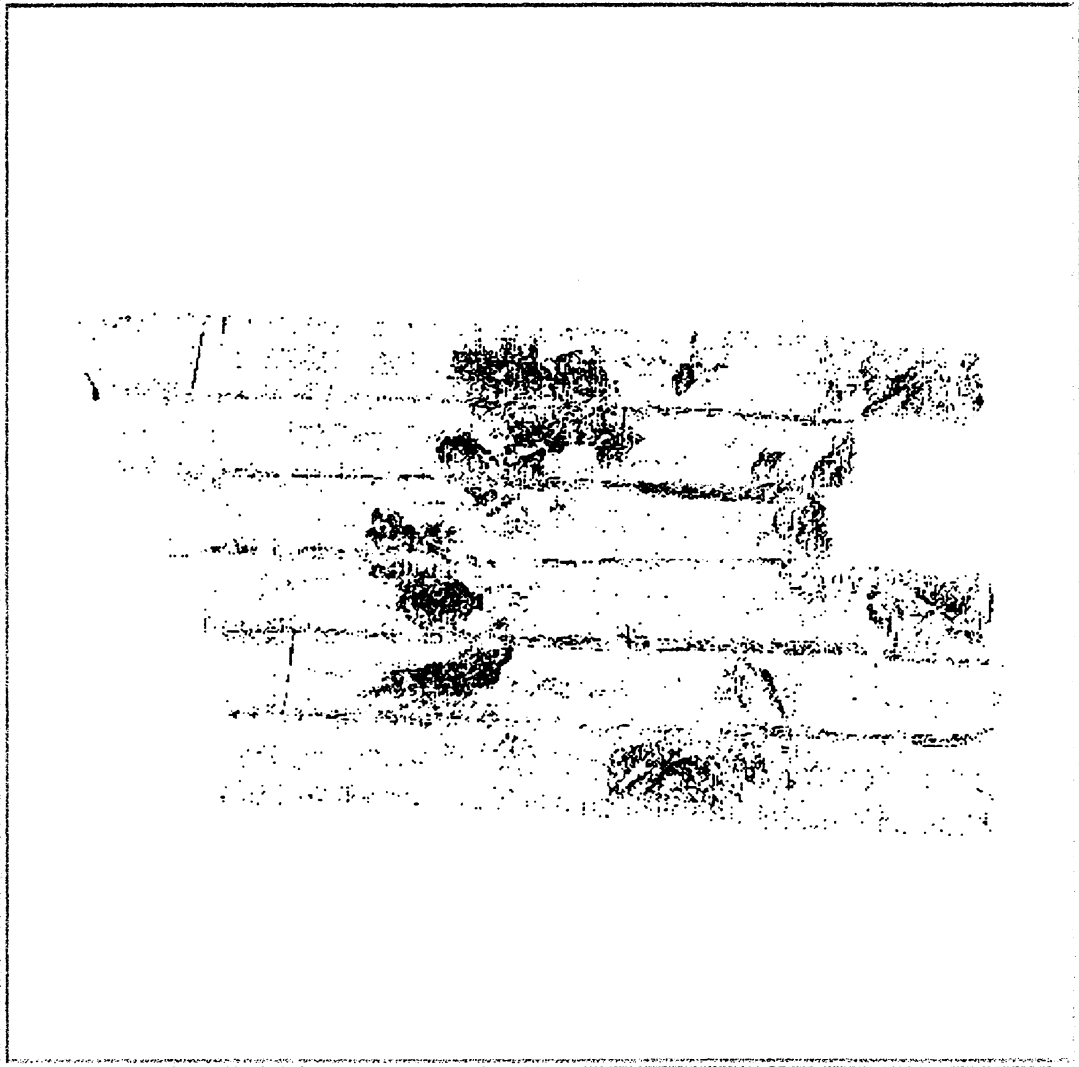


Figure b.17. Standard deviation surface from the data after being cleaned interactively with HDCS.

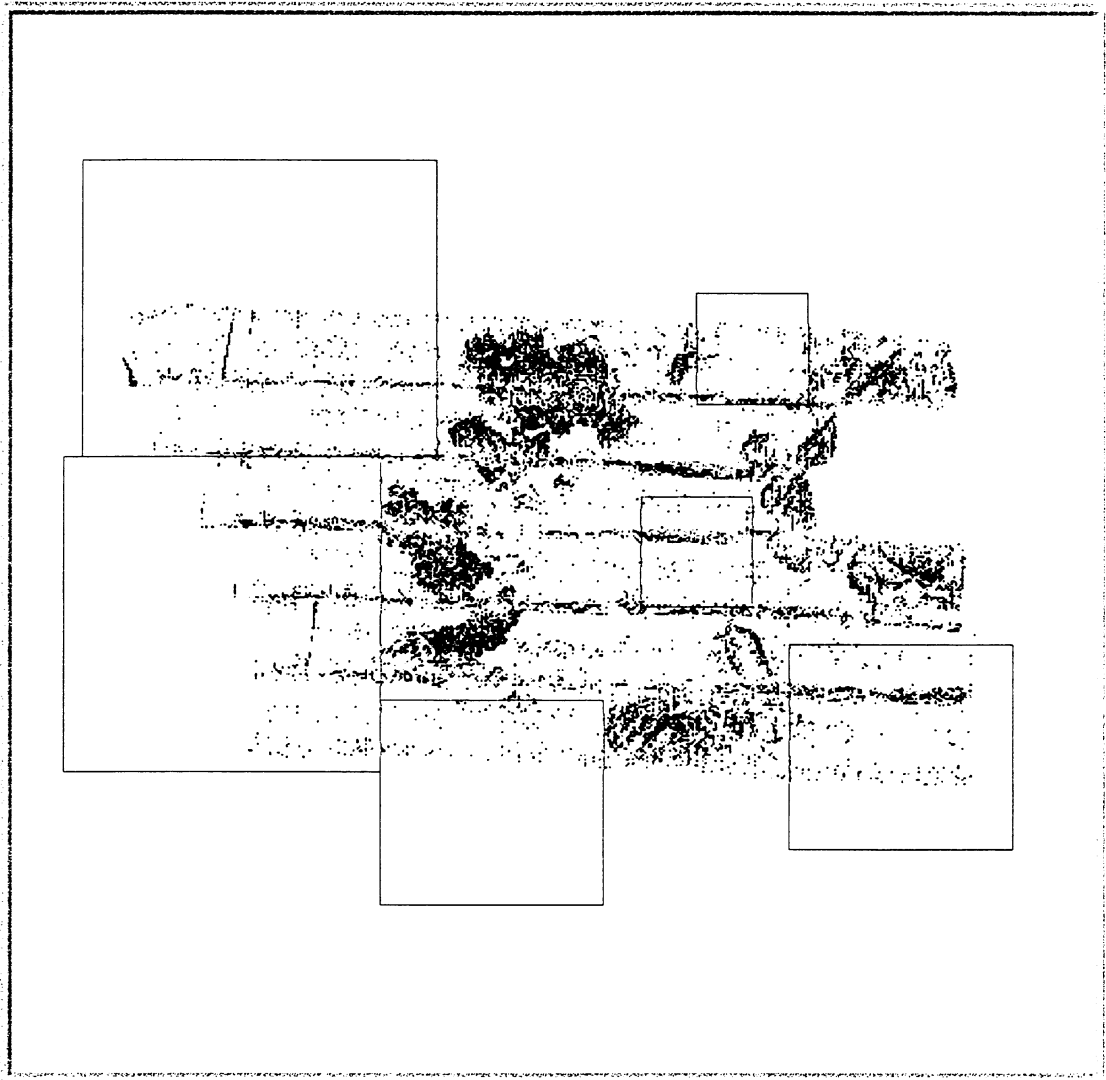


Figure b.18. Standard deviation surface from the data after being automatically cleaned with HDCS. The subsets cleaned automatically are represented by squares.

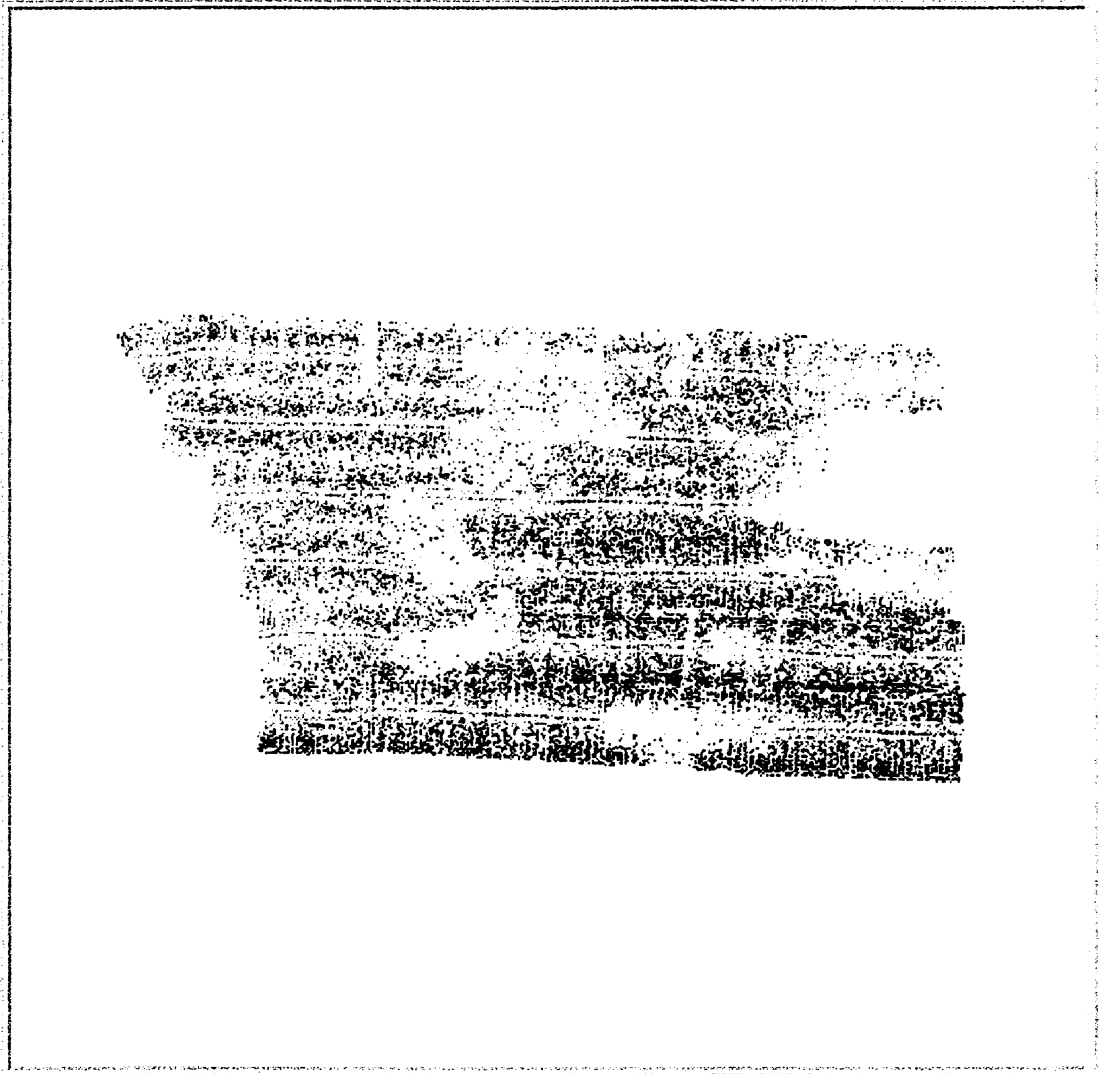


Figure b.19. Standard deviation surface from the data after the whole data set had been cleaned automatically.

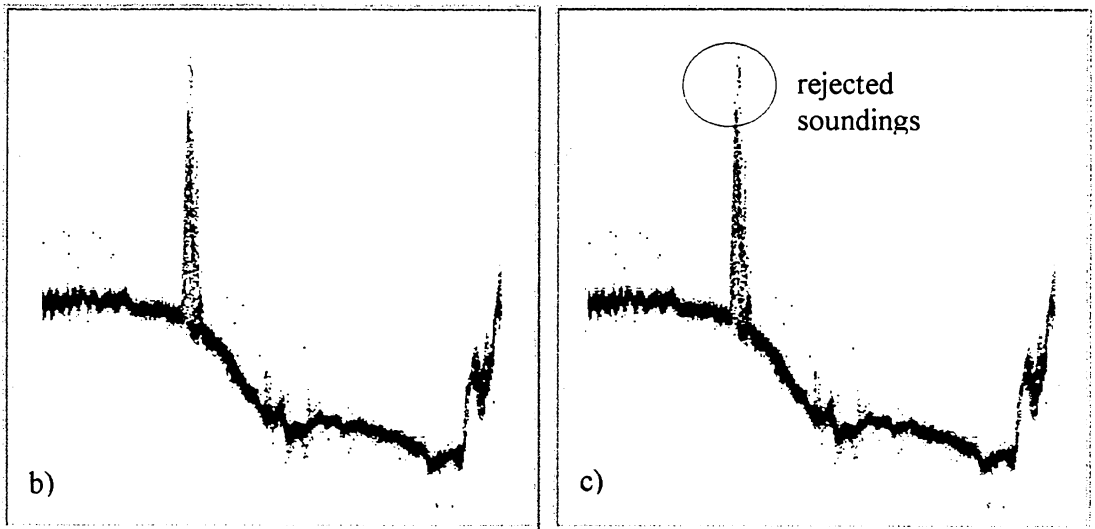
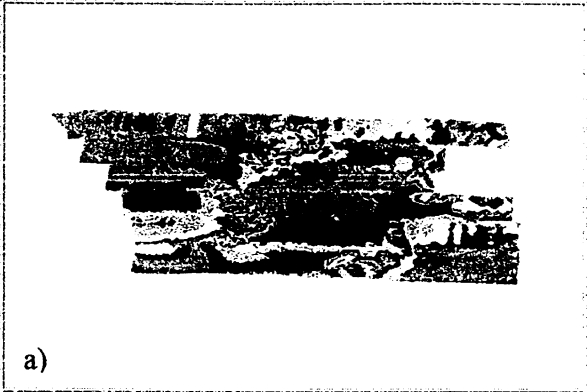


Figure b.20. Figures (b) and (c) are the result of the data cleaning performed on the profile defined in figure (a). The boulder is almost removed, figure (c), when applying the automatic method to the cross-section, defined in figure (a).

Appendix C.1

RESULTS OF INTERACTIVE AND AUTOMATIC DATA CLEANING WITH *BINSTAT* FOR THE *EMPRESS OF IRELAND*

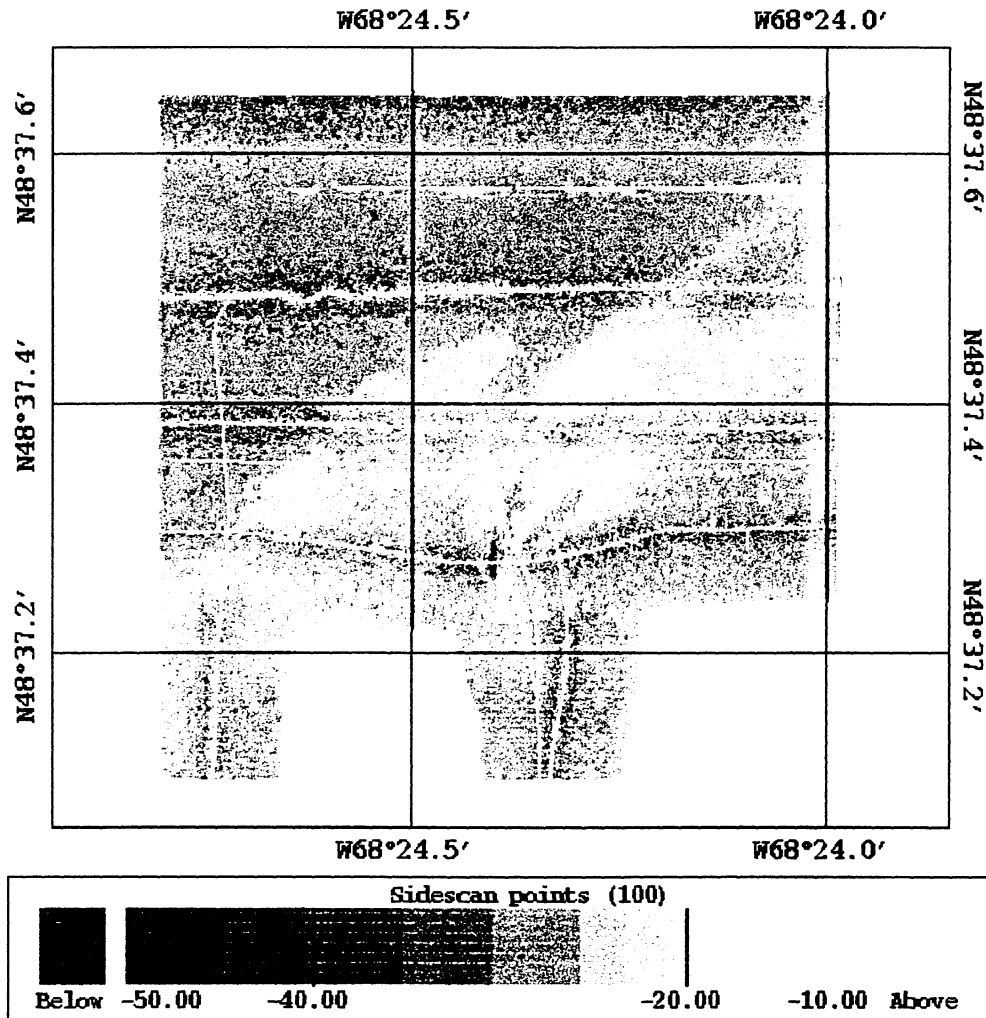


Figure c.1. Side scan image.

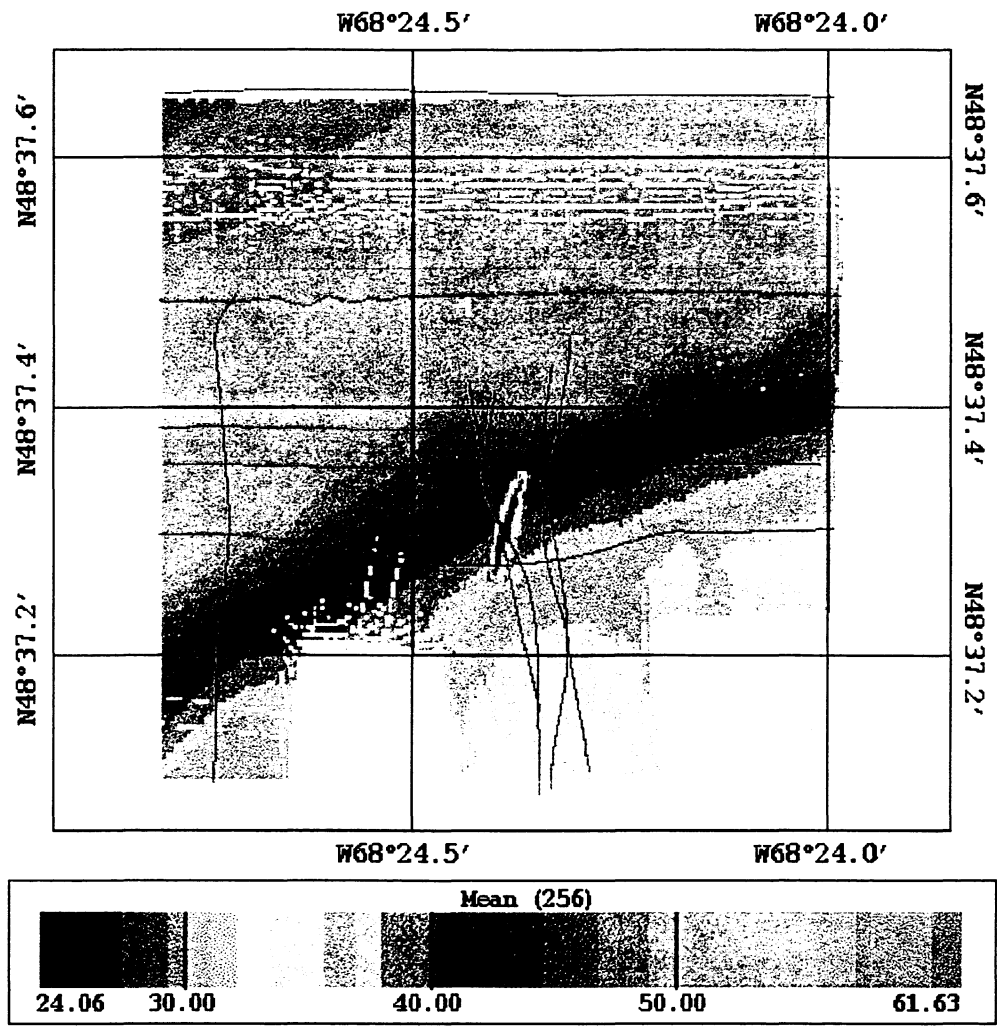


Figure c.2. Mean depth surface cleaned from systematic errors, using BINSTAT.

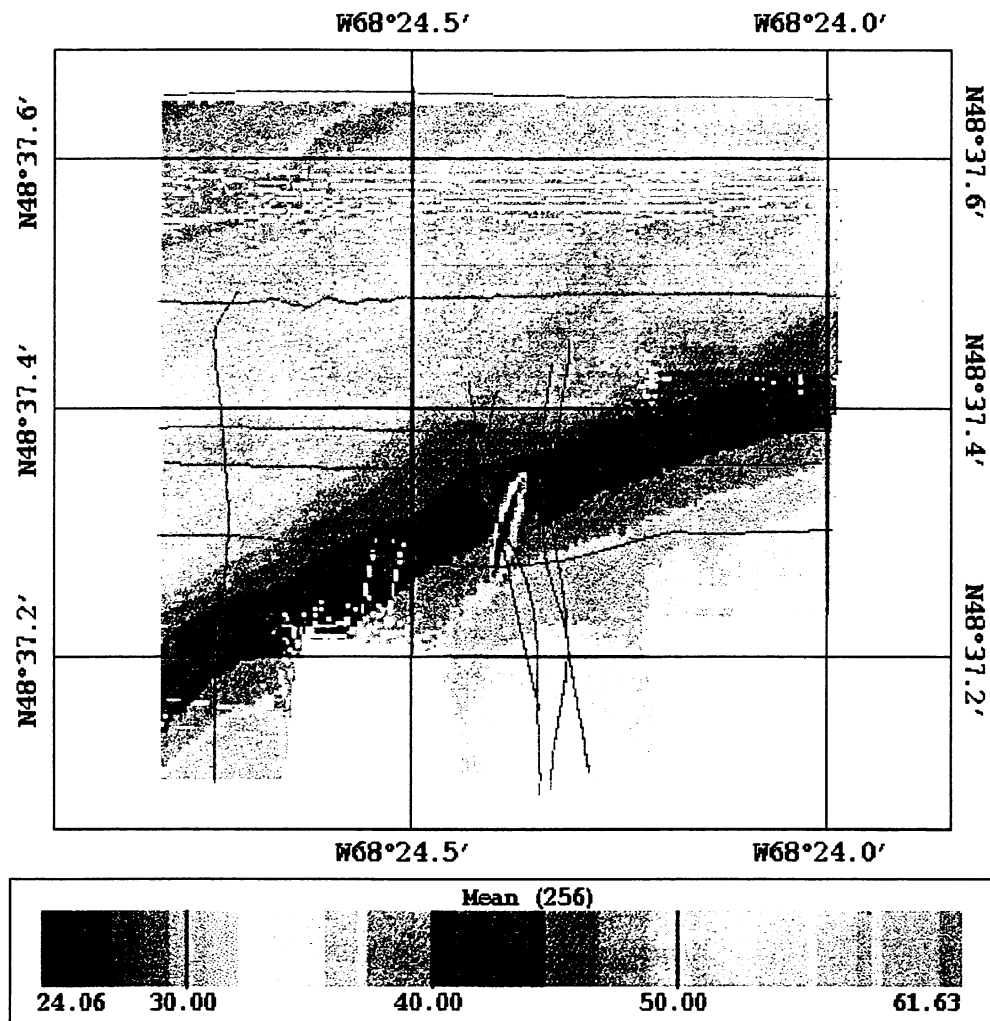


Figure c.3. Mean depth surface resulting from the interactive data cleaning, using BINSTAT.

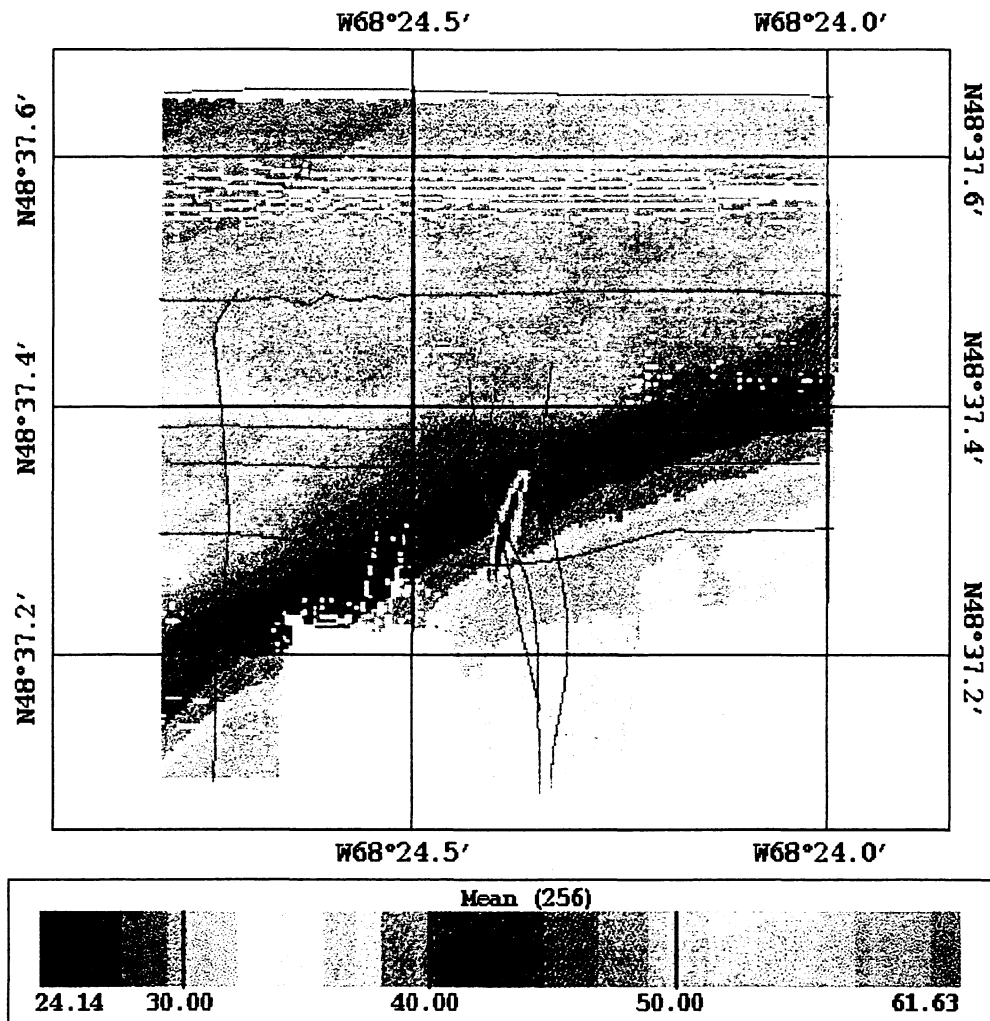


Figure c.4. Mean depth surface resulting from automatic data cleaning, using BINSTAT.

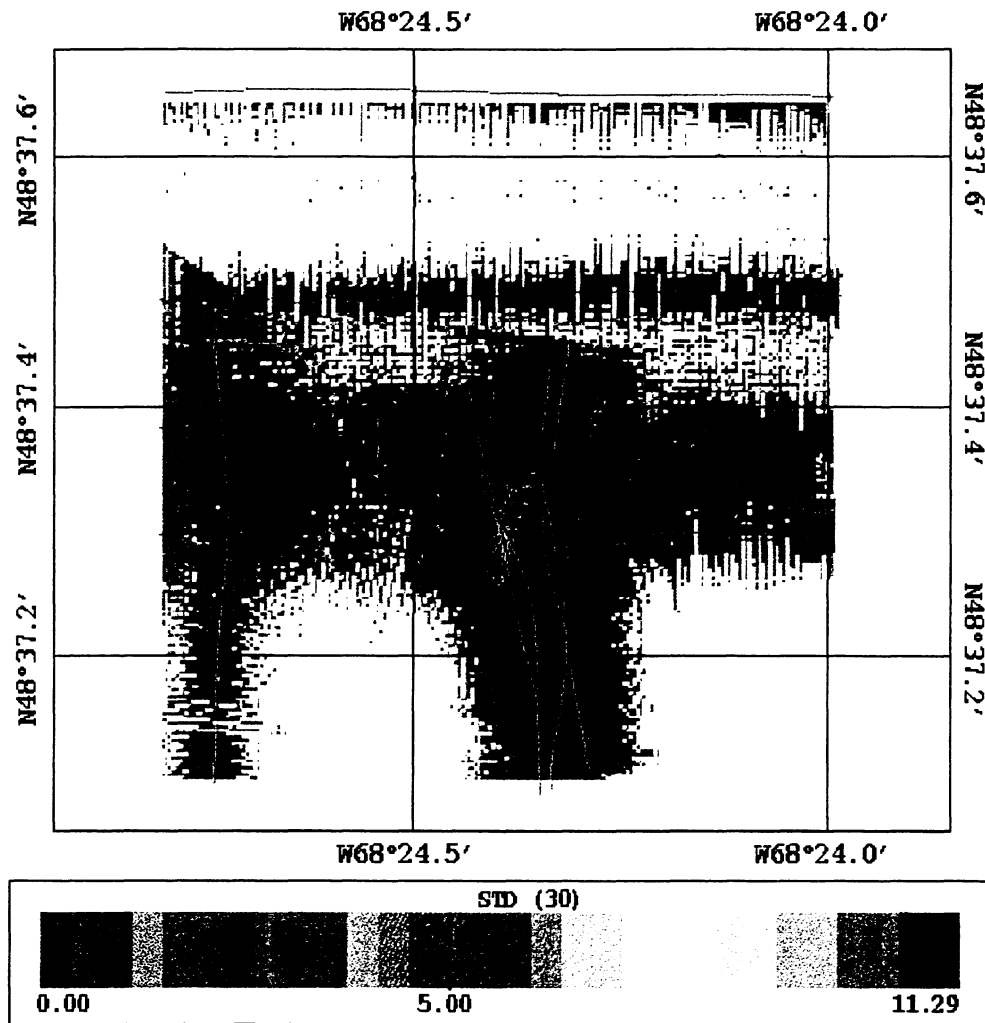


Figure c.5. Standard deviation surface corresponding to the data cleaned from systematic errors (Figure c.2), using BINSTAT.

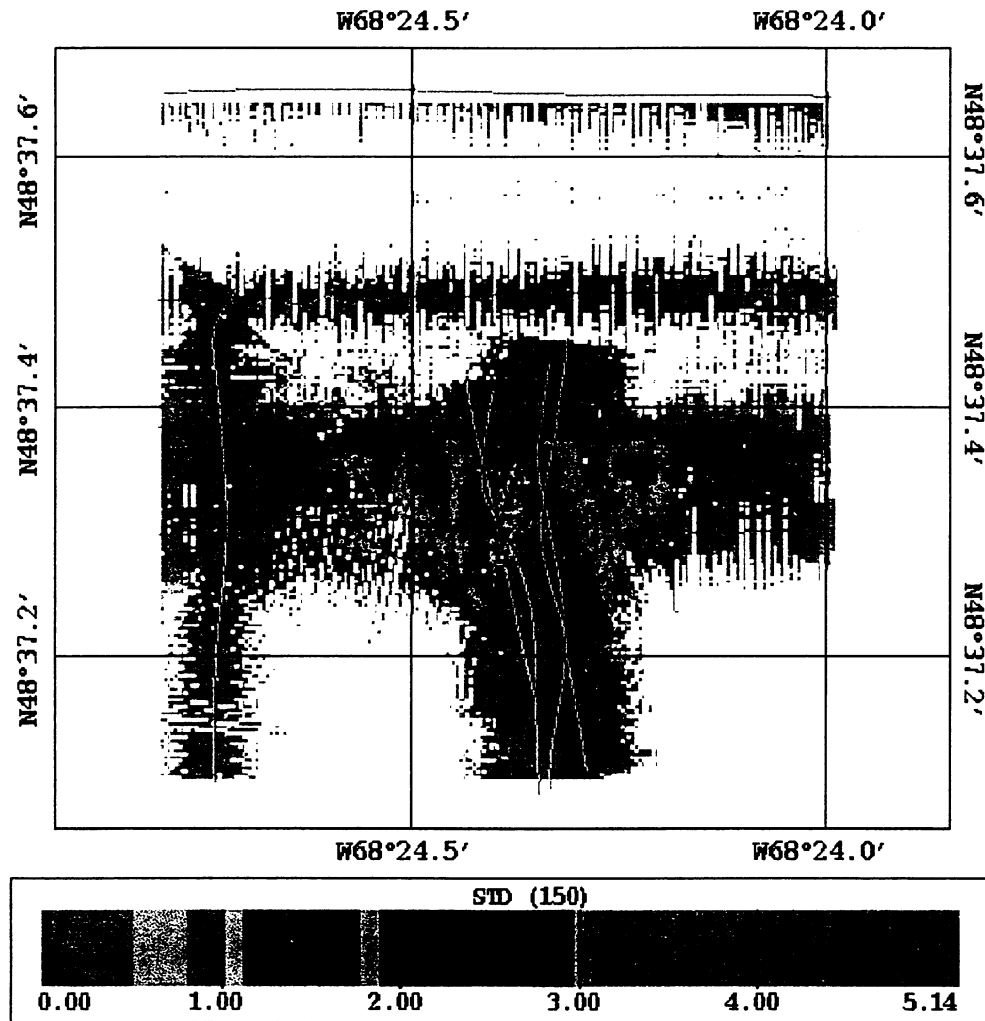


Figure c.6. Standard deviation surface corresponding to the data interactively cleaned (Figure c.3), using BINSTAT.

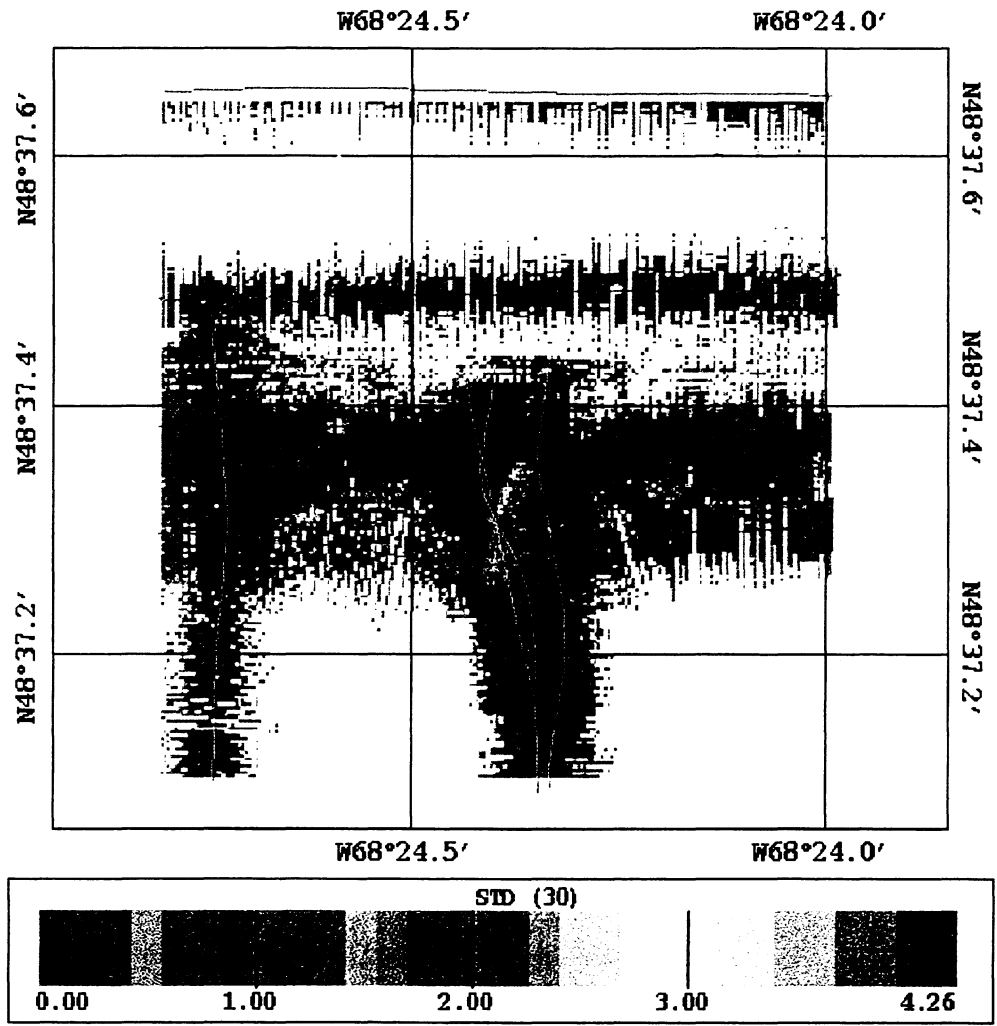


Figure c.7. Standard deviation surface corresponding to the data automatically cleaned (Figure c.4), using BINSTAT.

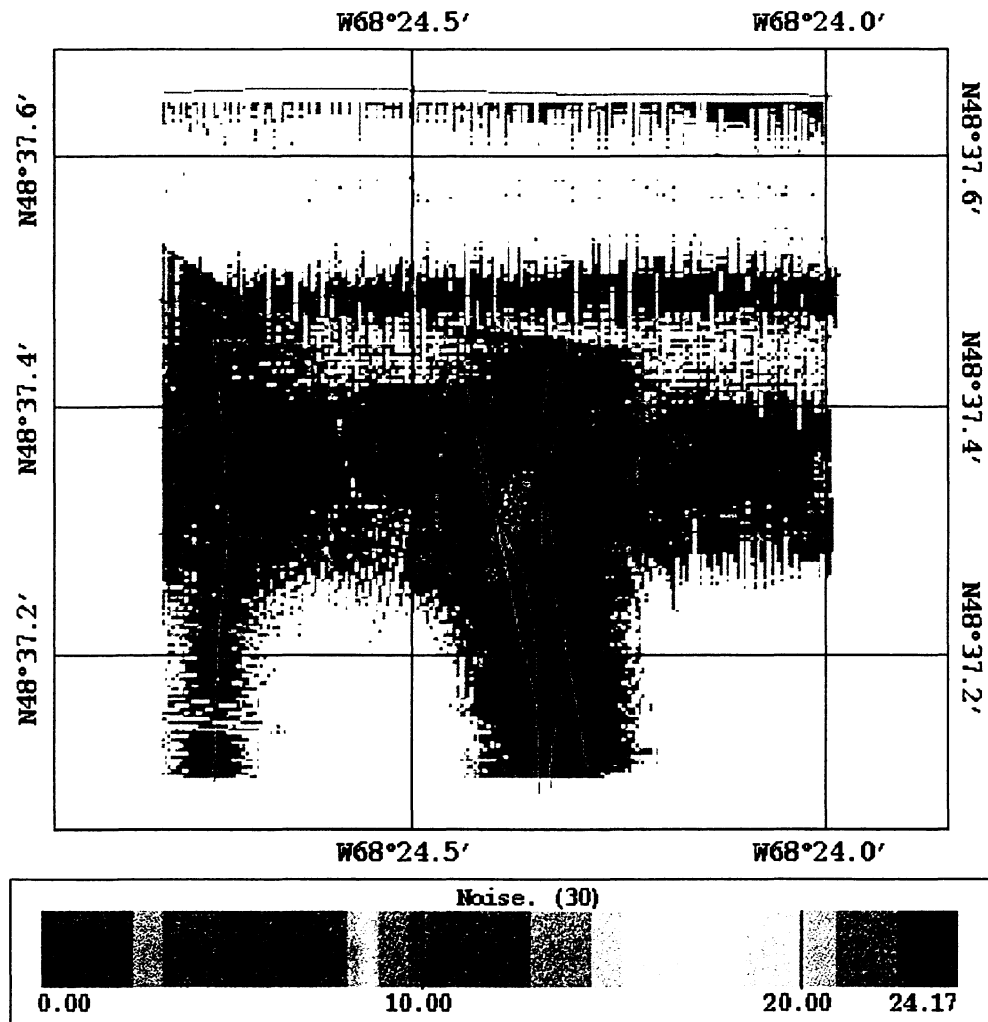


Figure c.8. Noise surface corresponding to the data cleaned from systematic errors (Figure c.2), using BINSTAT.

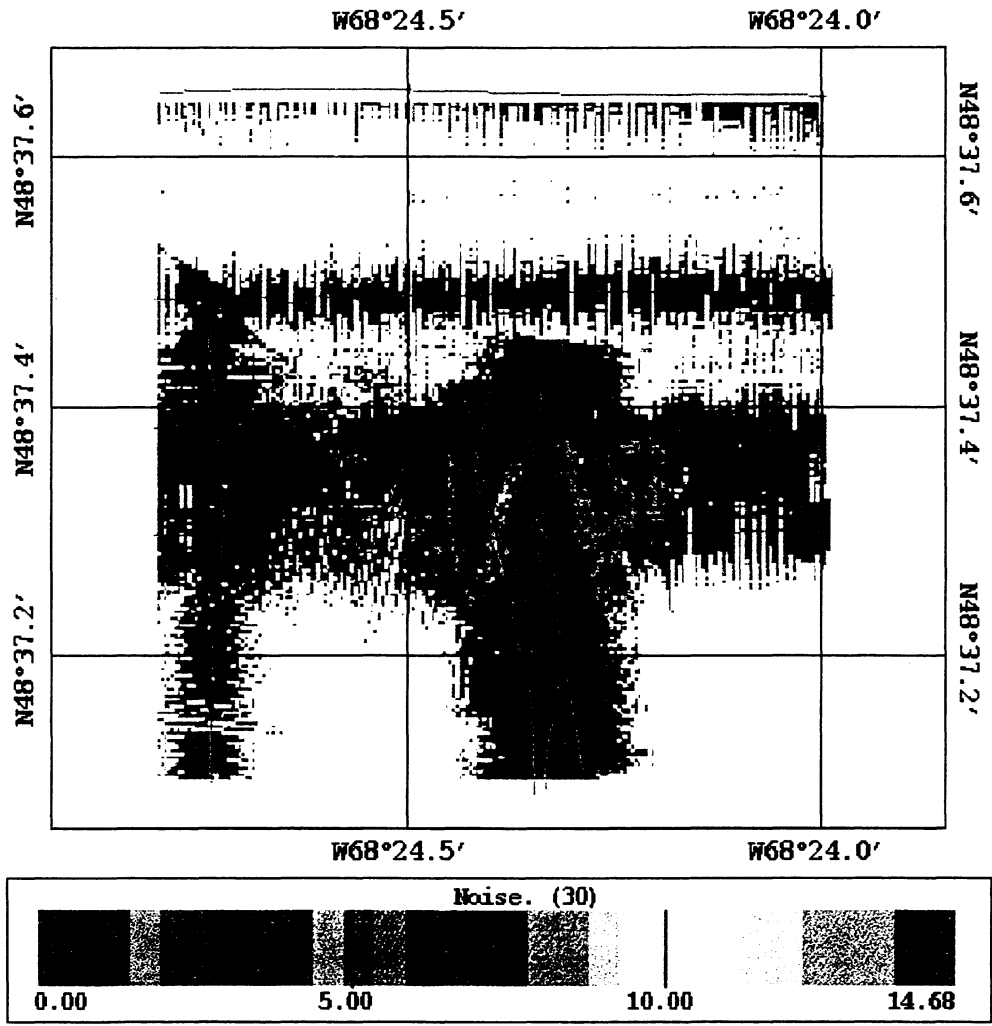


Figure c.9. Noise surface corresponding to the data interactively cleaned (Figure c.3), using BINSTAT.

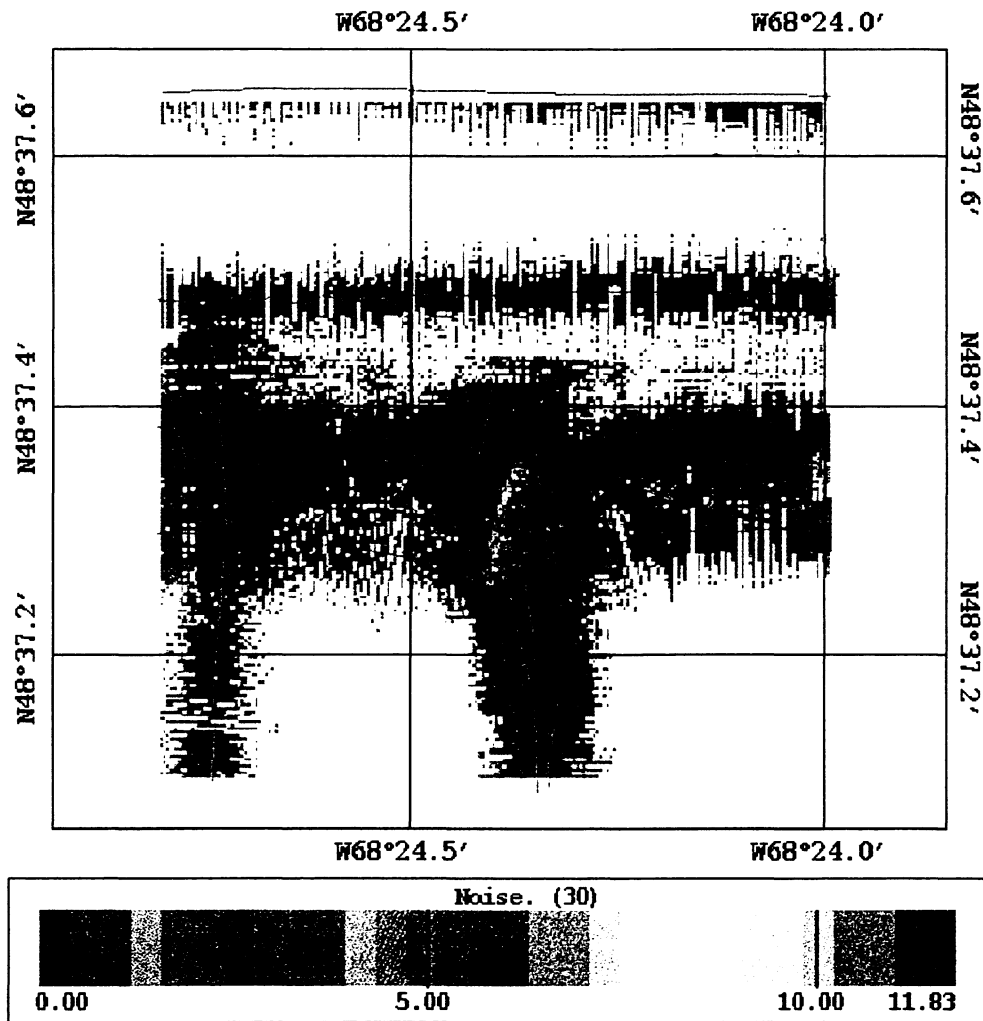


Figure c.10. Noise surface corresponding to the data automatically cleaned (Figure c.4), using BINSTAT.

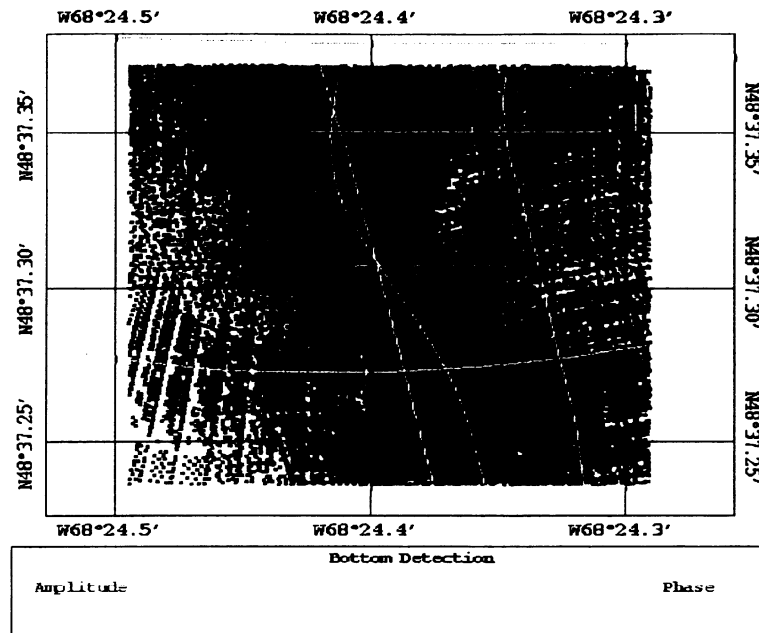


Figure c.11. Bottom detection for the area of the wreck, using BINSTAT.

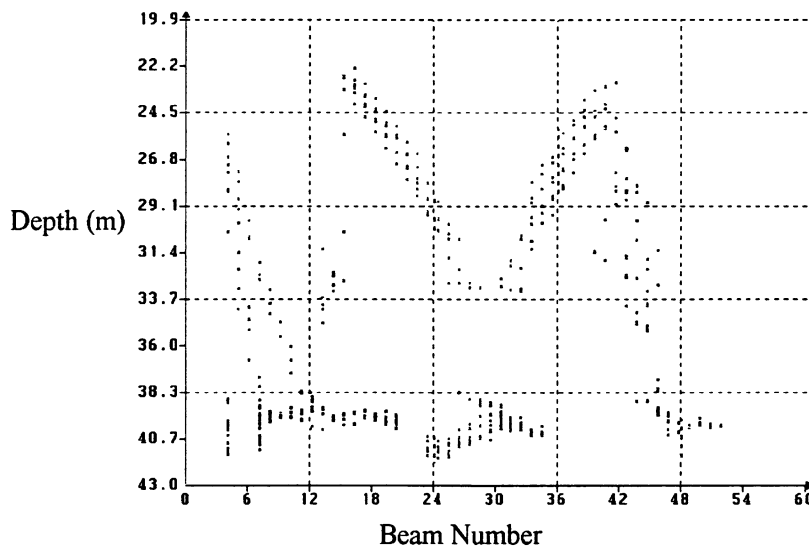


Figure c.12. Correlation plot of depth vs beam number for the area of the wreck, using BINSTAT. The overlapping of several swaths in the same area causes difficulties visualizing the depths as a function of beam number.

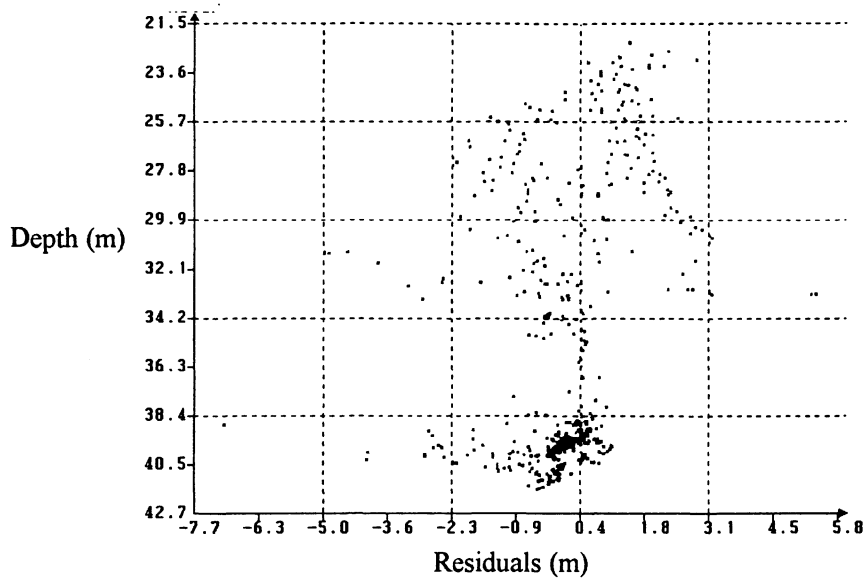


Figure c.13. Correlation plot of depth vs residuals for the area of the wreck, using BINSTAT.

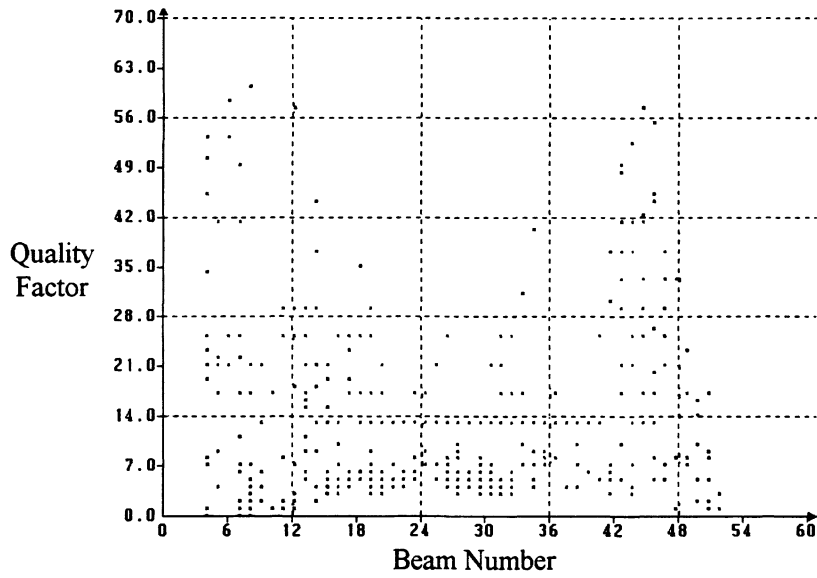


Figure c.14. Correlation plot of quality factor vs beam number for the area of the wreck, using BINSTAT. This correlation shows that even for the outer beams, where the variance of the phase curve fit vs time (proportional to the quality factor) is in general low, the obstruction creates additional variations which cause a depart of the phase samples from a straight line.

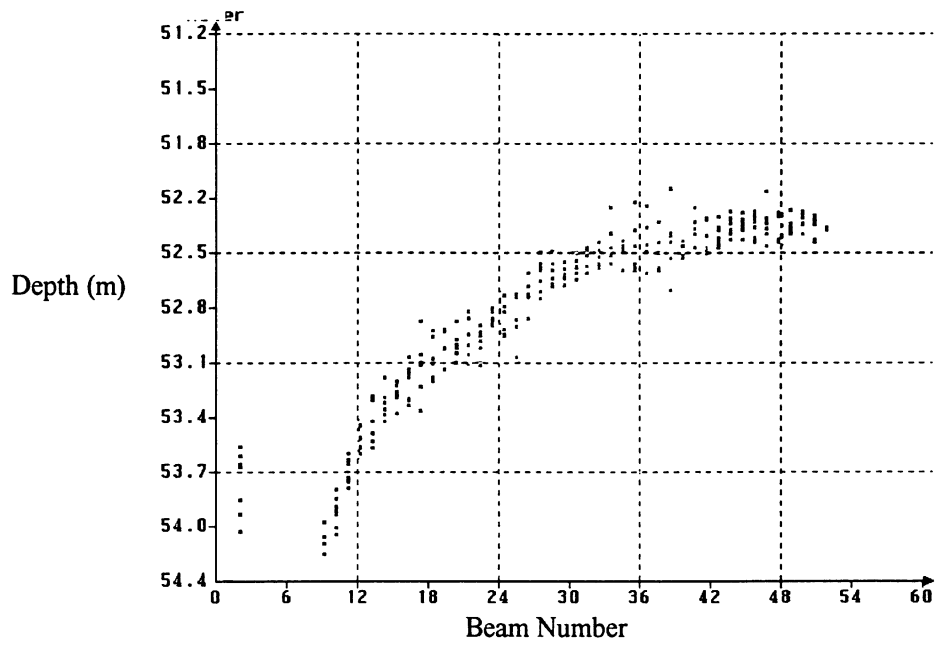


Figure c.15. Correlation plot of depth vs beam number, using BINSTAT.

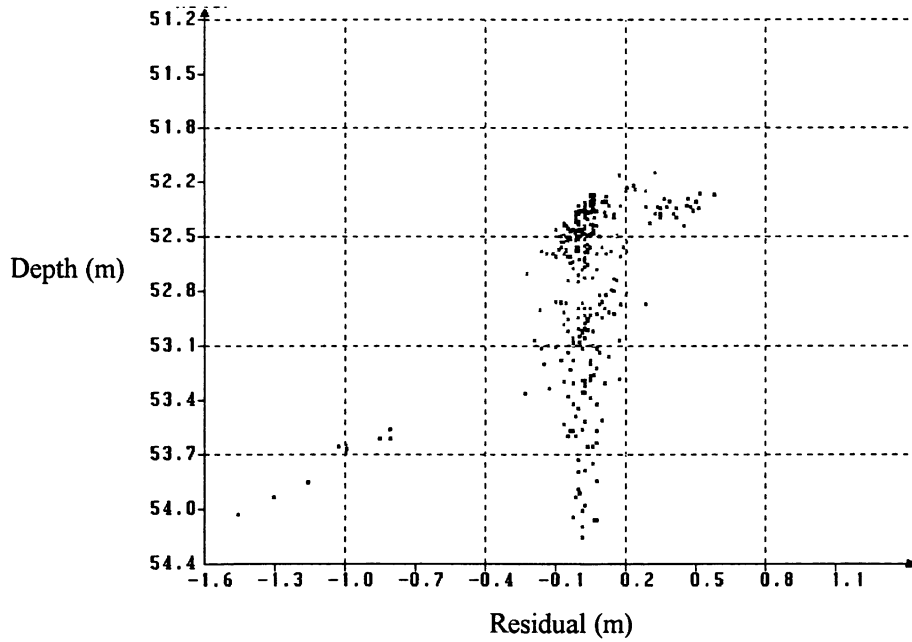


Figure c.16. Correlation plot of depth vs residuals, using BINSTAT.

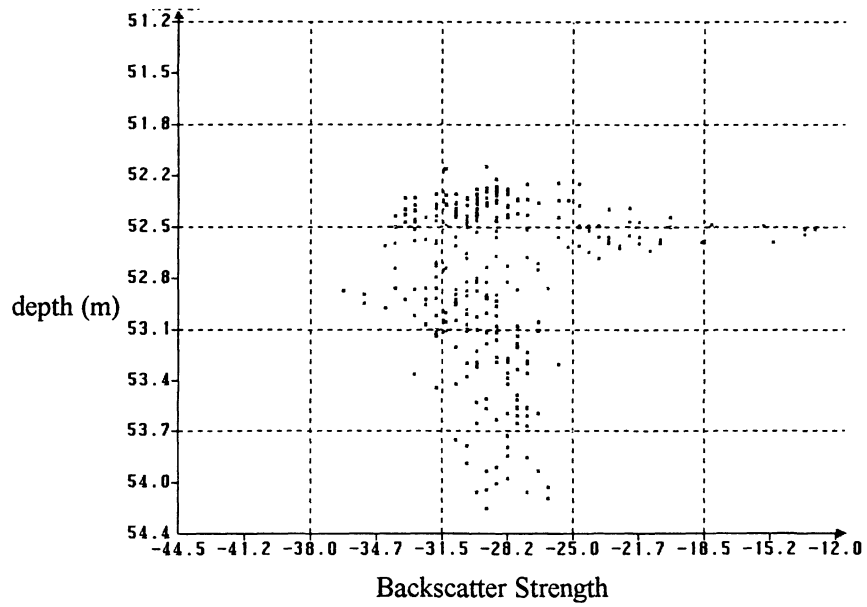


Figure c.17. Correlation plot of depth vs backscatter strength, using BINSTAT.

Appendix C.2

RESULTS OF INTERACTIVE AND AUTOMATIC DATA CLEANING WITH *BINSTAT* FOR *HALIFAX APPROACHES*

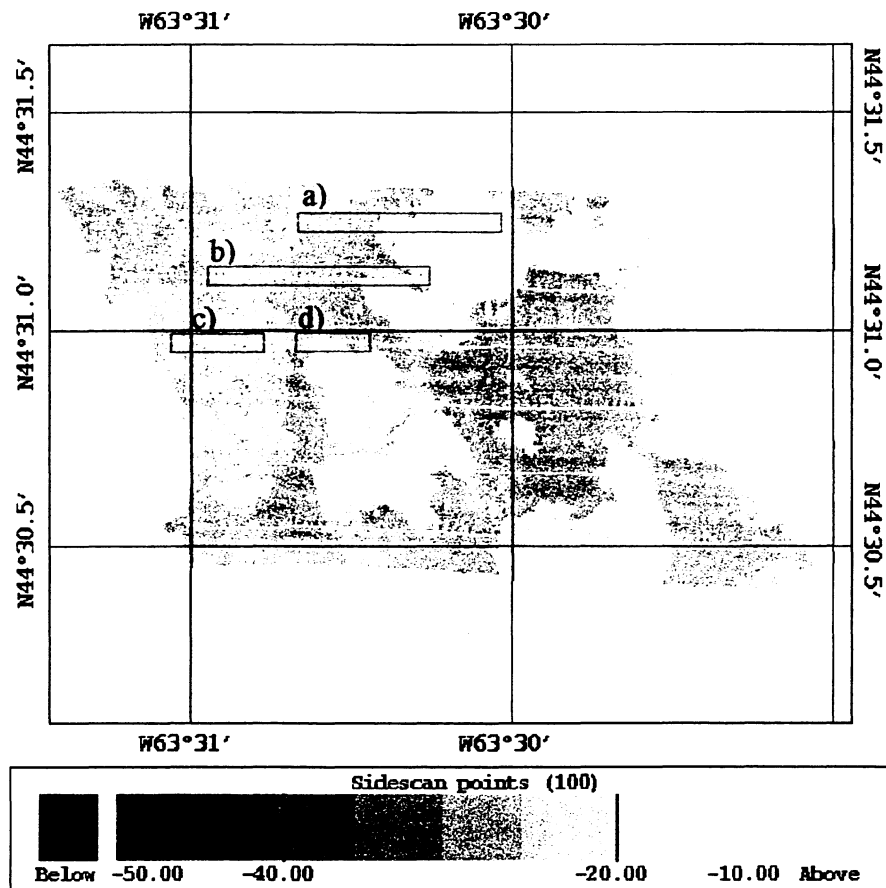


Figure c.18. Side scan image. The areas defined in this figure are investigated using the following correlation plots.

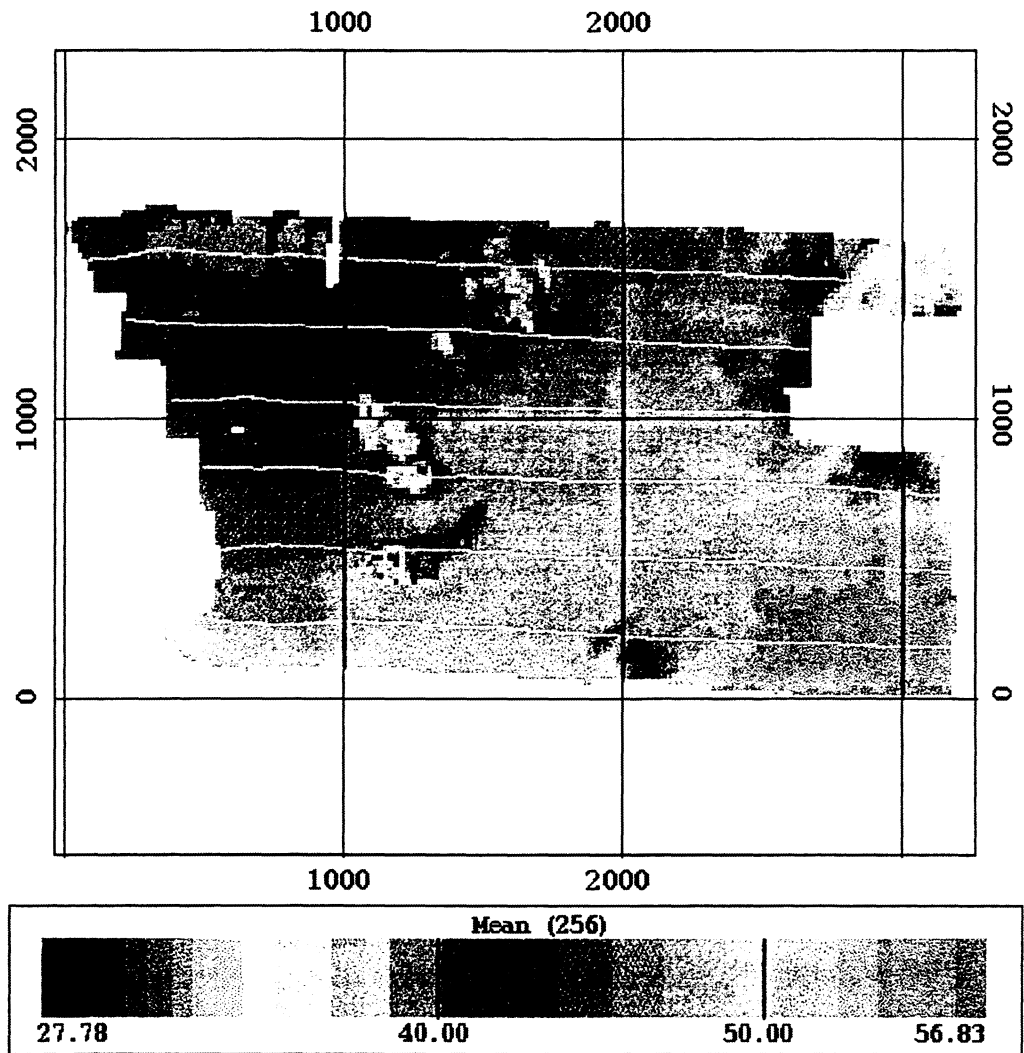


Figure c.19. Mean depth surface of the data set cleaned interactively, using BINSTAT.

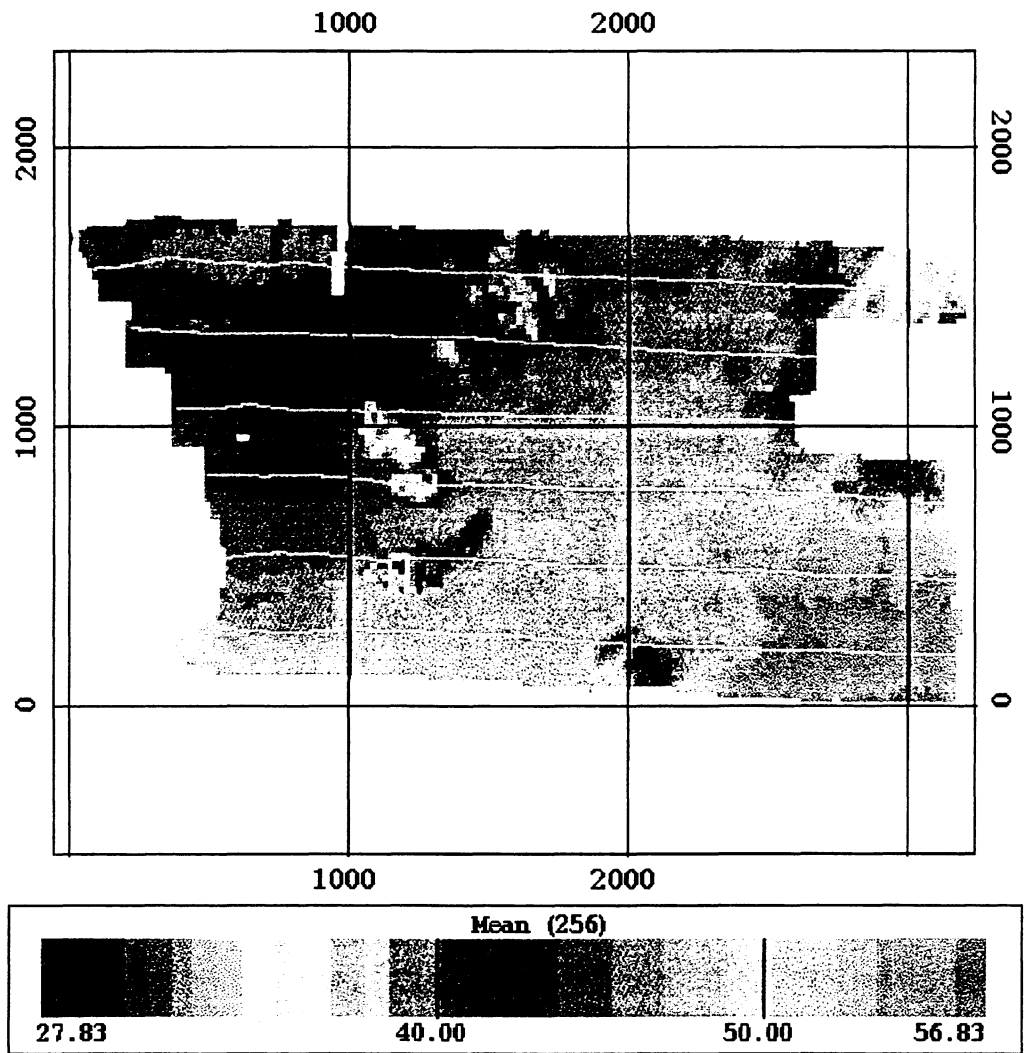


Figure c.20. Mean depth surface of the data set cleaned automatically, using BINSTAT.

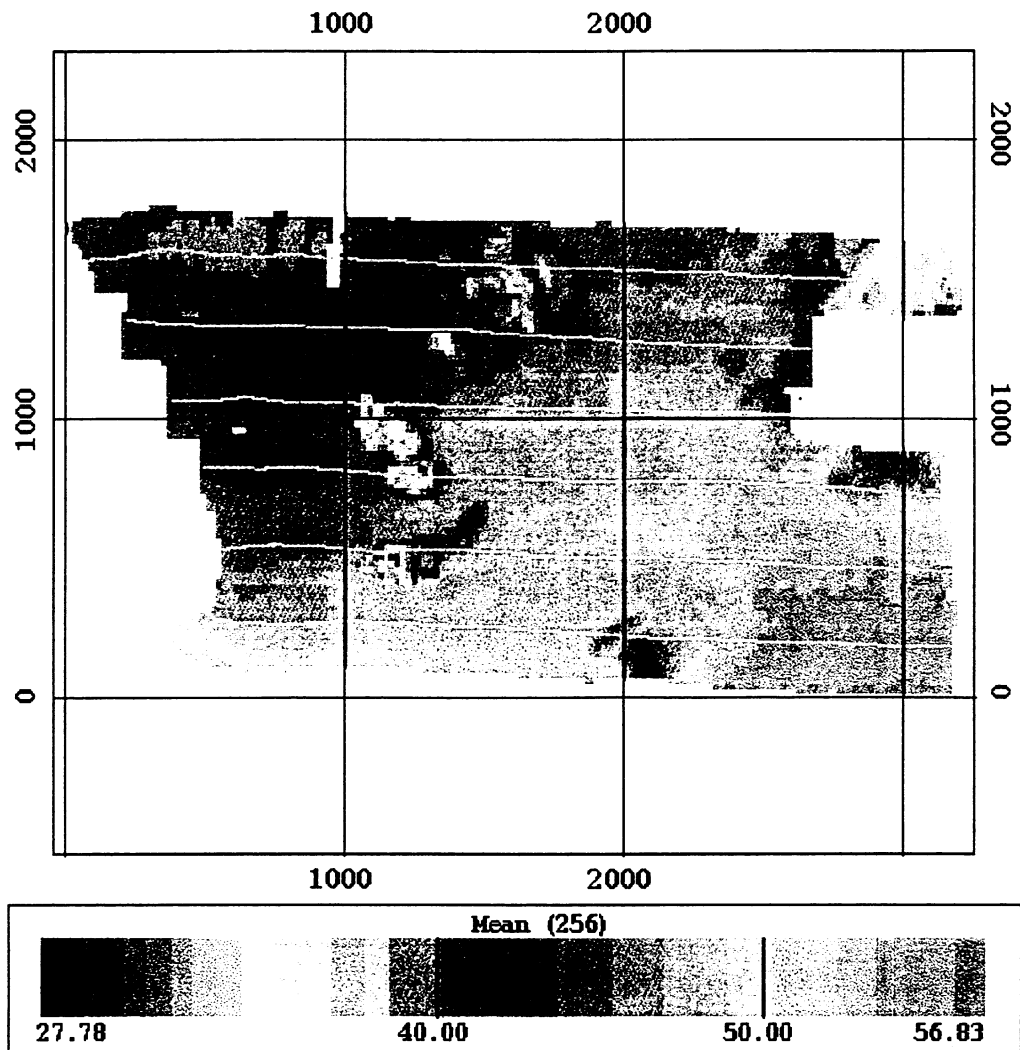


Figure c.21. Mean depth surface of the whole data set cleaned automatically, using BINSTAT.

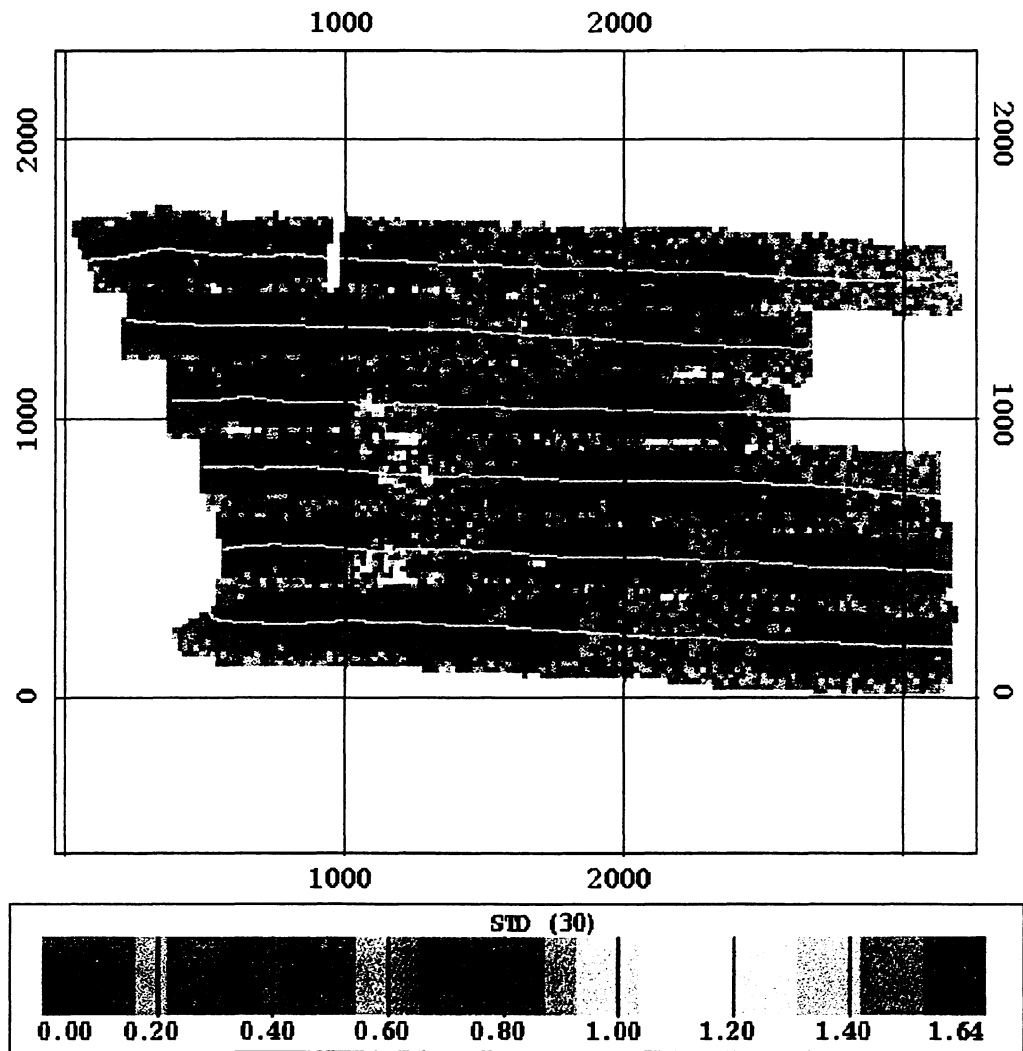


Figure c.22. Standard deviation surface of the data set cleaned interactively (Figure c.19), using BINSTAT.

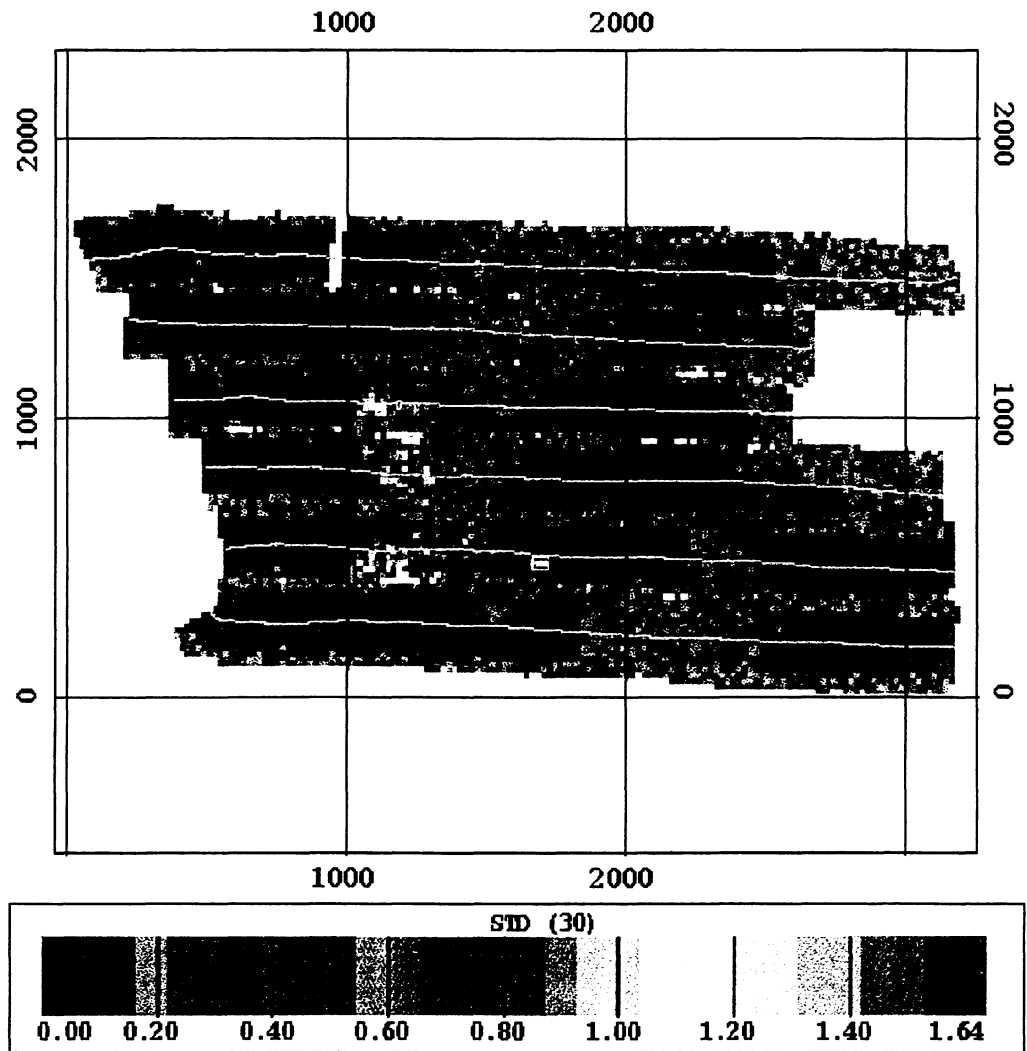


Figure c.23. Standard deviation surface of the dat set cleaned automatically (Figure c.20), using BINSTAT.

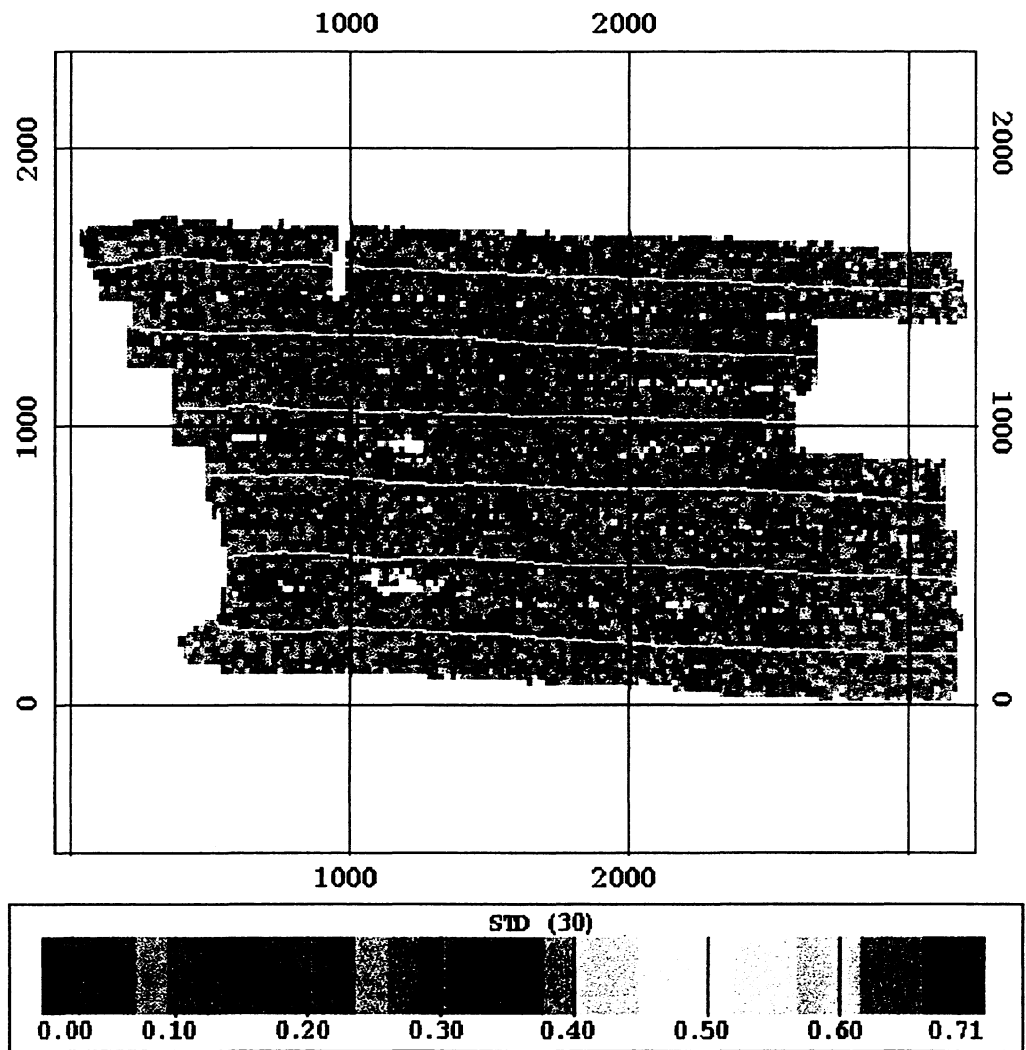


Figure c.24. Standard deviation surface of the whole data set cleaned automatically (Figure c.21), using BINSTAT.

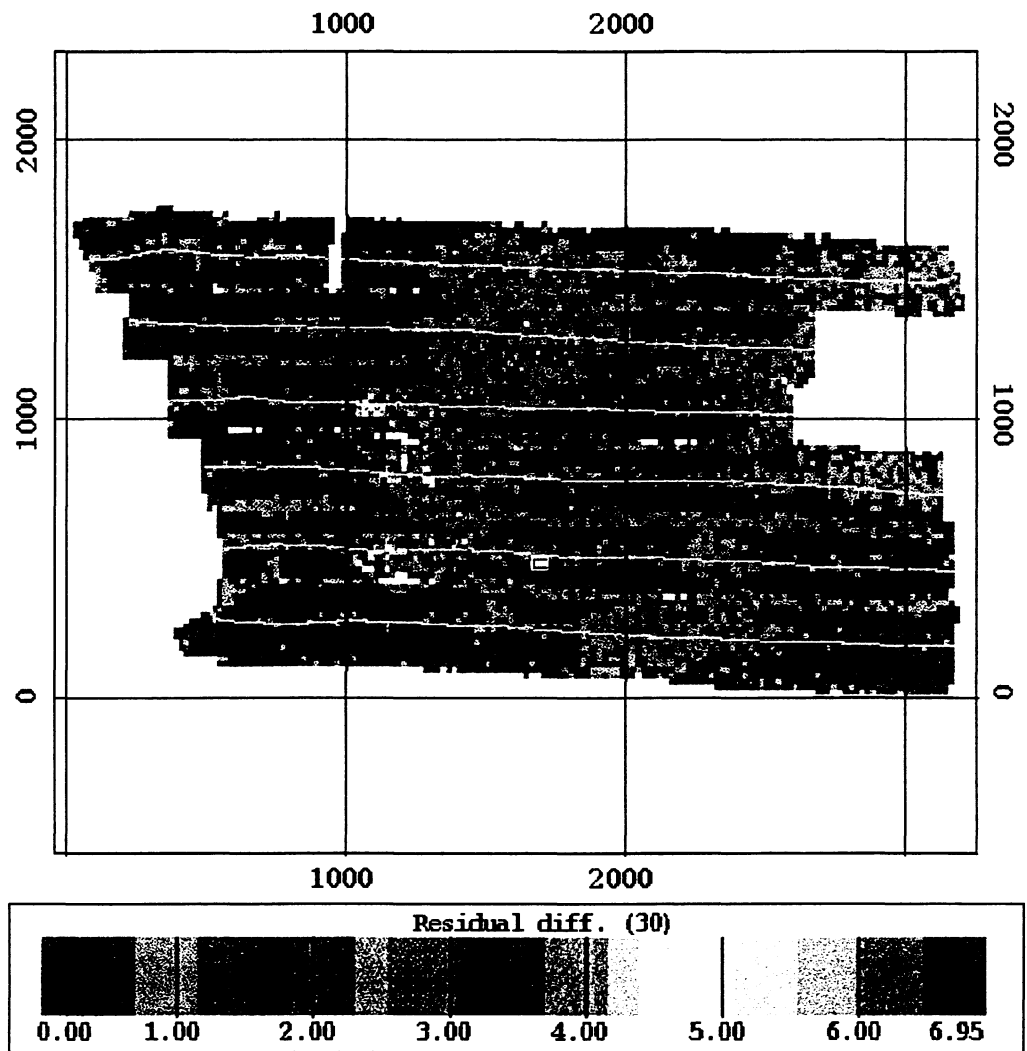


Figure c.25. Residual difference surface of the data set cleaned interactively (Figure c.19), using BINSTAT.

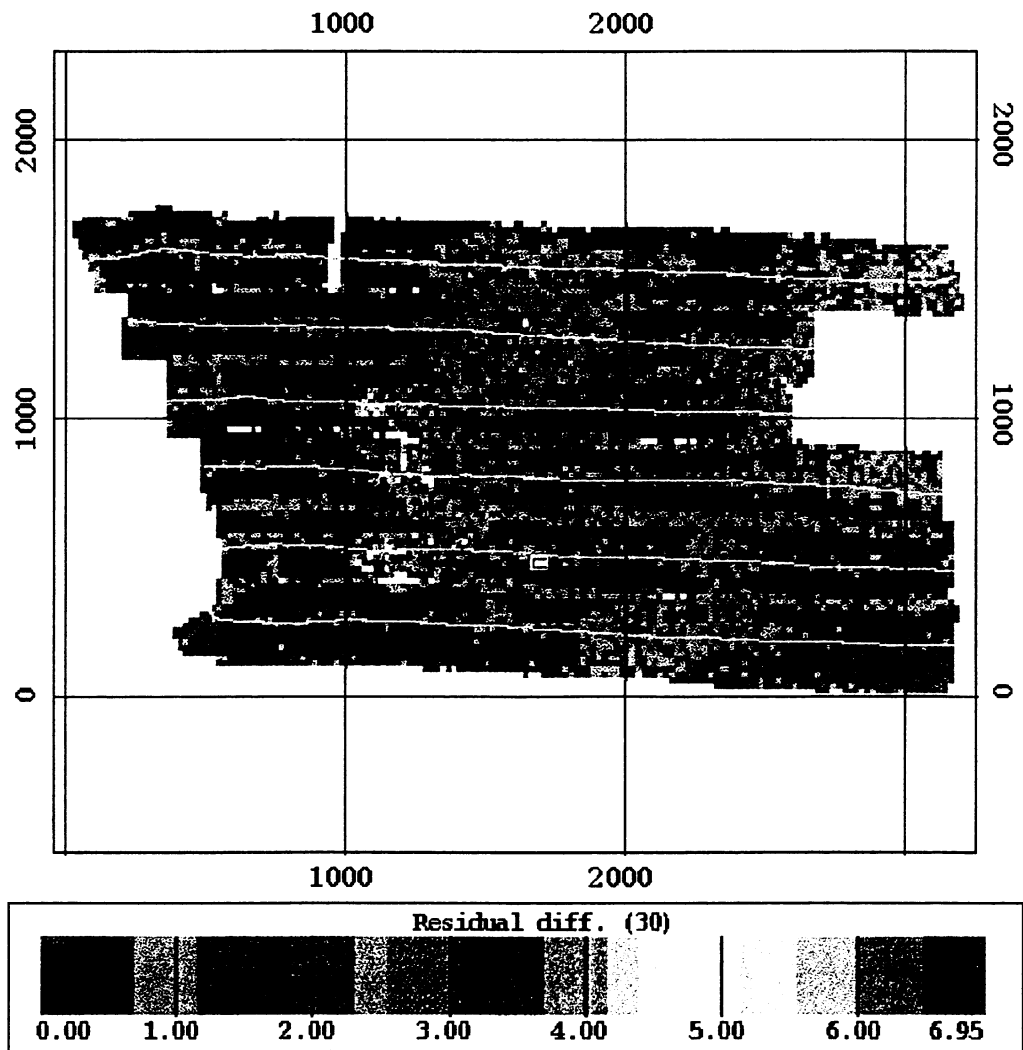


Figure c.26. Residual difference surface of the data set cleaned automatically (Figure. c.20), using BINSTAT.

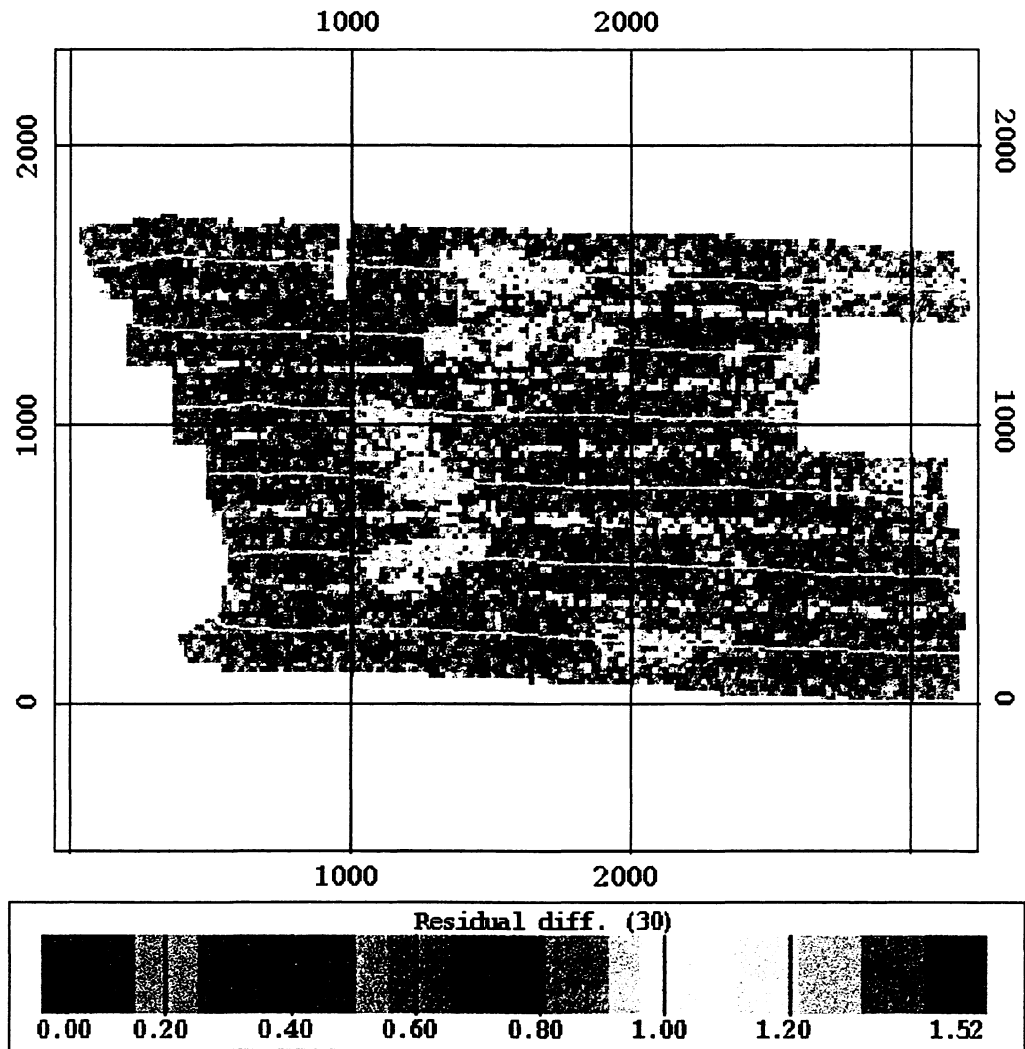


Figure c.27. Residual difference surface of the whole data set cleaned automatically (Figure c.21), using BINSTAT.

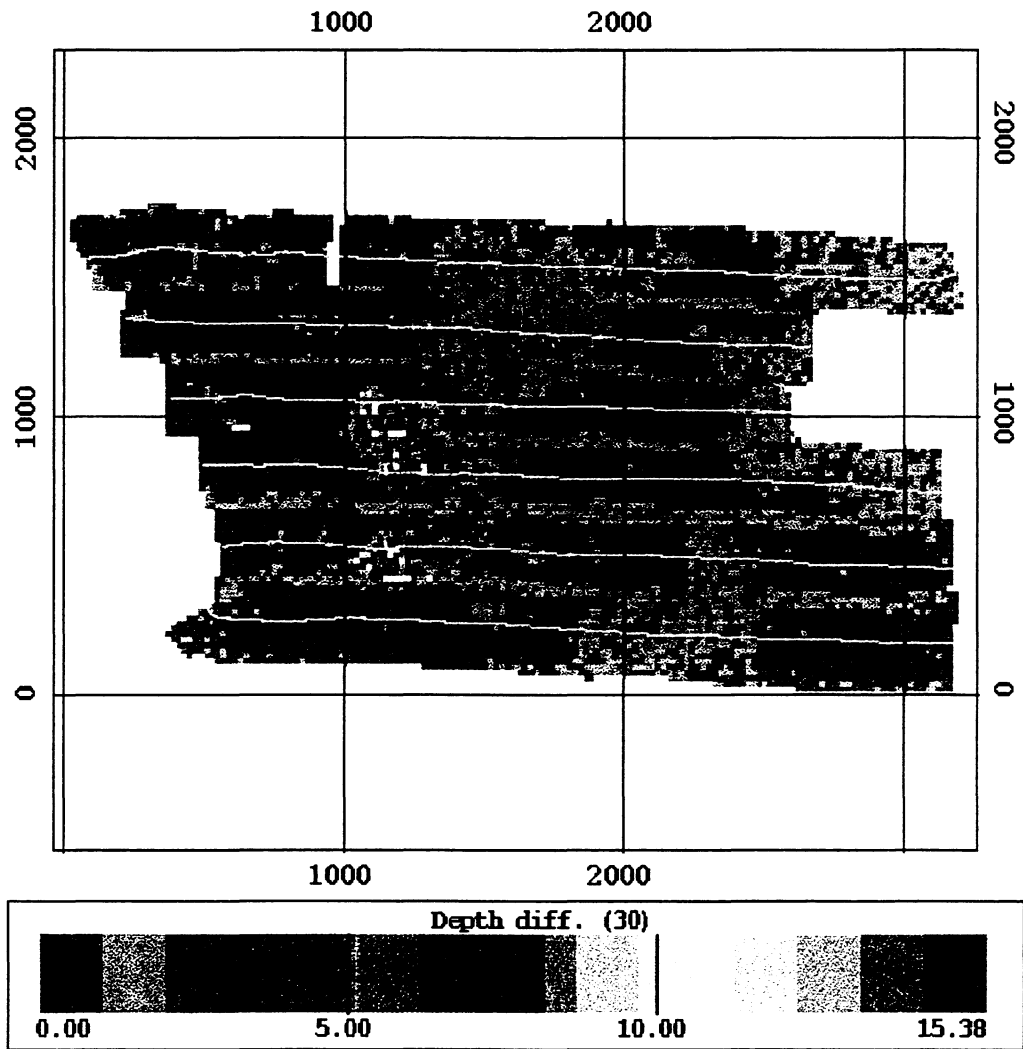


Figure c.28. Depth difference surface of the data set cleaned interactively (Figure c.19), using BINSTAT.

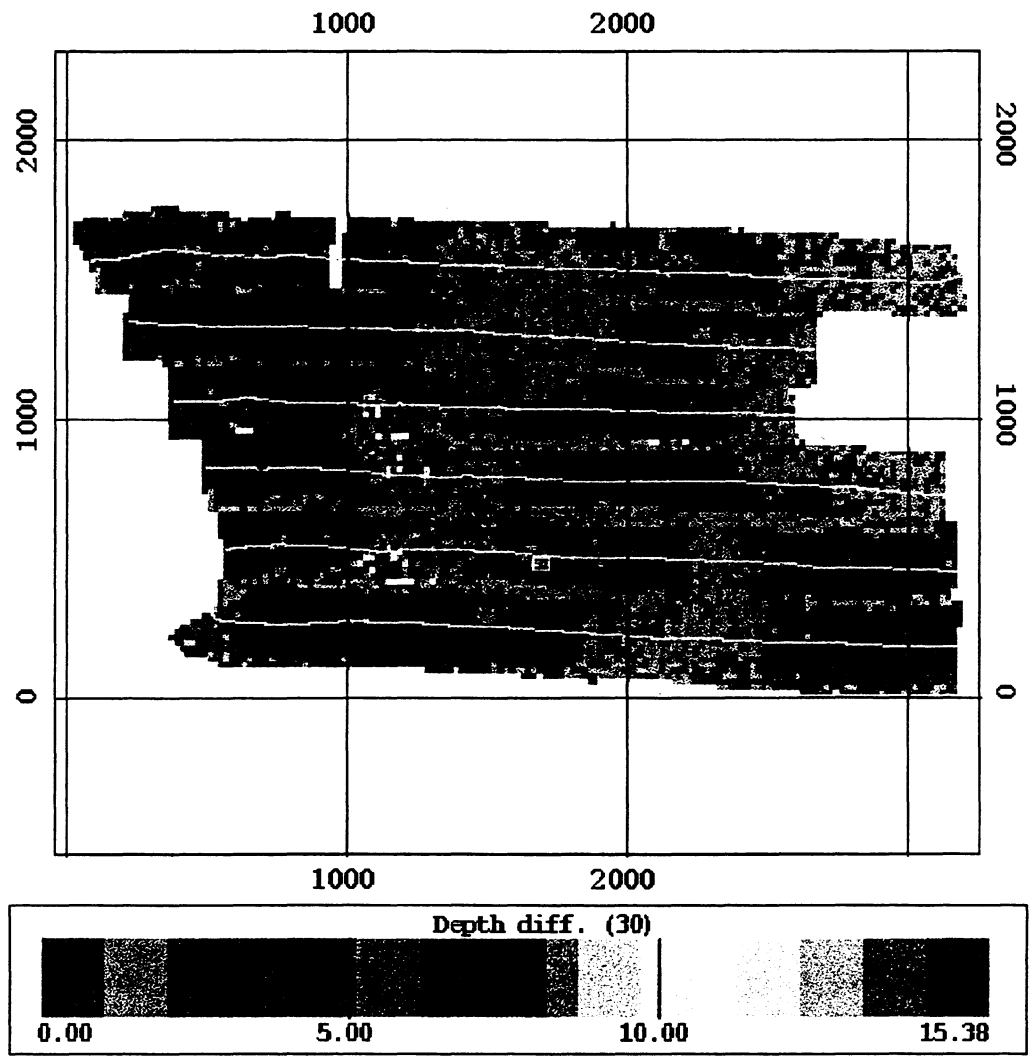


Figure c.29. Depth difference surface of the data set cleaned automatically (Figure c.20), using BINSTAT.

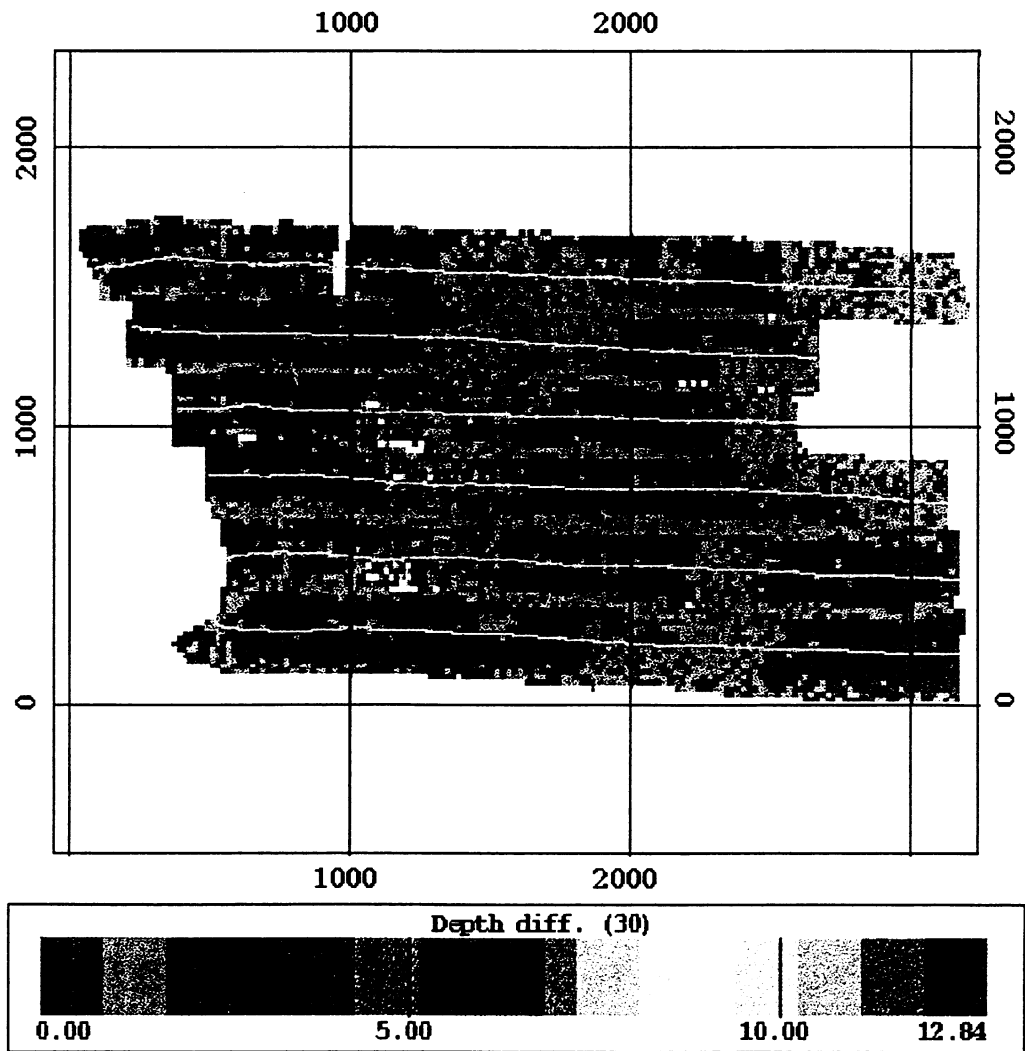


Figure c.30. Depth difference surface of the whole data set cleaned automatically (Figure c.21), using BINSTAT.

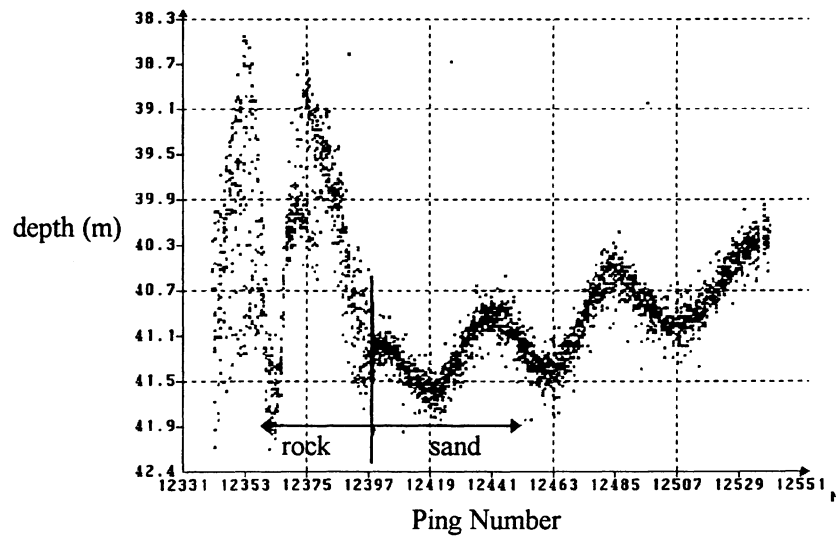


Figure c.31. Correlation plot of depth vs ping number for area *a* (Figure c.18).

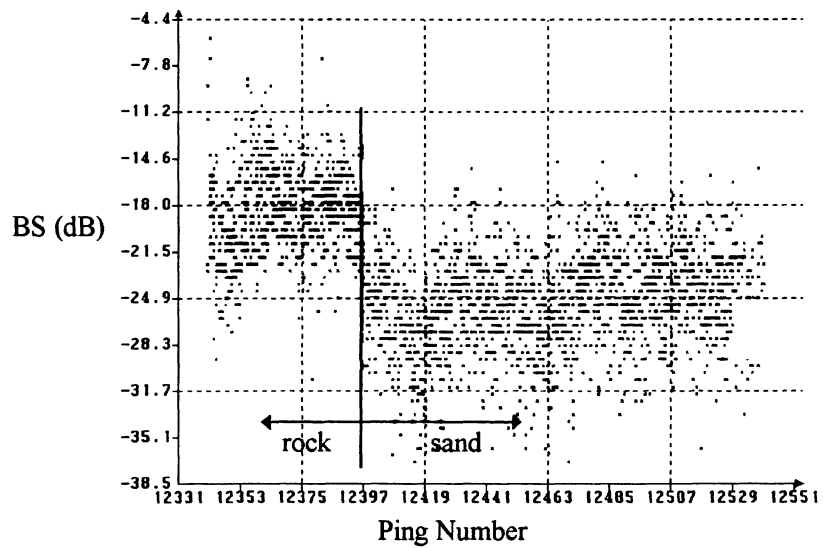


Figure c.32. Correlation plot of backscatter strength vs ping number for area *a* (Figure c.18).

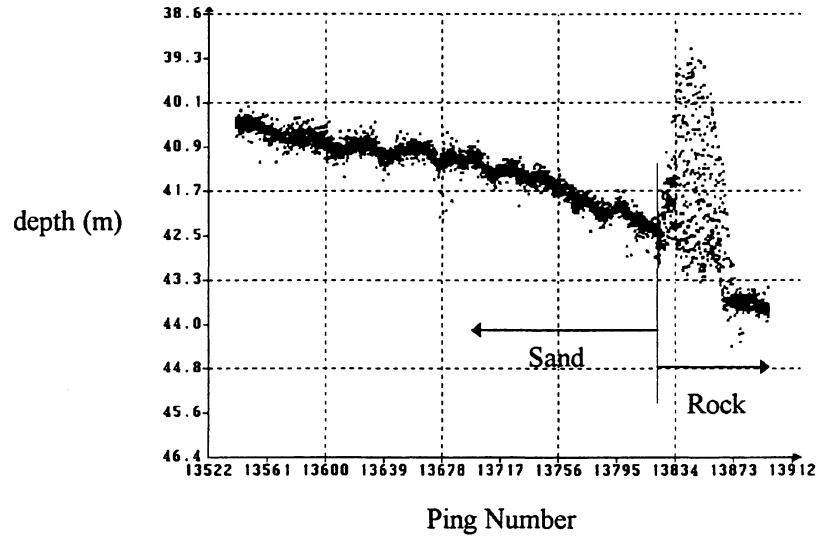


Figure c.33. Correlation plot of depth vs ping number for area *b*.

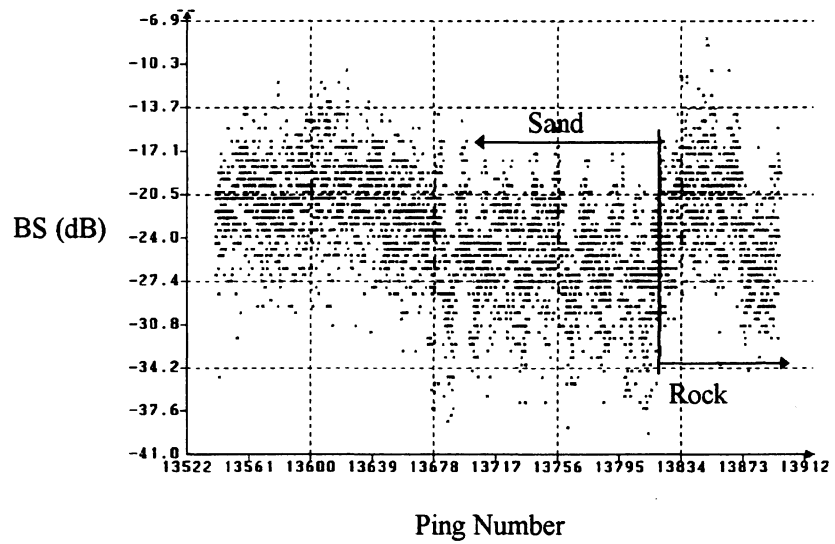


Figure c.34. Correlation plot of backscatter strength vs ping number for area *b*.

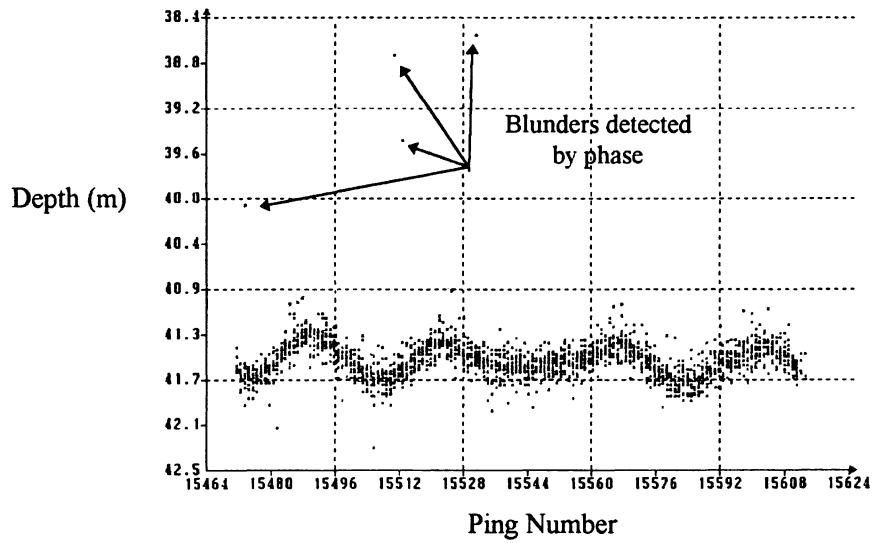


Figure c.35. Correlation plot of depth vs ping number for area *c* (Figure c.18). The blunders are positively identified in an area where topographic features should be detected by amplitude.

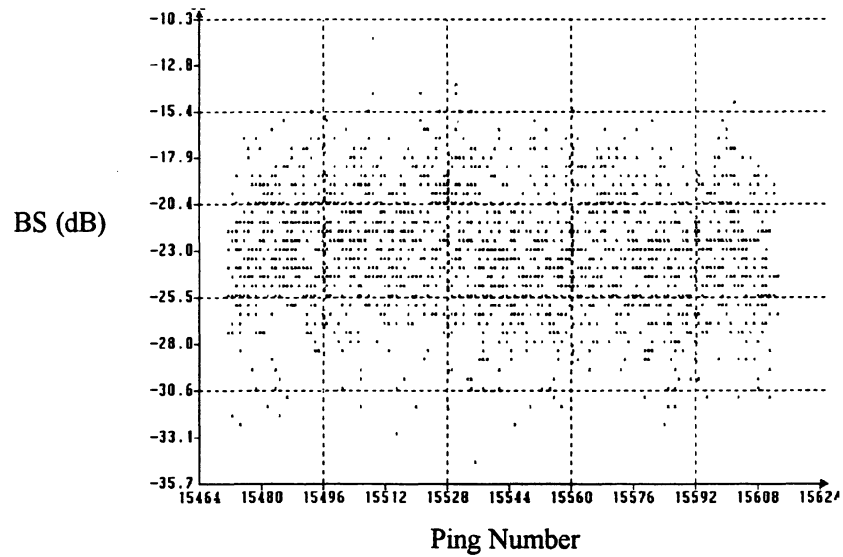


Figure c.36. Correlation plot of backscatter strength vs ping number for area *c* (Figure c.18).

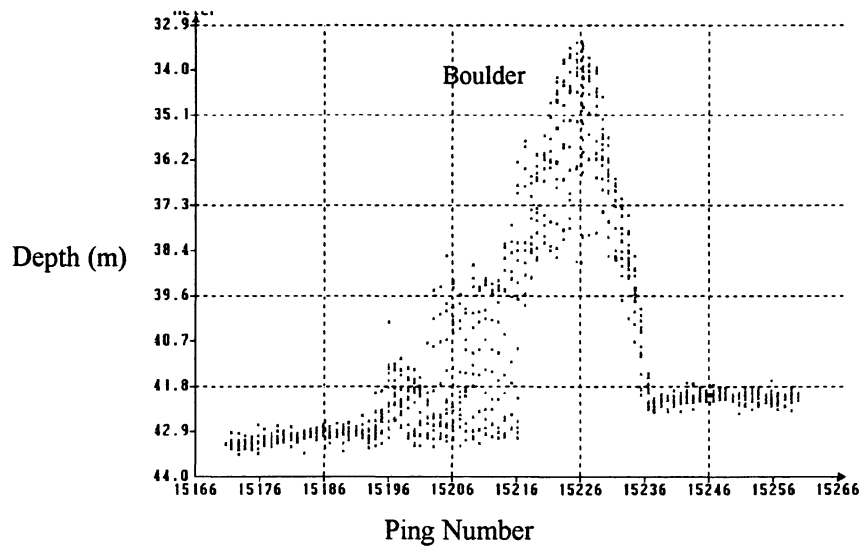


Figure c.37. Correlation plot of depth vs ping number for area *d* (Figure c.18).

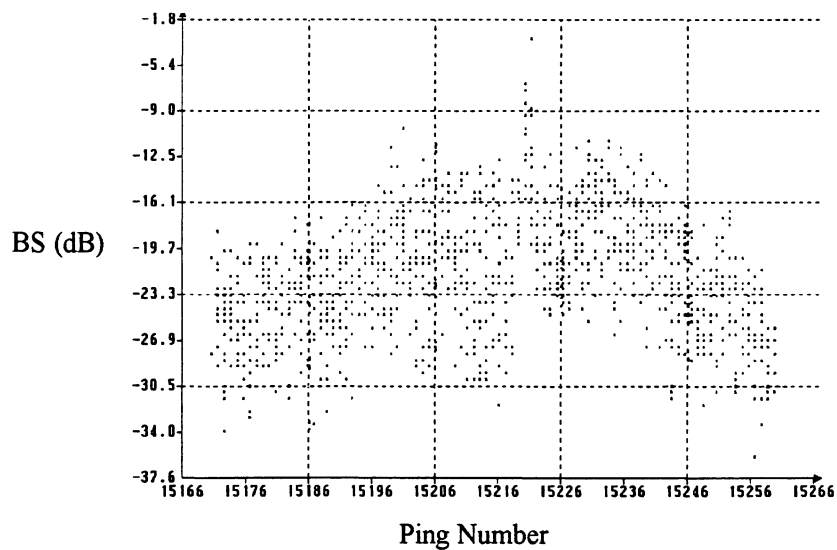


Figure c.38. Correlation plot of backscatter strength vs ping number for area *d* (Figure c.18). The boulder introduces an increase of the backscatter strength.

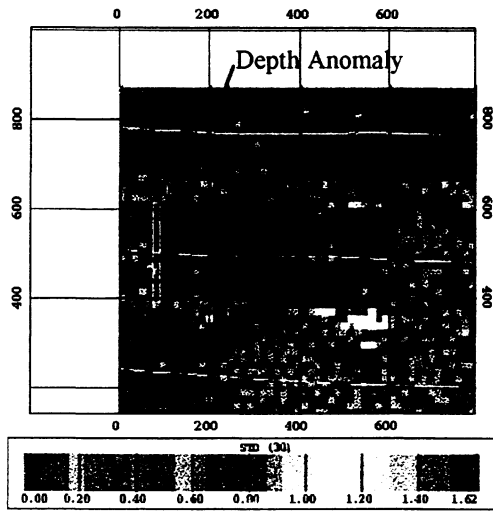


Figure c.39. Standard deviation surface.

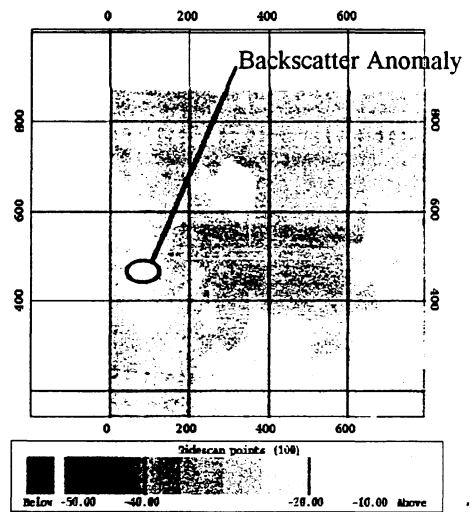


Figure c.40. Acoustic image.

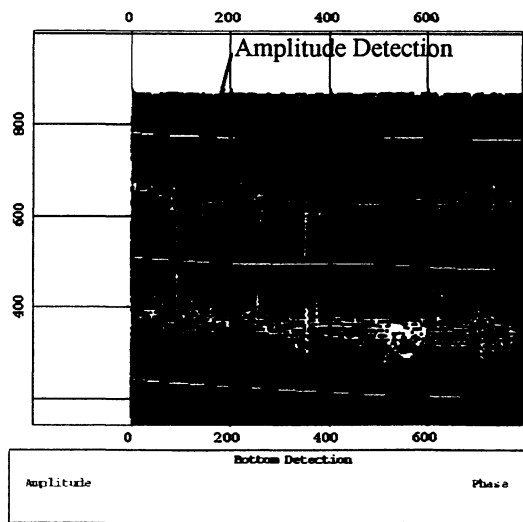


Figure c.41. Bottom detection surface.

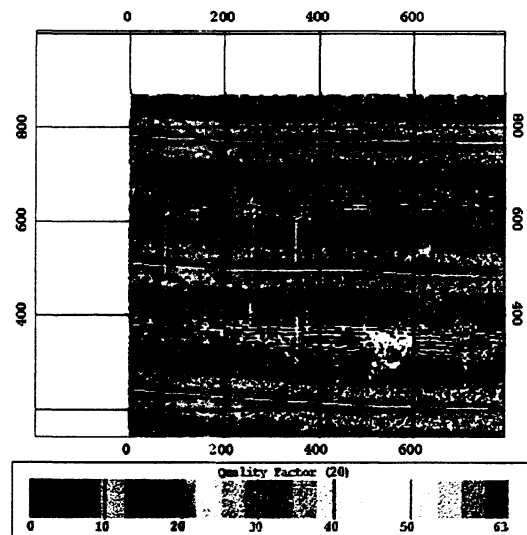


Figure c.42. Quality factor surface.

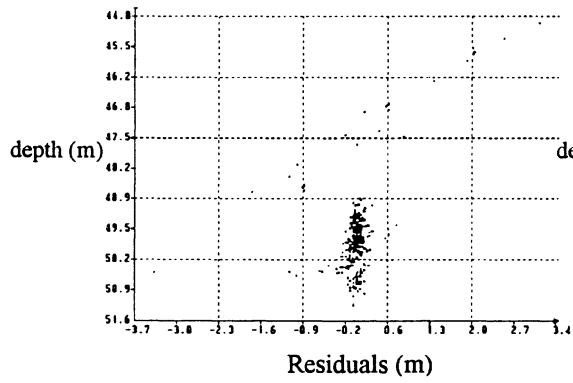


Figure c.43. Correlation of depth vs residuals.

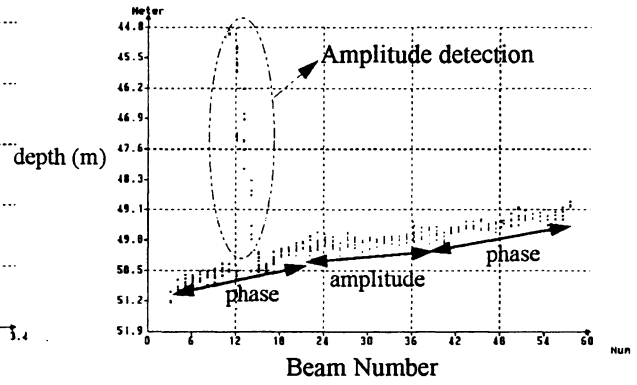


Figure c.44. Correlation of depth vs beam number.

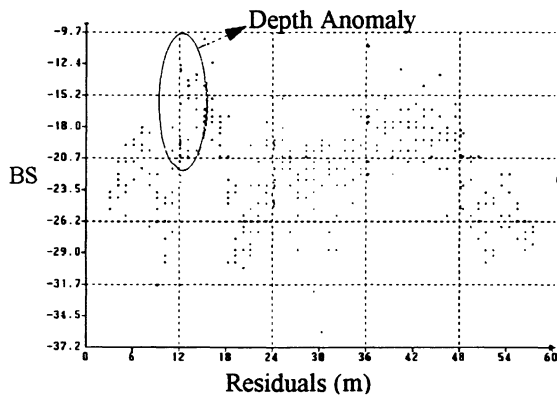


Figure c.45. Correlation of backscatter strength vs beam number.

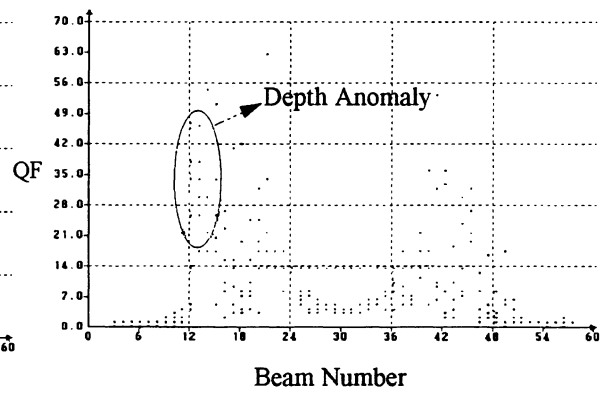


Figure c.46. Correlation of quality factor vs beam number.

VITA

Candidate's full name: Fernando Manuel Freitas Artilheiro

Place and date of birth: Albufeira, Portugal, on 5 August 1965

Permanent address: Avenida Bento Gonçalves, 33, 1° F
2800 Almada
Portugal

Schools attended: João de Deus High School, Faro, Portugal
(1977 - 1983)

Universities attended: University of the Algarve, Faro, Portugal
Marine Biology and Fisheries (1983 - 1985)

Naval Academy, Almada, Portugal
Diploma in Naval Military Sciences (1985 - 1990)

Hydrographic Institute, Lisbon, Portugal
Specialization Course in Hydrography
Certified with Category *A* from the International
Hydrographic Organization (1991 - 1992)

University of New Brunswick, Fredericton, Canada
Department of Geodesy and Geomatics Eng.
Master's of Engineering candidate (1994 - 1996)